UNIVERSITY OF PISA – FACULTY OF SCIENCE

SEARCH FOR THE TOP QUARK AT CDF IN EVENTS WITH TWO CHARGED LEPTONS, NEUTRINOS AND HADRONIC JETS

A Thesis presented by

Sandra Leone

to the Physics Department

in candidacy for the Degree of Doctor of Science

Advisor:	Coordinator:
Prof. Giorgio Bellettini	Prof. Pietro Menotti

FEBRUARY 1994

ACKNOWLEDGMENT

First of all I would like to thank the multitude of people in the CDF Collaboration, who with many hours of work built and maintained this excellent detector.

I would like to express my thanks to my advisor Prof. Giorgio Bellettini for giving me the opportunity to work on the CDF experiment. Without his support and encouragement this work would not have been possible. I thank him for letting me choose the topic of the analysis and for following my progress.

I thank particularly my supervisor Dr. Hans Grassmann for the innumerable discussions and his guidance in the analysis. I owe him most of what I learnt in high energy physics research. I appreciated his very careful reading of the thesis and his many helpful suggestions to improve the presentation.

I wish to express my appreciation to my friend and collegue Marina Cobal, with whom I spent, working side by side, these three years. Working together has been pleasant and productive.

I thank Prof. G.P. Yeh, responsible of the dilepton working group in CDF.

Finally I want to mention people to whom saying thanks is not enough. Enrico, for his constant encouragement and understanding through all of the long hours dedicated to this work. My parents, for the continuous support and the encouragement throughout the years: they, more than anyone else, helped me to believe that, despite all the appereances to the contrary, I was enjoying myself. This thesis is dedicated to them.

Index

Introduction

This thesis describes a search for the top quark. The analysis is based on a data sample of 21.4 pb^{-1} integrated luminosity collected by the CDF detector ("*Collider Detector at Fermilab*") from August 1992 to May 1993. During the data taking the detector, after more than 10 years of planning, construction, calibration and tests by the whole Collaboration, worked excellently.

This analysis has been done in collaboration with Dr. Hans Grassmann and under the supervision of prof. Giorgio Bellettini, in the context of the CDF heavy flavor working group, which periodically discussed its progress. The exchange of information with Dr. Marina Cobal, who was writing a thesis on the top search in a different decay channel, has been frequent.

The CDF experiment studies proton–antiproton interactions at the Fermilab Tevatron Collider. The Tevatron Collider is a synchrotron which provides a center of mass energy of 1.8 TeV, the highest available for hadron collisions. These interactions are the best available tools for frontier particle physics studies: b physics, QCD and jet properties, electroweak precision measurements, physics beyond the Standard Model. The search for the top quark, the last one predicted by the Standard Model, has been one of the major goals at hadron colliders.

In this thesis we have investigated the direct production of top–antitop pairs through the gluon–gluon fusion and the quark–antiquark annihilation: $gg \rightarrow t\bar{t}$ and $q\bar{q} \rightarrow t\bar{t}$. In the Standard Model each top quark decays to an intermediate vector boson W and a b quark ($t \rightarrow Wb$).

In particular, we studied the channel in which both W's decay leptonically. This channel has a small branching ratio, but it also has a small physical background. The observed final state is characterized by the presence of two isolated large transverse momentum charged leptons, an apparent energy unbalance in the plane transverse to the beam (due to the neutrinos), and two jets from the hadronization of the b quarks.

If the top quark is heavy enough ($M_{top} > 140$ GeV/c^2), some processes (e.g. the production of WW pairs) become competitive, from the point of view of the production cross section, with the production of $t\bar{t}$ pairs. These events are also characterized by two isolated high transverse momentum leptons, and by momentum unbalance. However, at the lowest order there are no hadronic jets. In our analysis strategy we required the presence of two jets to suppress the background from WW pairs and any other kind of background from QCD.

In order to gain efficiency, we required only one of the two leptons to pass the "*standard*" identification cuts. We applied looser cuts on the second lepton, which can still be tagged by exploiting the excellent performance of the CDF tracking system, and the isolation properties of leptons coming from heavy particle decays. This selection criteria will be discussed in detail in Chapter IV.

Besides studying the usual channels ee, $e\mu$ and $\mu\mu$, we extended the search to the channels $e\tau$ and $\mu\tau$, in which the τ decays into one charged hadron plus neutral particles. We tried to unify the analysis as much as possible amongst the various channels, using features common to all leptons (as for instance the isolation). We also studied the kinematical properties of the events in order to improve the signal–background separation.

Once we selected the candidate events, we looked for some evidence of secondary vertices from b quarks in the jets.

Until now, dilepton searches were used to extract a lower limit on the top quark mass from an upper limit on the production cross section. The purpose of the analysis described in this thesis was the observation of a signal and not the determination of an upper limit to it. Therefore a new limit has not been evaluated based on the candidate events found

by this analysis.

The thesis is organized as follows: Chapter I contains a short summary of the experimental results on top searches and of the relevant theoretical background. Chapter II describes briefly the Tevatron Collider and the CDF experiment, paying particular attention to those parts of the detector which provide the information which plays a major role in the analysis. The subject of Chapter III is the analysis strategy. As an example of the usefulness of studying the event structure, the application of this approach to the 88–89 CDF dilepton top candidate event is described. The most original part of this work was based on the tentative assumption that top is heavy. In this scenario, the presence of two jets in the events is required since the beginning of the analysis. In addition, by requiring one isolated track as the second candidate lepton, the decay $W \rightarrow \nu\tau$ has been included in the analysis. Till now the presence of the tau leptons had never been used for the top search.

In Chapter IV lepton and jet identification criteria are discussed. The variables used to select high momentum electrons and muons, the definition of leptons as isolated tracks and the efficiency studies are presented. Chapter V describes the background calculations for both technical and physical backgrounds. These studies have been made using Montecarlo programs and control data samples (events with many jets, events with non–isolated leptons, W + jets). Finally, Chapter VI reports the results of the analysis. The candidate events are discussed and a statistical interpretation of the result is made.

Appendix A presents a comparison between the analysis described in this thesis and a different analysis in the dilepton channel which has been developed by CDF collaborators. Appendix B briefly describes an application of the tau identification algorithm to the search for $Z^{\circ} \rightarrow \tau\tau$ events.

Chapter 1

Theoretical Framework

1.1 The Standard Model

The existing picture of the fundamental constituents of matter and their interactions (leaving aside gravitation) is currently summarized in a theoretical framework known as the "Standard Model". It consists of two parts: the Quantum Chromo–Dynamics (QCD) [1] which describes the strong interactions and is based on a non–abelian gauge symmetry SU(3) and the Glashow – Salam – Weinberg (GSW) model [2] which describes the weak and electromagnetic interactions and is based on a non–abelian SU(2)×U(1) symmetry.

Electromagnetic interactions are mediated by the massless photon γ. The conserved quantity related to the symmetry U(1) is the electric charge.

Weak interactions are mediated by massive bosons (Z° and $W^\pm$). The conserved charges associated with this symmetry are the weak isospin and the hypercharge. The breaking of the symmetry causes the Z° and the $W^\pm$ to become massive. The observation of the vector bosons at the CERN $p\bar{p}$ Collider in 1983 provided an important test of the Standard Model [3]. Later on, the LEP e^+e^- collider provided the possibility to make precision measurements of the Z° parameters and many checks of the predictions of theory [4].

Strong interactions are mediated by eight neutral massless gauge bosons called gluons, coupled to a conserved charge called colour. The amplitude of a strong interaction process

at a given momentum scale Q^2 can be parametrized in terms of a "*running*" coupling constant $\bar{\alpha}_s(Q^2)$. This coupling constant depends on the momentum scale Q^2 in the following way:

$$\bar{\alpha}_s(Q^2) = \frac{1}{b_o ln(\frac{Q^2}{\Lambda^2})}$$

where $b_o = \frac{33-2n_f}{12\pi}$ and n_f is the number of quark flavors. The momentum scale Λ is often referred to as the "QCD scale parameter" and it is the only adjustable parameter in QCD, except for the quark masses. It is determined by comparing QCD predictions to experimental data. From the above equation we observe that as the Q^2 of the interaction increases, the coupling constant $\bar{\alpha}_s$ decreases until the quarks and gluons are only weakly interacting with each other (asymptotic freedom). Therefore it turns out to be possible to apply perturbation theory at least for processes with large transferred momentum Q^2.

Gauge bosons properties are summarized in table 1.1.

Boson	Spin	Charge	Color	Mass (GeV/c^2)
γ	1	0	no	0
Z°	1	0	no	91.187 ± 0.007 [5]
$W^\pm$	1	± 1	no	80.22 ± 0.26 [5]
g_i $(i = 1, ..., 8)$	1	0	yes	0

Table 1.1: Gauge boson properties. The eight gluons correspond to the octet associated with the three color charges of the QCD SU(3) group.

All matter appears to be composed of quarks and leptons, which are pointlike, structureless, spin–1/2 particles. The quarks participate in all three interactions, while the leptons participate only in the weak and electromagnetic ones. The fundamental particles can be grouped in doublets and singlets of weak isospin, in three generations. The LEP experiments have shown that the e^+e^- annihilation cross section in the Z° mass energy region, primarily within the width of the resonance peak, is consistent with the Standard Model assumption of three light neutrino generations [5].

The picture of the fundamental interactions is completed assuming the existence of the Higgs boson. The Higgs field is responsible for the $W^\pm$ and Z° masses and for the

fermion masses through the process of spontaneous symmetry breaking [6]. In table 1.2 we present the scheme of the Standard Model fundamental particles and their quantum numbers. Right–handed fermions (labeled by the index R) are weak–isospin singlets ($T = 0$), while left-handed fermions (labeled by the index L) are weak–isospin doublets ($T = 1/2$).

Generation:	1	2	3	T_3	Y	Q
Fermions *lepton − type* (*spin* 1/2)	$\begin{pmatrix} \nu_e \\ e \end{pmatrix}_L$	$\begin{pmatrix} \nu_\mu \\ \mu \end{pmatrix}_L$	$\begin{pmatrix} \nu_\tau \\ \tau \end{pmatrix}_L$	1/2 −1/2	−1 −1	0 −1
	e_R	μ_R	τ_R	0	−2	−1
Fermions *quark − type* (*spin* 1/2)	$\begin{pmatrix} u \\ d \end{pmatrix}_L$	$\begin{pmatrix} c \\ s \end{pmatrix}_L$	$\begin{pmatrix} t \\ b \end{pmatrix}_L$	1/2 −1/2	1/3 1/3	2/3 −1/3
	u_R d_R	c_R s_R	t_R b_R	0 0	4/3 −2/3	2/3 −1/3
Higgs *bosons* (*spin* 0)	$\Phi = \begin{pmatrix} \phi^+ \\ \phi^0 \end{pmatrix}$			1/2 −1/2	1 1	1 0

Table 1.2: Particles in the GSW model. The quantum numbers of the third component T_3 of the weak isospin, the weak hypercharge Y and the electric charge Q are given ($Q = T_3 + \frac{1}{2}Y$).

Among these fundamental constituents, the ν_τ neutrino, the top quark and the Higgs boson have never been directly observed. One of the major goals of modern particle physics is the completion of this scheme. In particular the search for the top quark has always had high priority at hadron collider experiments.

1.2 Indirect evidence for the existence of the top quark

Despite the lack of direct experimental evidence, there are many results which give us rather good confidence that the top quark does indeed exist: the branching ratio for b decays to lepton pairs, the forward–backward asymmetry of the b quark production in e^+e^- collisions, and the Z° decays to b pairs [7]. They all come from measurements of the properties of b mesons.

If the b quark is a singlet, we expect the branching ratio for b decays to lepton pairs to be greater than 1.3×10^{-2} [8]. The value predicted by the Standard Model (where the b quark is a member of a doublet and the top quark exists) is 10^{-4} times smaller. The CLEO experiment reports a limit of less than 1.2×10^{-3} at 90% confidence level [9].

The forward–backward asymmetry in b quark production from e^+e^- collisions is proportional to $T^b_{3L} - T^b_{3R}$ [10]. One can conclude that the asymmetry would be zero for a b quark which is a singlet. Measurements made at LEP gave a value for the asymmetry corresponding to [11]:

$$T^b_{3L} = -0.504^{+0.018}_{-0.011}.$$

The value expected from the Standard Model is – 1/2.

Further evidence for the existence of the top quark comes from the observation of Z° decays to b quark pairs. The branching ratio for this process depends on the weak isospin quantum numbers of the b quark as follows:

$$\Gamma(Z \rightarrow b\bar{b}) \sim 24\ \Gamma_o[(T^b_{3L} + \tfrac{1}{3}\ sin^2\theta_W)^2 + (\tfrac{1}{3}\ sin^2\theta_W)^2]$$

where

$$\Gamma_o = \frac{G_F M_Z^2}{24\pi\sqrt{2}} \sim 82.9 \text{ MeV}.$$

G_F is the Fermi constant and M_Z is the Z°–mass. If one uses a value for the Weinberg mixing angle of:

$$sin^2\theta_W = 0.234,$$

the predicted values of the branching ratio are, for the two possible values of T^b_{3L}:

$$T^b_{3L} = -\frac{1}{2},\ \Gamma = 367 \text{ MeV}$$
$$T^b_{3L} = 0,\ \Gamma = 24 \text{ MeV}.$$

The measured value is:

$$\Gamma_{oss} = 362 \pm 19 \text{ MeV}$$

and it excludes $T^b_{3L} = 0$ [7].

There are also several theoretical arguments in the Standard Model which favour the existence of the top quark. For instance, an anomaly–free theory requires that the sum of the family charges be zero (taking into account the three color states for each quark). Given the b quark and the tau, there should be a charge 2/3 quark. Flavor changing neutral currents (FCNC) are suppressed by the GIM mechanism [12], provided that each family has the same singlet/doublet isospin structure (the GIM mechanism requires all the right–handed quarks (R) and left–handed quarks (L) in different families, which have the same electric charge, to also have the same weak isospin). Without this suppression, the FCNC should be observed in the B mesons well above the observed limits.

Further evidence comes from the oscillations of neutral B mesons to the corresponding $\bar{B}$. These oscillations proceed in a second order weak interaction through the exchange of virtual top quarks [13] (the top quarks represent the dominant contribution if the top mass is much bigger than the mass of the other quarks). The mixing coefficient depends on the mass difference ΔM between the weak lagrangian eigenstates relative to their width:

$$\mathrm{x} = \frac{\Delta M}{\Gamma} = \frac{\tau_B G_F^2 m_B}{6\pi^2}\ B_B\ f_B^2\ |V_{td}V_{tb}^*|^2\ M_t^2\ F\ (\frac{M_t^2}{M_W^2})\ \eta_{QCD}.$$

The B mean lifetime τ_B, its mass m_B, and the QCD corrections η_{QCD} are known. The Cabibbo–Kobayashi–Maskawa (CKM) matrix element V_{tb} is close to one. The B meson

decay constant f_B and the so–called *bag parameter* B_B cannot be evaluated but have to be determined from experiment. $F(\frac{M_t^2}{M_W^2})$ is a known function of $(\frac{M_t^2}{M_W^2})$. The mixing measurement gives information about a missing element of the CKM matrix, V_{td}, module the value of F $(\frac{M_t^2}{M_W^2})$ [14].

The mixing is often expressed as the ratio:

$$\chi = \frac{x^2}{2 + 2x^2}$$

which represents the number of times a particle oscillates to its antiparticle relative to the total.

The mean value of χ_d measured by the ARGUS [14] and CLEO [15] experiments is:

$$\chi_d = 0.153 \pm 0.031,$$

corresponding to an x value of [16]:

$$\mathrm{x} = 0.67 \pm 0.10.$$

The value measured by CDF for the inclusive mixing of B_s° and B_d° is [17]:

$$\chi = 0.176 \pm 0.031 \pm 0.032.$$

The value measured by ALEPH is [18]:

$$\chi = 0.119 \pm 0.012.$$

The relatively large observed B mixing is actually an indication of a fairly large top mass, since the mixing increases quadratically with the top mass.

The mass of the top often affects the cross section for other processes through radiative corrections [20]. This provides an indirect way to measure the top quark mass or place limits on it. An example of such a process is the ratio of the W and Z widths. The W and Z production cross sections depend on the top mass. By taking their ratio, some theoretical dependences as well as the dependence on structure function uncertainties cancel. Using the dilepton detection mode for the Z° and the single lepton plus missing E_T for the W, the ratio is:

$$R = \frac{\sigma_W}{\sigma_Z} \frac{\Gamma(W \to l\nu)}{\Gamma(Z \to ll)} \frac{\Gamma_Z}{\Gamma_W}.$$

By measuring this ratio and using the reliable Standard Model predictions for the branching ratio of Z°'s to lepton pairs and W's to leptons plus neutrinos and for the ratio of the production cross section, one can solve for the ratio of the total width of the Z° and W. Using the measured total width $\Gamma(Z)$ for the Z° [4] one can extract the total width for the W [21]. This measurement is sensitive to whether the top quark is light enough to open the $t\bar{t}$ channel for the Z° or the $t\bar{b}$ for the W. The total width obtained for the W is too low to be consistent with an open channel for W decays to top.

The value of the W mass also depends on the mass of the top quark through radiative corrections. In general, the W mass becomes heavier as the top mass gets heavier [22]. Actually the problem is more complex because, as is typical in such calculations, the W mass depends not only on the top mass but also on the assumed mass of the Higgs boson.

The partial width of Z° into fermions also depends on the value of the top and Higgs masses, with very large corrections becoming more sensitive to the top mass for heavier fermions (like the b quark) [23].

Finally, the value of the Weinberg angle in weak interactions is also changed by radiative corrections which depend on the top mass [4], [24].

A somewhat more unusual example of a process with top quark dependence comes from the B_s decay to $\gamma\gamma$. The rate of this process changes by nearly a factor of two for top masses between M_W and 2 M_W (nevertheless, the branching ratio is quite small and difficult to measure [25]).

Thanks to the precise measurements of the Standard Model parameters performed at LEP, it has been possible to estimate the top mass. The uncertainty due to the arbitrary value of the Higgs mass has been included in the systematic error. Using only data from LEP, a top mass of 166^{+17+19}_{-19-22} GeV/c^2 has been derived [4]. Combining the measurements made at LEP with the measurements of M_W and M_W/M_Z from CDF [22] and UA2 [26], and the measurements of the ratio of neutral and charged currents from CDHS [27],

CHARM [28] and CCFR [29] a value for the top mass of 164^{+16+18}_{-17-21} [4] has been obtained.

1.3 Top production in hadronic collisions

At the Tevatron energy ($\sqrt{s} = 1.8$ TeV) the top quark is primarily produced through the mechanism of pair production $p\bar{p} \rightarrow t\bar{t}$, for a top mass $m_t \leq 200$ GeV/c^2 (for a top mass ≥ 200 GeV/c^2 W–gluon fusion with production of only one top quark is the dominant process). In the QCD parton model the process of hard scattering between two hadrons is the result of the interaction among quarks and gluons inside the hadrons. If in the quark or gluon scattering there is a large momentum transfer (where "large" is compared to the QCD energy scale Λ), the hadronic cross section can be expressed as a convolution of the parton distribution functions with the partonic cross section. This can be evaluated in perturbation theory in terms of the strong coupling constant α_s. The cross section for top pair production at a $p\bar{p}$ collider can be written as:

$$\sigma(s) = \sum_{i,j} \int dx_1 dx_2 f_i^A(x_1,\mu) f_j^B(x_2,\mu) \hat{\sigma}_{ij}(\hat{s}, M_{top}^2, \mu)$$

where $f_i(x_1,\mu)$ ($f_j(x_2,\mu)$) is the probability of finding a parton of species i (j) inside the proton (antiproton) carrying a fraction between x_1 (x_2) and $x_1 + dx_1$ ($x_2 + dx_2$) of the proton momentum. M_{top} is the top mass, $\sqrt{s}$ is the center of mass energy while $\hat{s} = s x_1 x_2$ is the square of the energy available in the partonic reaction center of mass. μ is a scale factor which defines the characteristic scale energy of the strong process.

At lowest order (α_s^2) the gluon–gluon fusion and the quark–antiquark annihilation contribute to the $t\bar{t}$ production:

$$g + g \rightarrow t + \bar{t}$$
$$q + \bar{q} \rightarrow t + \bar{t}$$

The Feynman diagrams for these processes are shown in figure 1.1.

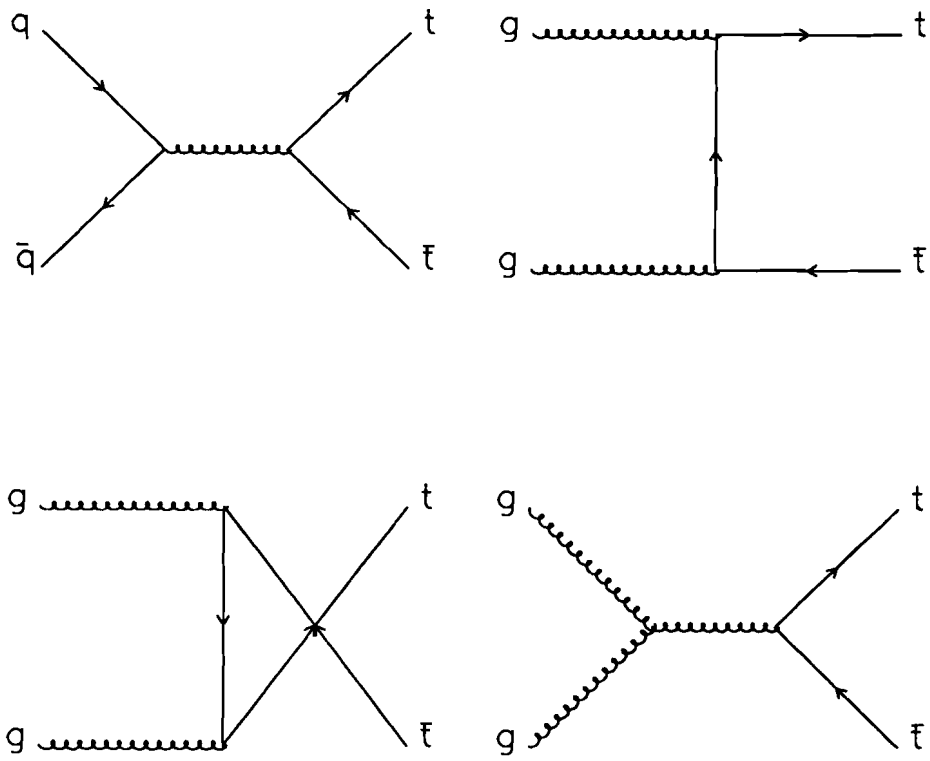

Figure 1.1: Lowest order Feynman diagrams for pair production of heavy quarks in $p\bar{p}$ collisions.

The corresponding partonic cross sections are:

$$\hat{\sigma}^{q\bar{q}\to t\bar{t}} = \frac{\pi\alpha_s^2\beta\rho}{27M^2}(2+\rho)$$

$$\hat{\sigma}^{gg\to t\bar{t}} = \frac{\pi\alpha_s^2\beta\rho}{192M^2}[\frac{1}{\beta}(\rho^2+16\rho+16)log\frac{1+\beta}{1-\beta} - 28 - 31\rho]$$

where $\rho = 4\ M^2/\hat{s}$ and $\beta = \sqrt{1-\rho}$. M is the top quark mass [30].

If the top mass is $> 100\ GeV/c^2$ the quark–antiquark annihilation dominates. Actually, on average the quarks inside the proton carry more momentum than the gluons, and large top masses require large x_1x_2 values.

The two top quarks are produced in opposite directions in the parton–parton center of mass system. In the plane transverse to the beam direction they are emitted in opposite

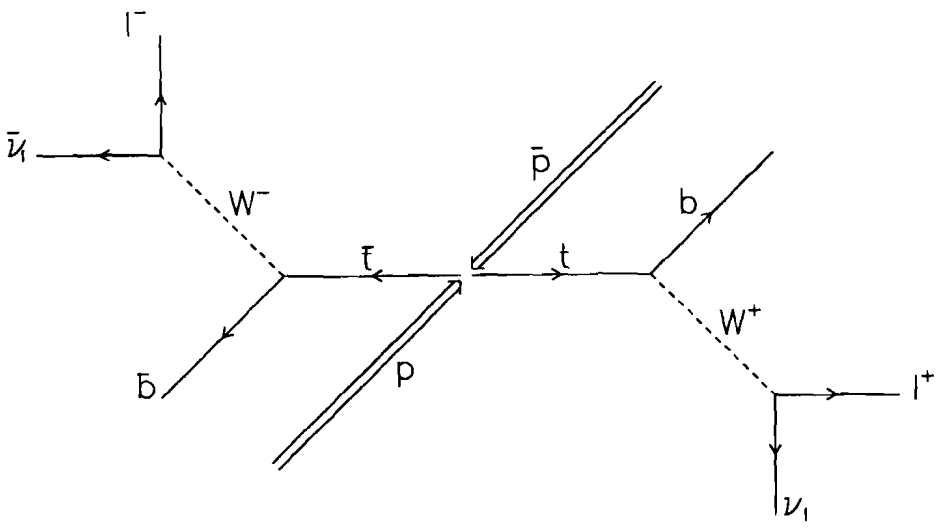

Figure 1.3: Illustration of top quark pair production and semileptonic decay.

The $t\bar{t}$ decay channels in which both W's decay hadronically present the highest branching ratio. In principle the two top quarks could be reconstructed because there are no neutrinos in the events. In practice this is very difficult. It is hard to separate these events from the multijet QCD background which has a much higher rate than top production [33].

The decay channels in which one W decays hadronically and the other one leptonically have a relatively large branching ratio (24/81 adding up the e and μ channels). In these channels also the background from direct W production in association with jets is relevant.

The branching ratio for the channels in which both W's decay leptonically is 2/81 for $e\mu$, $e\tau$, $\mu\tau$, and 1/81 for ee, $\mu\mu$, $\tau\tau$.

In spite of the small branching ratio, the dilepton channel offers a clean signal: the signature given by two high transverse momentum leptons is very difficult to obtain through other mechanisms. The most original part of this work is the inclusion of the $e\tau$ and $\mu\tau$ channels in the analysis. Till now the tau leptons had never been used for a top search.

1.5 Status of the top search (december 1993)

Although theory and some experimental observations make us to believe that indeed the top quark does exist, they give vague information about its mass. Precise knowledge of the top mass is important to make many tests of the Standard Model and to extract information about the Higgs boson mass. A first hypothesis on the top quark mass suggested the value 15 GeV/c^2, based on the comparison with the other quark masses: m_s(0.5 GeV/c^2), m_c(1.5 GeV/c^2), m_b(5 GeV/c^2). However, the lower experimental limit on the top mass has increased continuously, well beyond this naive estimate. The current lower limit on the top mass has been set by CDF at $m_t \geq 113$ GeV/c^2 [34], at 95% C.L. It is based on the analysis of data taken during the 1992–1993 run.

Concerning the top search done at e^+e^- machines, the AMY and VENUS experiments at TRISTAN put a lower limit at $m_t > 30.4$ GeV/c^2 [35]. Later on, the SLD experiment at SLAC and the experiments at LEP raised this limit to 40.7 and 46 GeV/c^2 respectively [36]. These studies are particularly interesting because they do not depend on the top decay mode. They are based on the hypothesis that the top electroweak coupling to the electron is the one predicted by the Standard Model.

At the CERN SpS Collider the UA1 and UA2 experiments put limits at 61 [37] and 69 GeV/c^2 [38] respectively. This search assumed the top quark to be lighter than the W: $m_t < m_W + m_b$. In this case, at the SpS energy top quark production would be dominated by the W decay: W $\rightarrow t\bar{b}$.

Direct searches for the top quark have been made in the past by CDF, analyzing the data sample corresponding to 4 pb^{-1}, taken during the 1988–1989 run. Two independent channels have been studied.

The analysis in the electron plus jets channel allowed the top quark to be excluded from the mass region: $40 < m_t < 77$ GeV/c^2 [39]. This analysis compared the shape of the transverse mass distribution of real W's with that of virtual W's coming from top decays ($m_W > m_t$). The data were in agreement with the absence of a top component.

This approach is not valid anymore if $m_t > m_W + m_b$, because the W from top decay becomes real.

The top quark search in the dilepton channels (ee, $e\mu$ and $\mu\mu$) provided a lower limit at 85 GeV/c^2. Combining this analysis with the result from the study of the lepton + jets + b channel, in which the b quark is identified through its semileptonic decay by looking for a low momentum muon in the event, a lower limit at 91 GeV/c^2 was extracted.

Chapter 2

Experimental Apparatus

2.1 The Tevatron Collider

The Tevatron Collider at Fermi National Laboratory is currently the world highest energy accelerator, colliding protons with antiprotons at a center of mass energy of $\sqrt{s} = 1.8$ TeV. The Tevatron shares the tunnel with the original Fermilab accelerator, called the "*Main Ring*", which reachs a maximum energy of 400 GeV. A schematic drawing of the Fermilab Collider is shown in figure 2.1.

Protons are accelerated in the Tevatron up to 900 GeV through several phases: first an electrostatic accelerator (*Cockcroft–Walton*) and a linear accelerator (*Linac*) accelerate the protons to an energy of 200 MeV. Then protons are focused and they are injected in a circular accelerator (*Booster*) where they reach 8 GeV. They are assembled in bunches and enter the *Main Ring*, where they are accelerated up to 150 GeV. Finally they enter the Tevatron, which is equipped with superconducting magnets. A 5.7 Tesla magnetic field allows the beam to reach energies of 900 GeV.

The *Main Ring* also provides primary protons at 120 GeV to the antiproton source. They collide with a tungsten target and produce antiprotons. The antiprotons are collected, focused through a lithium lens and the broad momentum spread is reduced by the stochastic cooling method. After that they enter the *Antiproton Debuncher–Accumulator* complex. There they are concentrated into dense bunches. After accumulation is com-

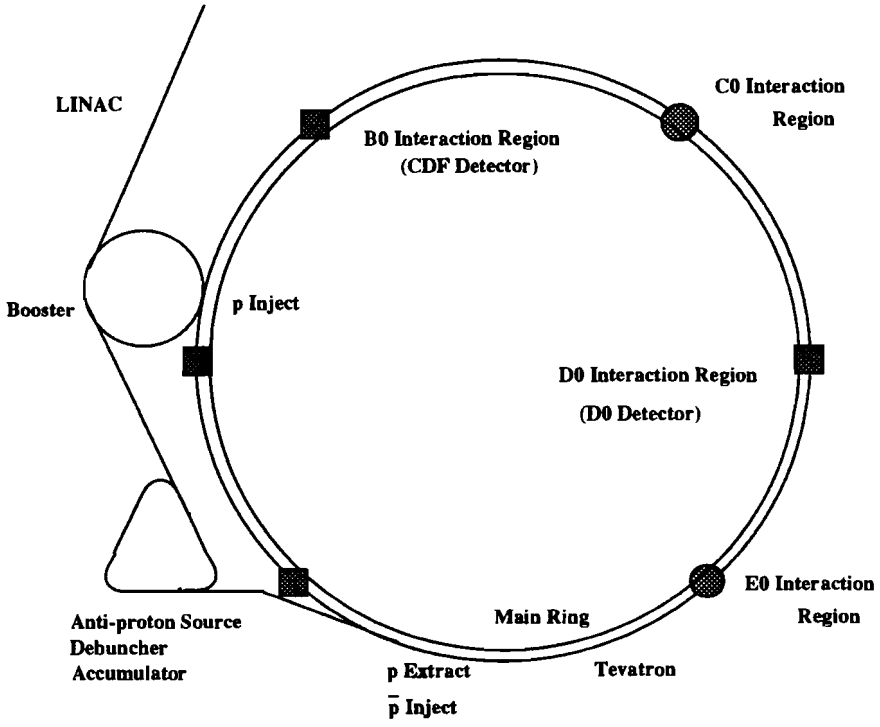

Figure 2.1: Schematic view of the Fermilab synchrotron.

pleted, the bunches of antiprotons are injected into the *Main Ring*, where they are accelerated up to 150 GeV. Finally, they are sent to the Tevatron, where they are accelerated together with the protons, in opposite directions, to 900 GeV.

There are six bunches of protons and six bunches of antiprotons. The proton bunches contain about 12×10^{10} particles, while the antiproton bunches contain about 4×10^{10} particles. The interval between two subsequent bunch–bunch collisions is ~ 3.5 μsec. The experiments CDF and D0 are located at two interaction points.

The most important parameter of an accelerator, besides the center of mass energy that it can reach, is the luminosity $\mathcal{L}$. The luminosity is defined by the following relation:

$$\mathrm{N} = \sigma \, \mathcal{L}$$

where N is the production rate for a given process and σ is the corresponding cross section. The luminosity is determined by the beam properties:

$$\mathcal{L} = \frac{N_p N_{\bar{p}} P f_0}{4\pi s^2}$$

where N_p and $N_{\bar{p}}$ are respectively the number of protons and antiprotons per bunch, f_0 is the revolution frequency (≈ 50 *kHz*), P is the number of bunches and s is the transverse beam size. During the 1992–1993 data taking the average luminosity was approximately 3×10^{30} cm^{-2} sec^{-1}. The highest instantaneous luminosity achieved was about 9×10^{30} cm^{-2} sec^{-1}.

2.2 The CDF detector

The *Collider Detector at Fermilab* (CDF) is a "4 π" (i.e. with almost complete angular coverage) general purpose detector designed to study $p\bar{p}$ interactions. Its characteristics allow the study of a wide range of physics processes. The basic goals of CDF are:

- to detect charged particles and measure their momentum;
- to measure the position and energy of electromagnetic as well as hadronic showers;
- to identify charged leptons;
- to observe indirectly non–interacting particles like neutrinos, by measuring the missing transverse energy.

In order to achieve this, the interaction region is surrounded by layers of different detector components. Particles encounter, in sequence, tracking detectors, sampling calorimeters and muon detectors. A flexible trigger system analyzes the events in a few microseconds and decides whether to record them or not. A schematic lateral view of the detector is shown in figure 2.2. A complete description of the detector in the 1989 configuration can be found in reference [41].

The CDF polar coordinate system has the origin in the center of the detector and the $+z$ axis along the beam line, in the direction of the proton beam. The azimuthal angle ϕ is defined with $\phi = 90°$ in the vertical upward direction. The polar angle θ is measured with respect to the beam direction and is defined with $\theta = 0$ along the $+z$

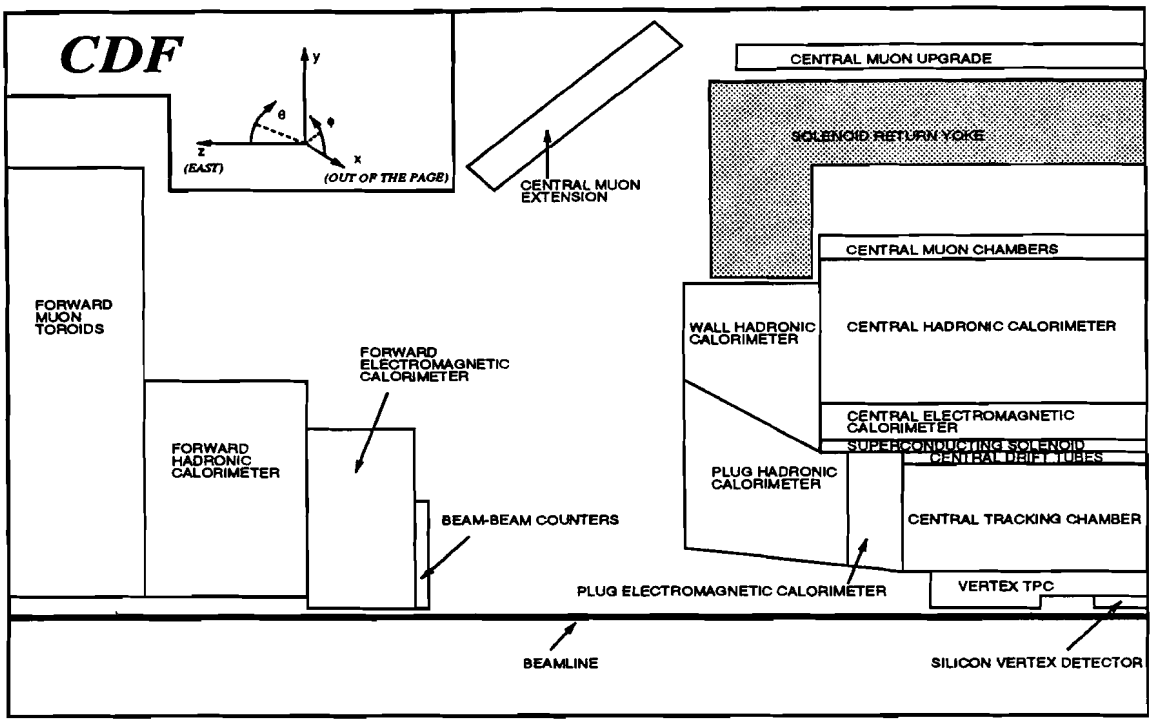

Figure 2.2: Schematic lateral view of a quarter of the CDF detector.

axis. The "natural" coordinate system for hadronic collisions is pseudorapidity η ($\eta = -ln\ tan\theta/2$), transverse momentum and azimuthal angle. For this reason an approximately cylindrically symmetric configuration of the detector has been chosen, with segmentation almost uniform in η and ϕ.

CDF is built in three major pieces: forward and backward spectrometers, covering the region from 2° to 10° in polar angle away from the beams, and a central detector measuring particles at larger angles from the beam. For the analysis described in this thesis we used essentially data taken with the central part of the detector. Therefore we will focus our attention on that.

2.2.1 The tracking system

The central tracking system is located inside the superconducting solenoidal coil. The solenoid provides a uniform magnetic field of about 1.4 Tesla, parallel to the beam axis. The magnetic field allows charge and transverse momentum measurement for charged

particles, by measuring the bent trajectories in the transverse plane.

The vertex detector SVX

The detector component closest to the interaction point is the silicon vertex detector (SVX) [42]. This detector was installed for the 1992–1993 run, as part of the upgrade of the original CDF tracking system. The inner and outer radii are approximately 3 and 7.9 cm. The $p\bar{p}$ interaction vertex is distributed along the beamline as a gaussian distribution with $\sigma \sim 30$ cm. Consequently a long vertex detector is required to have good acceptance. The SVX is 51 cm long and its acceptance covers about 60% of the interaction region. It consists of two independent cylindrical modules (*barrels*), left and right of the nominal beam–beam interaction point. The SVX contains 4 radial layers of silicon strip detectors with the strips parallel to the beam. It provides information in the $r - \phi$ plane, with a resolution of approximately 13 μm in each layer. One of the two barrels is shown in figure 2.3. The detectors are arranged in a 12–sided geometry. A section of $\Delta\phi = 30°$ is called *wedge*. In order to obtain a length of 25.5 cm along the beam direction, three silicon detectors of 8.5 cm each were electrically bonded together. A goup of three connected detectors is called a "*ladder*" and it is the basic subdivision of the device. The structure of one ladder is shown in figure 2.4. The total number of readout channels is 46080.

The VTX

The SVX is located inside the VTX (*Vertex Time Projection Chamber*) [43], which consists of 8 adjacent octogonal chambers. They track charged particles at angles greater than $\approx$ 3.5° from the beam line and cover about seven units in pseudorapidity ($|\eta| < 3.5$). The VTX has reconstruction capabilities in the $r - z$ plane and provides information on the event vertex (or vertices, in the case of events with multiple interactions in the same bunch crossing) with a precision of about 1 mm.

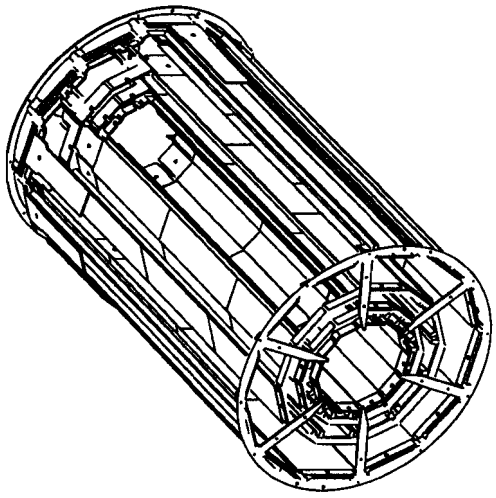

Figure 2.3: Perspective view of one of the two SVX barrels.

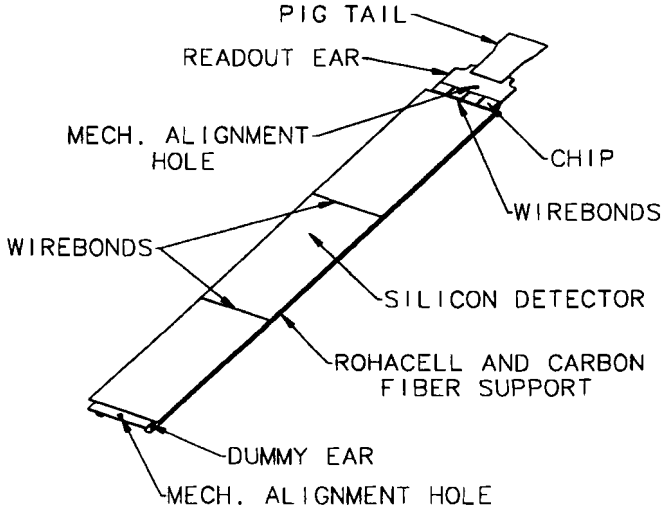

Figure 2.4: Schematic view of one SVX ladder.

The CTC

Outside of the VTX is the Central Tracking Chamber (CTC), a 3.2 m long cylindrical drift chamber with inner radius 0.3 and outer radius 1.3 m [44]. The CTC gives precise momentum measurements in the pseudorapidity region $|\eta| < 1.2$. It consists of 84 layers of anode wires, grouped in 9 *superlayers* . Five of these superlayers (axial) have 12 wires parallel to the beam, providing tracking information in the $r - \phi$ plane (perpendicular to the beam). The remaining four stereo superlayers contain 6 wires which are tilted by $\pm$ 3° alternatively with respect to the beam line. The stereo layers give track information in the $r - z$ plane.

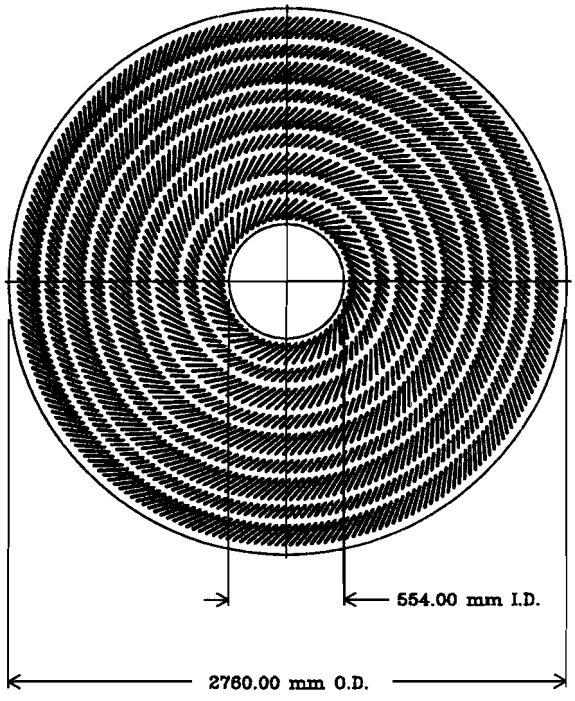

Figure 2.5: The layout of wires in the Central Tracking Chamber showing the grouping into 9 superlayers and the 45° rotation angle.

The wires are arranged in cells, which are tilted to form an angle of 45° relative to the radial direction, to compensate for the Lorentz angle of the electrons drifting in the magnetic field. Tilting allows cells in the same superlayer to overlap in the radial direction, so that every radial high P_T track at some point passes close to one sense wire in each

superlayer. This property is used to generate a prompt trigger signal for high P_T muon candidates. It also helps in the offline to resolve closely spaced tracks.

A charged particle passing through the CTC causes a chain of signals along its trajectory. The reconstruction code provides tracks, which are reconstructed in the $r - \phi$ and $r - z$ planes, by fitting arcs of helices to the hits detected in the chamber. If a charged particle has a transverse momentum smaller than 350 MeV, it spirals inside the CTC and it does not reach the calorimeter because of the magnetic field.

The design resolution on each wire is 200 μm. This results in a momentum measurement resolution of the "*stand-alone*" CTC equal to: $\frac{\sigma_{P_T}}{P_T} \sim 0.002 \times P_T$. When the SVX information is used to reconstruct the track the resolution becomes: $\frac{\sigma_{P_T}}{P_T} = [(0.0009 P_T)^2 + (0.0066)^2]^{1/2}$.

Before starting the last data run the 54 outer layers of the CTC were instrumented with the electronics needed to measure the particle energy ionization losses ($\frac{dE}{dx}$). This allows partial discrimination between electrons, charged pions and K mesons for momentum less than a few GeV/c.

The CDT tubes

On the outer perimeter of the CTC (and immediately inside the magnet coil) there are three layers of *Central Drift Tubes* (CDT) [45]. For particles produced in the central region ($|\eta| < 1.0$) each tube at a location in ϕ provides high accuracy $r - z$ tracking information, at a radius of 1.4 m from the beam line. Both drift time and charge division are measured, potentially providing a more accurate z measurement than the stereo layers of the CTC.

2.2.2 The central calorimeters

Outside of the magnetic coil there are the central electromagnetic (CEM) [47] and central hadronic (CHA) [48] calorimeters, which cover the angular region $30° < \theta < 150°$. They are sampling calorimeters. Layers of sampling material (plastic scintillator) are interleaved

with layers of absorber. The CEM uses lead as an absorber, while the CHA uses steel. The shower energy deposits are summed over the sampling layers of the two separated electromagnetic and hadronic sections. CEM and CHA are divided into two polar halves by the plane $z = 0$. Each polar half is organized into 24 azimuthal modules, called *wedges.* Each wedge contains a number of projective towers oriented towards the nominal interaction point. The segmentation in η and ϕ is $\Delta\eta \times \Delta\phi = 0.1 \times 15°$. Located at a depth of six radiation lengths into the CEM calorimeter, approximately at shower maximum for electromagnetic showers, there are central proportional chambers (CES) with strip and wire readout. They provide shower position measurements in both the $r - z$ and $r - \phi$ views. They help to distinguish γ and $\pi°$. The $\gamma/\pi°$ separation has been further improved by inserting wire proportional chambers before the last data taking period (CPR: *Central Preradiator*) [46] between the solenoid and the CEM. The CEM extends from 1.7 to 2.1 m in radial distance from the beam axis, providing a total of $\sim$ 18 radiation lengths. The single particle energy resolution is:

$$\frac{\sigma_E}{E} = \frac{0.14}{\sqrt{E_T}} \oplus 0.02.$$

The constant term is added in quadrature to the first term and takes into account the uncertainties in the single tower calibrations.

The central hadronic calorimeter surrounds the CEM. It extends from 2.1 and 3.5 m in radial distance from the beam axis, for a total of $\sim$ 5 absorption lengths. The single particle energy resolution is:

$$\frac{\sigma_E}{E} = \frac{0.50}{\sqrt{E_T}} \oplus 0.03.$$

Signal collection for the CHA is identical to that for the CEM: wavelength shifters absorb blue light from the scintillator and transmit light of longer wave length to light guides. These run radially out of the calorimeter to photomultiplier tubes on the two azimuthal sides of each tower.

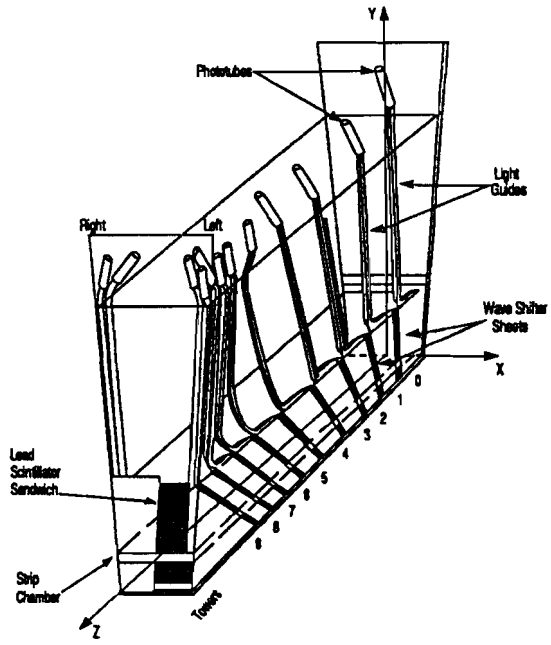

Figure 2.6: Perspective layout of a CEM module. The wavelength shifter plastic collects the light from the scintillator and shows the cell structure in η.

2.2.3 The muon chambers

The muon detectors are located just outside of the central hadron calorimeter, at a radial distance of about 3.5 m from the beam axis. The calorimeter acts as an absorber for the muons. Energetic muons ($P_T > 1.5$ GeV/c) can reach the chambers.

The central muon detector (CMU) consists in total of 48 modules [49]. Each module covers approximately 12.6° in ϕ, with a 1.2° gap on both sides of the wedge. The layout and dimensions of one module are shown in figure 2.7. The CMU covers 84% of the angular region between $56° < \theta < 124°$ (that means $|\eta| < 0.65$ in pseudorapidity). The loss of 16% in acceptance is due to the 2.4° gap between each wedge and the gap between the two calorimeter arches at $\theta = 90°$.

The muon chambers are proportional drift chambers. Each module consists of 4 layers in the radial direction, which are segmented in ϕ to form three towers of 4.2° each. Figure 2.8 shows the geometry of one of these towers, consisting of 16 rectangular drift cells.

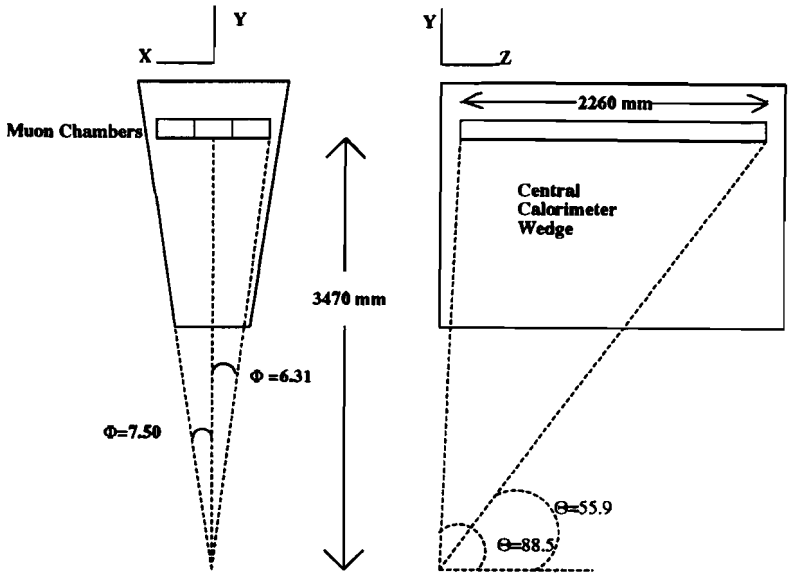

Figure 2.7: Geomety of the central muon chambers in one of the central wedges.

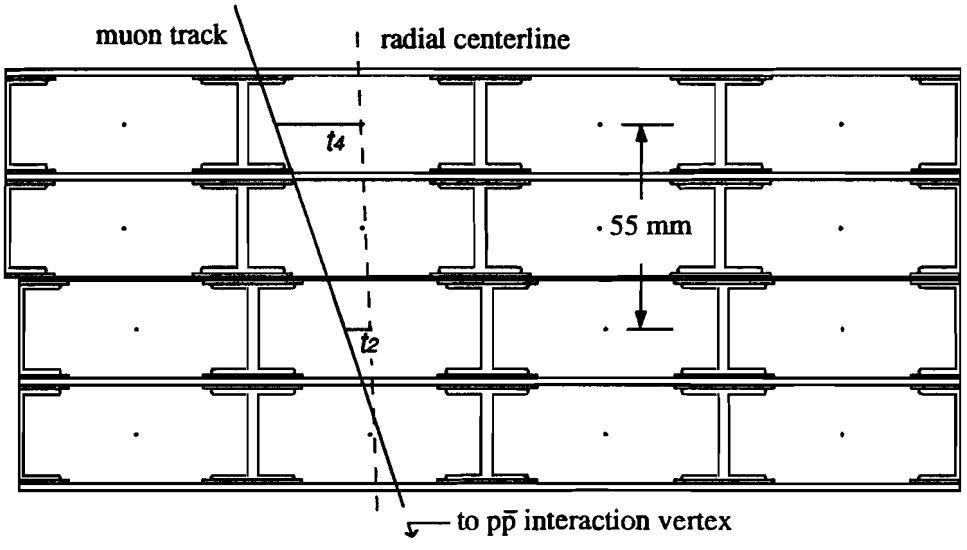

Figure 2.8: The arrangement of the four planes of central muon chambers in a view along the beam direction. A possible traversing particle and the associated drift times are also shown.

Four sense wires, one from each layer, form a muon tower. One pair of these four wires, from alternating layers, lies on a radial line which passes through the interaction point. To avoid left–right ambiguity, the remaining two wires of a tower lie on a line which is offset from the radial one by 2 mm at the midpoint of the chamber. Using the drift time information, the chambers measure 4 points on a particle trajectory with a precison of 250 μm. If there is a signal in at least three of the four chamber layers a segment called a "*stub*" is reconstructed. If this segment corresponds to a track reconstructed in the CTC, then the track is labelled as a muon candidate.

The track angle with respect to the sense wires can be measured by comparing the arrival times of hits from alternating layers. The track angle is related to the transverse momentum of the particle, since the solenoidal B field deflects the track away from the radial line by an amount:

$$\alpha \approx \frac{eL^2B}{2DP_T}$$

where L = 1.44 m is the radius of the solenoidal field, B is the field magnitude and D = 3.47 m is the radial distance from the beam line to the muon chambers. The information on the momentum derived from the α angle is also used in the trigger (see following paragraph). The multiple scattering the particle undergoes modifies the effective α value, so that the correspondance with the actual P_T of the particle is only approximate.

CMU tracks are reconstructed independently in the $r - \phi$ plane, using TDC information, and in the $r - z$ plane, by the use of charge division information: the position of a particle along the sense wire is found by measuring the charge deposited at each end of the wire.

With respect to the 1988–1989 data taking the CDF muon detection system has been improved and extended [43]. A set of drift chambers (CMP) [50] which cover roughly the same range in η as the CMU has been placed at larger radius behind additional steel shielding (60 cm) which doubles the number of interaction lengths and so decreases the background from hadrons which cross the calorimeter without interacting.

Moreover new drift chambers (CMX) [51] have been added in the pseudorapidity region $0.6 < |\eta| < 1.0$ together with two layers of scintillators used for the trigger (CSX), in order to increase the muon coverage to $|\eta| = 1.0$.

2.2.4 The trigger

The interaction rate at the Tevatron is about 130 kHz with an average luminosity of 3×10^{30} $cm^{-2}sec^{-1}$. The rate at which data can be logged to tape is only few Hz, thus the trigger has to provide the proper reduction factor. In principle, this is acceptable since the rate of interesting events is only a very small fraction of the total rate. However, the trigger must be able, in a very short time, to reject the majority of the events while accepting interesting events with a high efficiency. It also must be versatile enough to be changed during the run, depending on the results of the experiment.

The CDF trigger for the 1992–1993 data taking was organized into three different levels [52]. Each level is a logical OR of a number of triggers designed to select events with electrons, muons, jets or other interesting parameters.

The lowest level trigger uses fast information from the central detectors for muon triggers and fast information from the calorimeters for electron and jet triggers. The calorimeter segmentation which is used for the trigger towers is $\Delta\eta = 0.2 \times \Delta\phi = 15^{\circ}$ for both the electromagnetic and the hadronic section. The central electron trigger requires an energy deposit in the CEM with $E_T > 6$ GeV. The central muon trigger [53] requires a track segment in the CMU with $P_T > 6$ GeV/c in coincidence with hits in the CMP, or a track segment in the CMX with $P_T > 10$ GeV/c in coincidence with hits in the scintillators placed on both sides of the chambers. The CMX inclusive muon trigger was fully functional for 30% of the data taking. In order to preserve the efficiency for CMX muons from top decays, CMX muon candidates were accepted even when they passed the level 1 single tower calorimeter trigger. This trigger was present for 83% of the collected data.

The second level trigger uses calorimeter and CTC information, with greater sophis-

tication. A list of calorimeter energy deposits (*clusters*) is provided. For each cluster the transverse energy E_T, the average ϕ and the average η are determined. This information is combined with a list of bidimensional tracks (in the $r - \phi$ plane) provided by a hardware track processor of the CTC tracks called CFT ("*Central Fast Tracker*") [54]. The CFT gives information on CTC high momentum tracks ($P_T > 2.5$ GeV/c) in 2.5 μs. The momentum resolution is $\frac{\sigma_{P_T}}{P_T} \sim 0.0035 \times P_T$ and the efficiency is 93.5 $\pm$ 0.3 % for isolated tracks with $P_T > 10$ GeV/c. In addition, muon track segment information is available in the second level trigger from CMU, CMP and CMX. CFT tracks can be matched to an electromagnetic cluster to form electron candidates, or they can be matched to muon track segments to form muon candidates. The electron level 2 trigger requires a CEM energy cluster with $E_T > 9$ GeV, associated with a CTC track with $P_T > 9.2$ GeV/c. The ratio of hadronic to electromagnetic energy in the cluster is required to be less than 12.5%. The muon level 2 trigger requires a match between CFT tracks in the $r - \phi$ plane with $P_T > 9.2$ GeV/c and a track segment in the muon chambers.

The level 3 trigger is a software trigger running on commercial processors (*Silicon Graphics multi-cpu Power Servers*), which combined can process one billion instructions per second. The processors use a Fortran code which reconstructs events, with particular attention to the three dimensional tracking in the CTC. This level reduces the output rate of the events which are stored on magnetic tape to about 5 Hz. For central electrons the level 3 algorithm requires the reconstructed cluster energy to be $E_T > 18$ GeV, and the presence of a reconstructed track with $P_T > 13$ GeV/c pointing to the cluster. The central electron trigger efficiency is 92.8 $\pm$ 0.2 % for electrons with $20 < E_T < 150$ GeV. The level 3 muon trigger requires a match better than 10 cm in $r \times \phi$ between the extrapolation of the CTC track with $P_T > 18$ GeV/c and the track segment in the muon chambers. In addition, the energy deposited in the hadronic tower traversed by the muon must be less than 6 GeV. The CMU and CMX muon trigger efficiency is 87 $\pm$ 2% e 54 $\pm$ 5% respectively, for muons with $P_T > 20$ GeV/c.

Chapter 3

Analysis Strategy

3.1 The channel with two high P_T leptons in the final state

Events from the process $t\bar{t} \rightarrow W^+bW^-\bar{b}$ in which both W's decay leptonically are characterized by two high transverse momentum isolated leptons, two neutrinos and two jets from b quark hadronization. The background to this signal comes from $b\bar{b}$, WW, WZ and $Z^\circ \rightarrow \tau\tau$ production. A proper choice of the event selection criteria allows reduction of the background maintaining a good efficiency for $t\bar{t}$ events. Requiring large lepton P_T's reduces the background from $b\bar{b}$ and $c\bar{c}$ quark pair production, where the leptons have in average lower momentum. Further discrimination from lighter quark decay processes is provided by the lepton isolation request.

The analysis described in this thesis is tuned to a heavy top quark search ($\geq$ 140 GeV/c^2). For a large top mass the background from WW production is comparable, from the point of view of the production cross section, to the $t\bar{t}$ signal ($\sigma_{t\bar{t}}(m_{top}$=160 GeV/$c^2$) = 8.2 pb [32], σ_{WW} = 9.5 pb [55]). The WW events are also characterized by two high P_T isolated charged leptons and two neutrinos. However, at the lowest order there are no hadronic jets.

3.2 The jet requirement in top candidate events

The only way to reduce the background from WW and WZ boson pairs production is by requiring jets in the events [56]. This cut strongly reduces also the background from $Z^\circ \rightarrow \tau\tau$. Moreover it reduces the background contamination from misidentified leptons. The efficiency of the jet requirement to accept top events depends on the b quark jet energy. The b jet energy depends on the top mass and increases with it.

We studied from Montecarlo the jet E_T distributions in top events, for various top masses [1]. We used the Isajet Montecarlo program to produce $t\bar{t}$ events [57]. This Montecarlo simulates strong, electromagnetic and weak processes in $p\bar{p}$ interactions. Isajet has been used during this analysis to produce samples for several processes ($t\bar{t}$, WW, WZ, Z°). It uses the Eichten structure functions [58]. The cross section is obtained from $2 \rightarrow 2$ matrix elements, and it does not include higher order terms. Higher order processes are accounted for by adjusting phenomenological parameters, as well as the parton fragmentation to hadrons. From the Montecarlo one obtains a list of the produced particles and their four-momenta. At this point a CDF detector simulation (called "QFL") is applied, which outputs events to be analyzed exactly as the experiment real data.

We used the Isajet standard version (except when stated otherwise), which includes gluon radiation in both the initial and final states.

The E_T distributions of the first and second leading jet are shown in figure 3.1, for a top mass of $M_{top} = 170$ GeV/c^2 (solid line) and of 140 GeV/c^2 (broken line). From these studies we have determined that the efficiency of the jet requirements which we will use (see Chapter IV) varies from about 30% for a top mass of 100 GeV/c^2 to over 85% for a top mass of 180 GeV/c^2.

[1] This Montecarlo studies were made in collaboration with Marina Cobal and Hans Grassmann.

3.3 Isolation

In order to gain back some of the efficiency lost with the jet requirement, we used very loose identification criteria for one of the two charged high momentum leptons. Contextually we could extend the search to the $e\tau$ and $\mu\tau$ channels. We tried to unify as much as possible the lepton identification criteria, for them being e, μ, or τ. Because of the large top quark mass, the decay products tend to be distributed over a wide solid angle. Therefore the leptons from top decay are usually well separated from the b quark jet and from the decay products of the other top. The maximum transverse momentum which a lepton from Q quark decay can have with respect to the other decay particles is $M_Q/2$ [59]. In b quark decay this is about 2.5 GeV/c. Therefore leptons from b decays will be close in angle to the semileptonic decay hadrons. Exploiting this difference among the b quark and heavier quarks, it is possible to distinguish between the two processes studying the energy deposited in a cone centered on the lepton. This property is referred to as the lepton "isolation". Obviously this separation is statistical. In top decay an incidental energy deposition close to the lepton can be due to the gluon radiation in the initial and final states or from the spectator partons of the $p\bar{p}$ interaction (*underlying event*).

We expect all the leptons from W decays to behave similarly, from the point of view of isolation. Therefore we started requiring a high P_T track isolated in the CTC. Next the track was classified as electron, muon or tau candidate based on the calorimeter energy deposition (see chapter IV). In figure 3.2 we show the P_T track distribution for electron and muon candidate tracks; in figure 3.3 the same distribution is shown for tau candidate tracks (Montecarlo Isajet, $M_{top} = 170$ GeV/c^2).

3.4 The large missing E_T requirement

Requiring a large missing transverse energy in the event (as expected if there are one or more energetic neutrinos) helps to reduce several sources of background:

- $b\bar{b}$ and $c\bar{c}$, where in general the missing energy is smaller than in $t\bar{t}$;

- ee, $\mu\mu$ Drell–Yan pair production, where there are no neutrinos; $\tau\tau$ pair production where neutrinos are less energetic than in $t\bar{t}$;

- background due to hadrons misidentified as leptons.

The missing energy distribution in top events with two leptons in the final state is shown in figure 3.4 (Montecarlo Isajet). The solid line corresponds to a top mass of M_{top} = 170 GeV/c^2, the dashed line to a top mass M_{top} = 140 GeV/c^2.

3.5 The ee and $\mu\mu$ channels

From the point of view of the branching ratio, the sum of the ee and $\mu\mu$ channels is equal to the $e\mu$ channel. However, the Drell–Yan mechanism represents a considerable additional background to the ee and $\mu\mu$ channels, since it has a cross section much larger than the top cross section. In Drell–Yan processes a quark–antiquark pair annihilates to give either a virtual photon or a Z° which decays to an unlike sign lepton pair. Requiring jets and missing energy in the event helps to reduce this background. Since the Drell–Yan cross section has a resonance at the Z° mass, most of this background can be removed by cutting away the Z° region ($75 < M(\ell^+\ell^-) < 105$ GeV/c^2). However, this cut can fail when the Z° is misreconstructed. There are of the order of 50 Z° + 2 jet events in the 21 pb^{-1} data sample. For a heavy top the expected number of events is very small.Therefore in order to quantify the background due to misreconstructed Z°'s one must understand the instrumental problems to a level of 1%. Relying on a channel with this kind of problems (difficult to quantify) to identify a top signal would be dangerous and was not attempted in this thesis.

3.6 The $e\mu$ channel

The $e\mu$ channel provides the final state with the lowest background. There is no W + jets background, as in the single lepton channel, and there is no Drell–Yan background

as in the ee, $\mu\mu$ channel. The background from WW and WZ pair production can be considerably reduced by requiring jets. $b\bar{b}$ production gives origin to non–isolated leptons which in average have lower P_T than leptons from $t\bar{t}$. However, since our identification criteria for one of the leptons are very loose, significant background could come from hadrons wrongly identified as leptons. The study of this background will be presented in Chapter V.

3.7 The $e\tau$ and $\mu\tau$ channels

In order to observe a top signal, it is reasonable to use all channels which can give valuable information. The $e\tau$ and $\mu\tau$ channels have been included for the first time in this kind of analysis [60]. Considering just the branching ratio, these two channels would increase the efficiency of the standard dilepton search by a factor of two, assuming the same detection efficiency for all leptons. As a matter of fact, the efficiency for taus must be lower, because of the ν_τ which carries out some momentum in the tau decay (compare the electron–muon and tau P_T distributions in figures 3.2 and 3.3). The loss in efficiency depends on the top mass. On the other hand, a small fraction of events in which the tau decays to electron or muon will enter the ee, $e\mu$ or $\mu\mu$ samples. It is not possible to distinguish these events from direct W decays to electron or muon. A true additional efficiency can be contributed if the hadronic decay channels of the tau are exploited.

We studied only the following hadronic tau decay channel:

$$\tau \rightarrow 1 \text{ charged hadron} + 1 \text{ or more neutral particles.}$$

This channel represents 50% of the tau total decays. The tau shows up as a single track in the tracking chamber, similarly to what happens for its decay to electron or muon. The track is a "jet" in as much as it corresponds to a localized energy deposition in the calorimeter. The tau jet is characterized by its narrowness and a relatively large fraction of hadronic energy. The identification of the tau signature in hadron collisions is not easy. The signal is the product of a double sequential decay (the W to tau first, the tau to

hadron next). The kinematics of the final prong is more diluted than in direct W decay to electron or muon.

However, the collimated jets from energetic isolated tau decays appear usually very different from the QCD jets, which typically are wider and have higher multiplicity. Because of fluctuations in the fragmentation process or of measurement errors, we still expect the background from hadrons misidentified as tau–leptons to be larger than for the other leptons.

CDF already showed its capability to identify taus in the analysis which studied $W \rightarrow \tau\nu_\tau$ and verified the lepton universality hypothesis in W decays [61]. However, if we compare the $W \rightarrow e\nu, \mu\nu$ sample in reference [62] with the number of candidates selected in the $W \rightarrow \tau\nu$ channel in reference [61] (which is about ten times smaller) we can understand that using this channel is more problematic. In Chapters IV and V we will see how the tau definition we used still allows the suppression of the QCD background.

By including the tau lepton in the top search we not only increase the analysis efficiency, but we can also verify the Standard Model prediction. An abnormal high P_T tau production can be a possible indication of new physics. For instance, in an extension of the Minimal Standard Model, the top could decay to charged Higgs bosons (if they exist and have a mass smaller than the top mass) [59]. The decay $t \rightarrow H^+ b$ could reduce the rate of the standard $t \rightarrow W\ b$ decay and thus provide an indirect signature. The direct way to identify this possible charged Higgs boson is through its tau decay, since its couplings are proportional to the parton masses.

3.8 Event structure study

We briefly describe here a method that we are planning to use in the near future as an extension of the present analysis of $t\bar{t} \rightarrow \ell\ell$ candidates. An interesting application of it is illustrated in paragraph 3.9. In spite of the low statistics of the present data sample (see Chapter VI), this method provided already interesting results and it promises

improvements in the signal–background separation.

Many jets from QCD production come from initial state gluon radiation or from scattering of initial state particles. Those jets will mostly be emitted in the forward direction, close to the beam. This behaviour has indeed been observed for various types of QCD processes. In contrast, the decay products of centrally produced heavy particles are expected to be less correlated to the beam direction. It has been shown that the correlation between the jet emission direction and the beam direction can be used to distinguish between top production events and QCD background. In particular this study has been applied to the top decay channel with one charged lepton in the final state. In general, this is an effect of kinematic origin that can be used to distinguish QCD–dominated background processes from decays of heavy particles of any kind [63], [64], [65].

In the top decay channel we are interested in, the requirement for the jets to be central discriminates against WW + jets, Z° and Drell–Yan + jet events. It also helps to reduce the background due to misidentified leptons, which is mostly due to multijet events.

We studied the pseudorapidity ($\eta = -\ln\tan\theta/2$, θ is the production angle in the laboratory frame) of the jets produced in top decays. This variable is convenient to give a measurement of the "centrality" of a production process.

The pseudorapidity distribution of the two leading jets in top Montecarlo events in which both W's decay leptonically, for two different top masses, is shown in figure 3.5 (Isajet, M_{top} = 170 GeV/c^2 and 140 GeV/c^2).

Requiring for instance that the two jets in top decay are both at $|\eta| < 2.0$ the efficiency loss is very small ($\sim$ 5 %).

A different variable which one could use is $cos\theta^*$(jet), where θ^* is the angle between the jet and the proton beam in the event center of mass system. This variable showed itself to be very powerful in the study of the single lepton top decay channel [63], [66].

However, since the top decay channel which we studied in this thesis contains two energetic neutrinos, the center of mass frame is not well measured. Using the $cos\theta^*$ variable could therefore be problematic.

Since Isajet reproduces the gluon radiation based on a phenomenological model, we used a W + 2 jets sample of real data to show the jet pseudorapidity distribution. This distribution is shown in figure 3.6, with many more jets emitted at small angles (large $|\eta|$). One can observe a difference from what expected for top (figure 3.5).

3.9 Application of the event structure analysis to the 88–89 top candidate event

The study of the event characteristics has been useful already to investigate the nature of the top candidate event found by CDF during the 1988–1989 data taking [40]. This event was selected requiring a high P_T electron and muon. In addition to these high P_T leptons, the event also contains two jets, one central and one relatively forward. There is also a low P_T muon candidate near to the smaller jet in the forward direction. The event characteristics are summarized in table 3.1. The values have been obtained from reference [67].

Run=19250 Event=20435	Charge	E_T (GeV/c)	ϕ (deg)	η
Electron	+	31.7	132	-0.81
Central muon	-	42.5	269	-0.80
Forward muon	+	8.0	97	-1.96
Jet 1		19.7	341	1.07
Jet 2		8.9	85	-2.76

Table 3.1: Characteristics of the top candidate event from the 88–89 run.

The presence of a third lepton is not typical of the main background processes expected for this event. On the other hand, a muon in the forward region is not likely in top decay events, where muons from b decays tend to be produced in the central region. The CDF analysis compared the number of dilepton events expected from top production to one observed electron + muon event. For the purpose of obtaining a limit that event was assumed to be a top event. No other statement was made on its nature [40]. Nevertheless some authors outside the CDF collaboration tried to reconstruct the event as production

and decay of a $t\bar{t}$ pair. In the study described in reference [67] the event turned out to be compatible with being from a top decay, where the forward jet and the nearby muon are from the $\bar{b}$ and the central jet is from the b. Based on these assumptions the authors find that production and decay of a top with a mass of about 125 GeV/c^2 would explain the overall event parameters best.

We studied the available information to see whether the above interpretation of this event is likely, and to verify the consistency of the kinematical parameters with the $t\bar{t}$ hypothesis. We considered the variables displaied in figures 3.5 and 3.6 (jet pseudorapidity) without trying to reconstruct the event [68].

We used the Isajet Montecarlo program for the simulation of top production and decay at parton level. In figure 3.7 we show the pseudorapidity distribution of b and $\bar{b}$ quarks from top decay for $M_{top} = 130$ GeV/c^2. In order to avoid a bias from detector geometry a cut $|\eta|$(high–P_T lepton) < 1.0 has been applied, as it is also done in the experiment. Also shown in figure 3.7 is the position of the two beauty candidates observed in the CDF electron + muon top candidate event, based on the kinermatical values given in [67]. The forward jet and the forward muon have been combined to reconstruct the rapidity of the original $\bar{b}$ ($|\eta(\mu + jet)| = 2.47$). We ignore the neutrino from the $\bar{b}$ candidate since the invariant mass of the jet and the muon is already quite high (~ 7 GeV/c^2) relatively to the b mass. Therefore the possible neutrino should either have little energy or be close to the muon–jet system. The forward jet and forward muon together have a P_T of 16.8 GeV/c.

In table 3.2 we show the fraction of Isajet top events which have at least one b or $\bar{b}$ at $|\eta(b, \bar{b})| > 2.47$, for different cuts on $P_T(b, \bar{b})$ and two different top masses. The probability of finding a beauty from top decay at such a large rapidity is of the order of 1%.

The pseudorapidity of the b is determined by its emission angle in the rest system of the reaction, but also by the longitudinal boost of the system, due to the energy difference between the primary partons in the hard scattering. A variable which is less sensitive to the boost is the rapidity difference between the two jets. From a kinematical point of

M_{top} : P_T min.	130 GeV/c^2 Prob.	stat. error.	100 GeV/c^2 Prob.	stat. error
5 GeV/c	2.5%	0.5%	5.%	2.%
10 GeV/c	1.5%	0.4%	0.5%	0.5%
15 GeV/c	0.4%	0.3%	0.%	<0.2%

Table 3.2: Probability of a top event to have at least one beauty at $|\eta|>2.47$ for different cuts on $P_T(b)$ and $P_T(\bar{b})$ and for two different top masses, with Montecarlo statistical error (M_{top} = 130 GeV/c^2).

view, this variable provides an independent information from the previous one (however, one must observe that error measurements could strongly correlate the two quantities). The value of the η difference of the two jets in the data event is 3.54. We found that the probability for the two b's in top events to be at this large distance from each other is about 0.5%, according to Isajet. In figure 3.8 we show the distribution of the η difference versus the maximum of $|\eta(b)|$, $|\eta(\bar{b})|$. This presentation summarizes the global available information.

Based on these observations we find that the interpretation of the jets in the $e\mu$ top candidate event from the 1988–89 data as being due to b quark decays has a probability of less than 1%.

The numbers we showed have been obtained at parton level, without any detector simulation. Detector related effects could modify the results. It is however hard to imagine how these effects could bring to an interpretation very different from what said above.

In order to examine carefully this point, the study has been repeated after applying the CDF detector simulation (QFL) to the events produced by Isajet. First we used the Isajet version without gluon radiation, in order to be sure that the jets we find can be only from b quarks or from some fluctuation of the underlying event. The result was similar to that obtained at parton level.

Finally, we investigated whether the $e\mu$ event could be top, allowing the low E_T forward

jet to come from gluon radiation. In order to do that, we used the standard Isajet version which produces gluon radiation. The jet configuration observed in the data event becomes only slightly more likely (of the order of 2%).

The study presented in this paragraph was the first top dilepton analysis which made use of the jet information in a quantitative way [68]. The result, namely that the probability for this event to be top can be quantified by this method, encouraged us to develop an improved dilepton + jets analysis to apply to the 1992–1993 data sample.

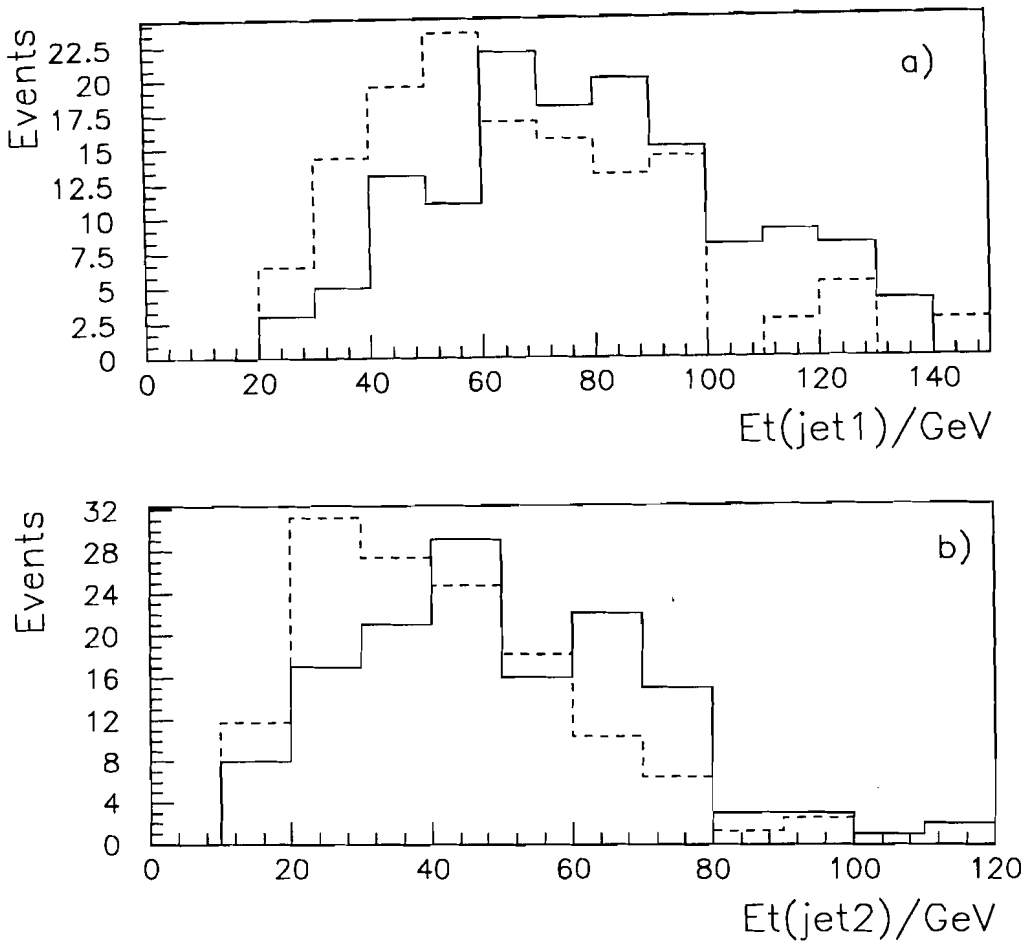

Figure 3.1: E_T distribution of the first (a) and the second leading jet (b) in top event (Isajet + QFL) where both W's decay leptonically. The solid line corresponds to M_{top} = 170 GeV/c^2, while the dashed line to M_{top} = 140 GeV/c^2. The two histograms have been normalized to the same number of events.

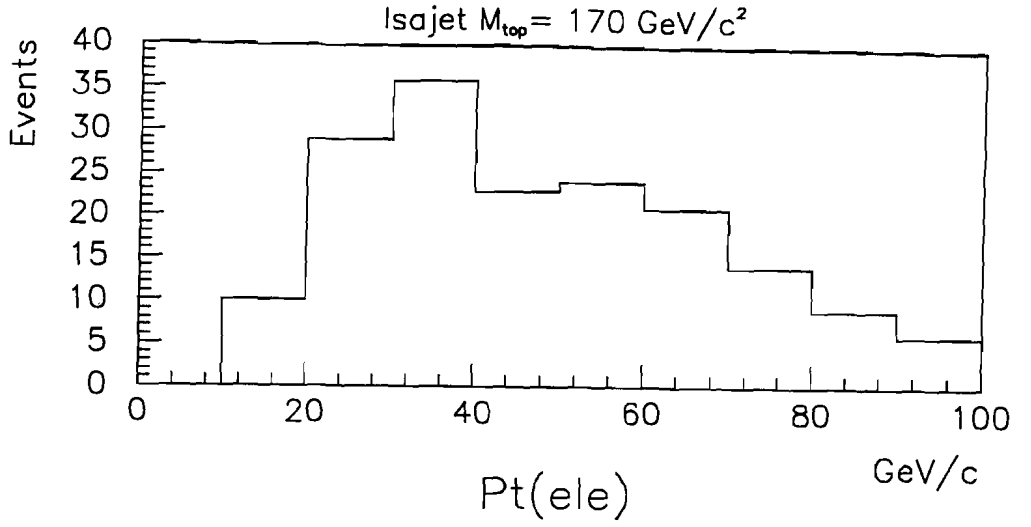

Figure 3.2: P_T distribution of electron and muon candidate tracks in top events (Isajet + QFL, M_{top} = 170 GeV/c^2).

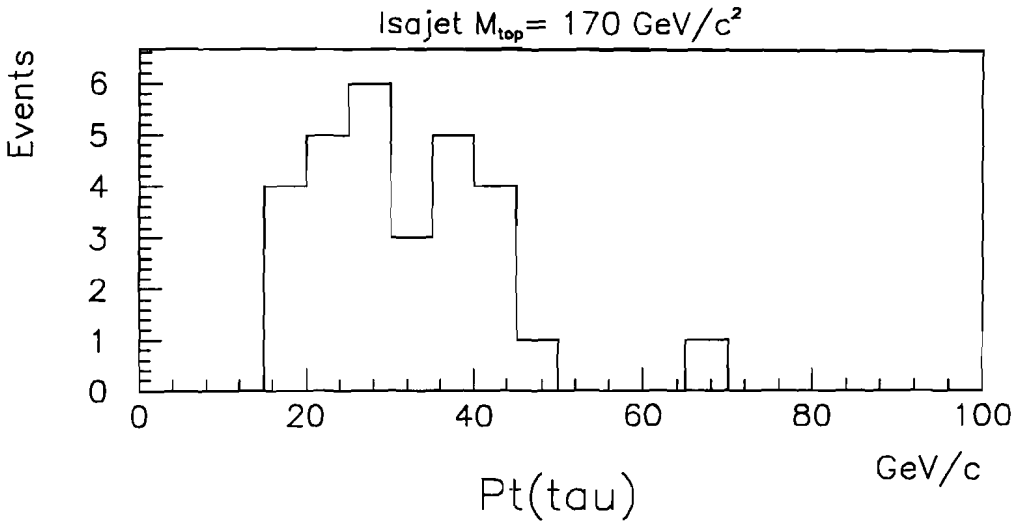

Figure 3.3: P_T distribution of tau candidate tracks in top events (Isajet + QFL, M_{top} = 170 GeV/c^2).

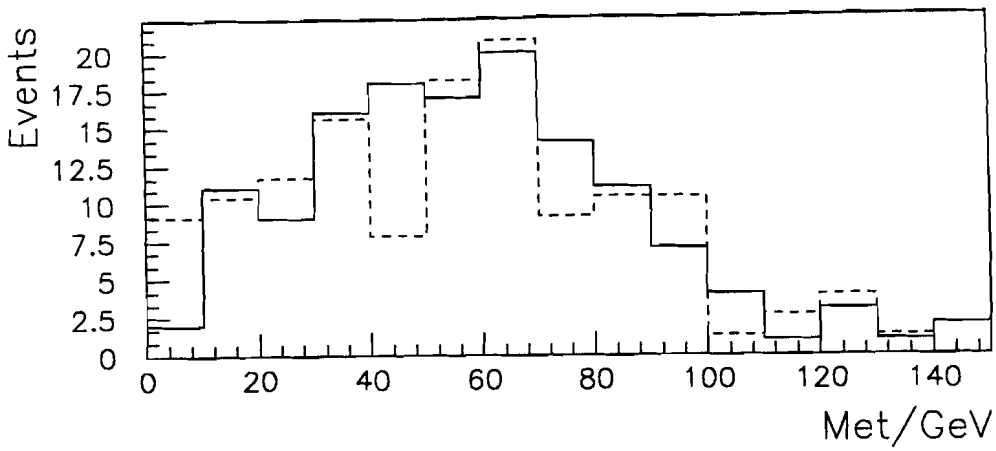

Figure 3.4: Missing E_T distribution in top events (Isajet + QFL) in which both W's decay leptonically. The solid line corresponds to M_{top} = 170 GeV/c^2 while the dashed line to M_{top} = 140 GeV/c^2.

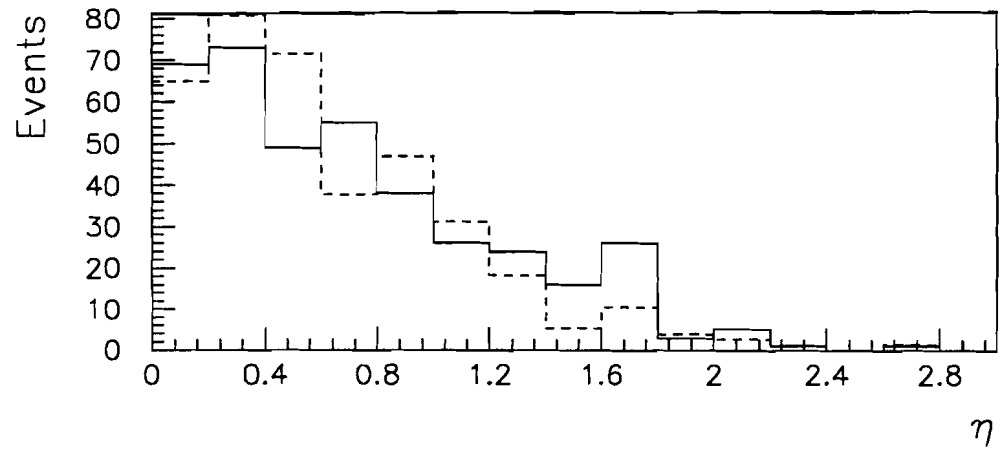

Figure 3.5: Pseudorapidity $|\eta|$ of the two leading jets in top events (Isajet + QFL) where both W's decay leptonically. The solid line corresponds to M_{top} = 170 GeV/c^2 while the dashed line to M_{top} = 140 GeV/c^2.

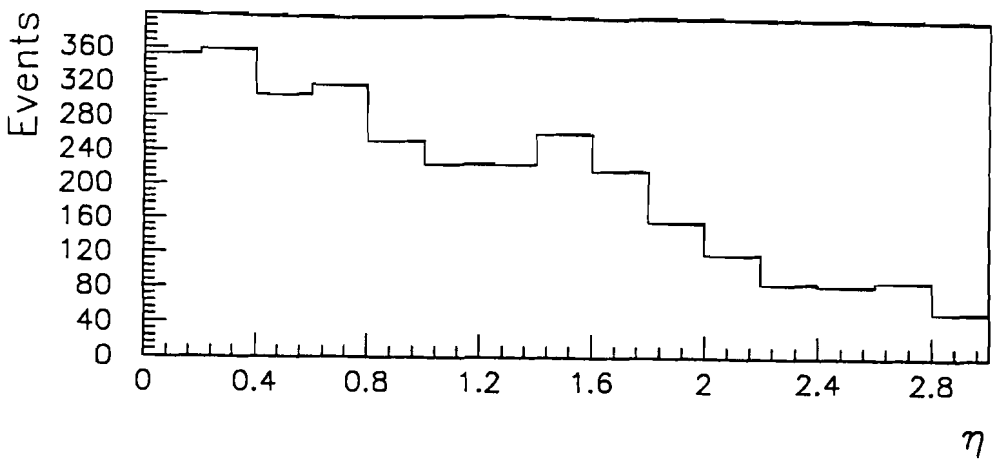

Figure 3.6: Pseudorapidity $|\eta|$ of the two jets in W + 2 jet data events.

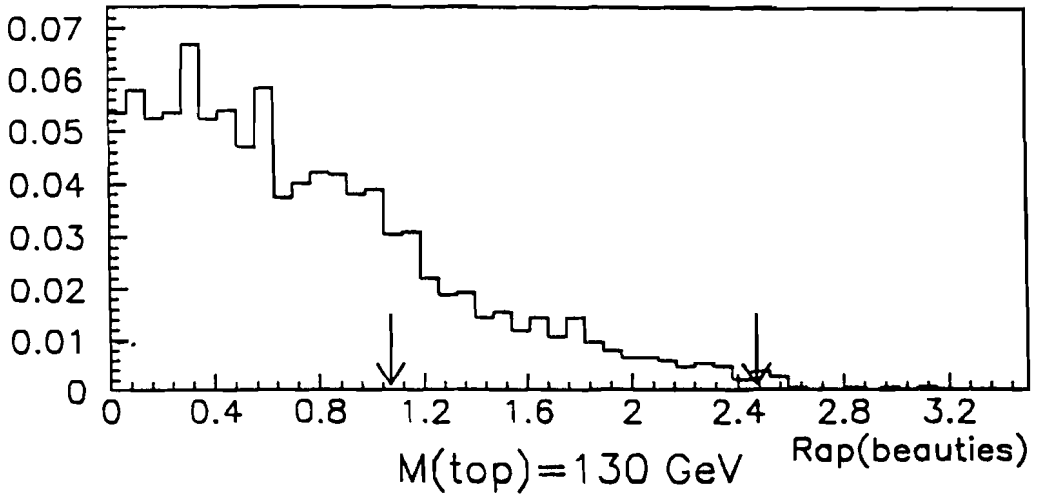

Figure 3.7: Pseudorapidity $|\eta|$ of b quarks from top decay at parton level, Montecarlo Isajet (M_{top} = 130 GeV/c^2). The arrows indicate the position of the b candidates in the $e\mu$ event found by CDF in the 88-89 data.

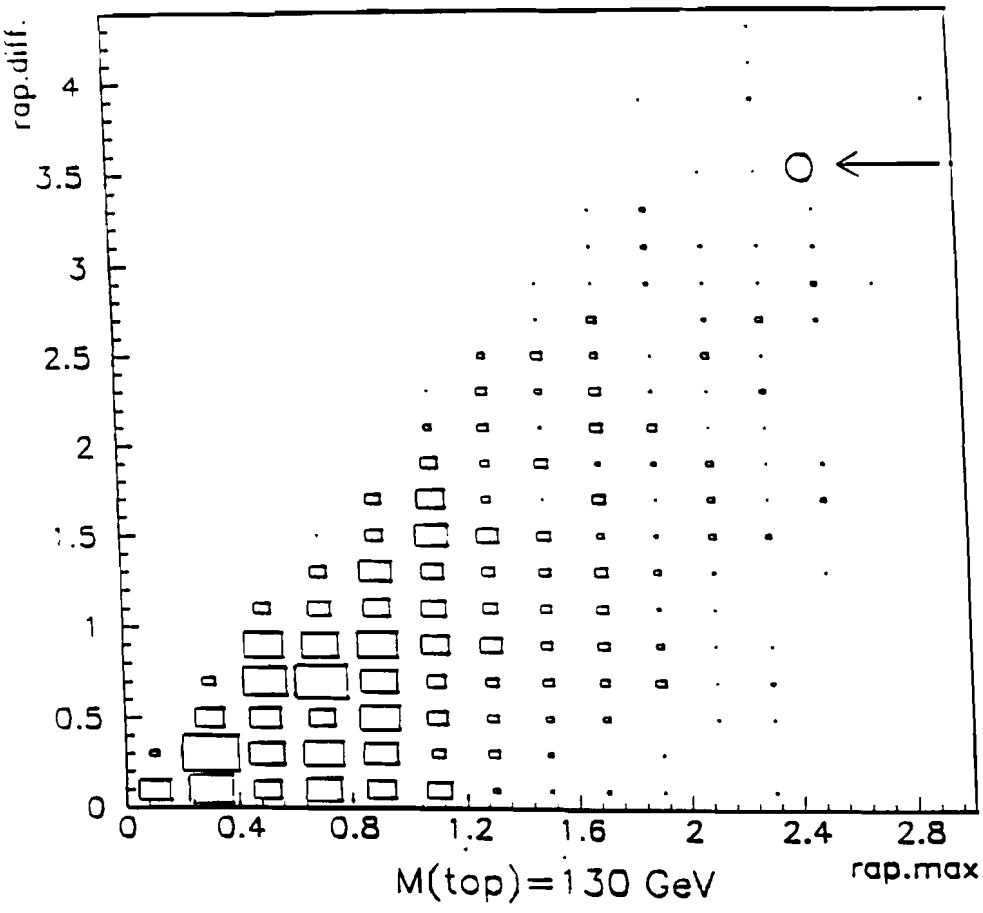

Figure 3.8: Pseudorapidity difference between b and $\bar{b}$ versus the maximum of $|\eta(b)|$, $|\eta(\bar{b})|$, Montecarlo Isajet (M_{top} = 130 GeV/c^2). The plot contains 980 entries, there are no overflows.

Chapter 4

Data Selection

4.1 Event processing and reconstruction

During the collision period which started in august 1992 and lasted till may 1993, the accelerator provided an integrated luminosity of 30.2 pb^{-1}. CDF collected about 15.5 million events, corresponding to an integrated luminosity of 21.4 pb^{-1}. The CDF efficiency was about 71%. During the data taking a system which analyzed immediately the data was available (called "*express-line*"). Electrons and muons over a P_T threshold were selected, which was chosen in order to limit the number of events to process, and at the same time to include a large fraction of the most interesting events. The raw data were written on magnetic disk and later transferred on tape for a permanent storage. The data on disk were read by an IBM–UNIX system on which quality control and reconstruction processes were activated.

First, the tracks were reconstructed and the digital information indicating the pulse height in the calorimeter were converted to energy values. Subsequently the "parton" (i.e. electrons, muons, jets) reconstruction was performed, using the track information and the energy deposits in the calorimeters. The events reconstructed through the *express-line* were about 1.7 millions.

The events were available in two different formats: DST (*Data Summary Tape*), more complete, and smaller PAD, where several banks had been dropped.

A first selection of the reconstructed events has been made in order to create smaller samples easy to handle, each finalyzed to the specific requests of the variuous analyses.

4.2 Electron identification and selection

The CDF electron candidates in the central region ($|\eta| < 1.0$) have a CTC track extrapolating to a CEM energy deposit (*cluster*). The electromagnetic cluster is built around a "seed" tower with $E_T > 3$ GeV, including the neighboring towers with $E_T > 100$ MeV. The size of the cluster is limited to 3 towers in pseudorapidity ($\Delta\eta = 0.3$) and one tower in azimuth ($\Delta\phi = 15°$). Fiducial cuts on the shower position as measured in the CES are applied to ensure that the electron candidate is away from calorimeter boundaries and therefore that the energy is well measured. This cut reduces to 84% the solid angle available for the electron fiducial region at $|\eta| < 1.0$. Any electron without a matching VTX track or with an opposite sign CTC track forming a low mass e^+e^- pair is rejected as a conversion candidate. Using this method, electrons from converted photons can be removed with high efficiency (88 ± 4 %) using tracking information, with a loss for good quality electrons of only 5%.

The following identification variables are used to discriminate electrons from charged hadrons:

- the ratio of hadronic energy to electromagnetic energy of the cluster: E(had)/E(elm);
- the ratio of electromagnetic cluster energy to track momentum: E/P;
- the variable $\mathcal{L}_{shr}$ which gives a measurement of the lateral shower profile in the calorimeter (for a detailed description of this and the other electron technical variables see reference [39]);
- the shower is reconstructed in the *strip chambers*. A χ^2 comparison of the strip chamber shower profiles with those of test beam electrons is made: χ^2_{strip};

- the distance between the extrapolated track position and strip chamber shower position measured in the $r - \phi$ and $r - z$ views: Δx (Δx=$x_{CES} - x_{CTC}$) and Δz (Δz=$z_{CES} - z_{CTC}$); usually a tighter cut is applied in the x direction, because of the better CTC resolution in that direction.

- the distance along the beam between the interaction vertex and the reconstructed track: z–vertex match.

Since in the decay channels studied in this thesis we always require one lepton to be a high P_T electron or muon, for the electrons we used three "subsamples" referred to as ICE (*Inclusive Central Electron*), WENU ($W \rightarrow e\nu$) and ZEE ($Z \rightarrow ee$). The ICE data sample consists of central electrons with $E_T > 18$ GeV, passing certain loose quality cuts. The WENU sample consists of central electrons with $E_T > 22$ GeV energy and missing transverse energy greater than 22 GeV. The ZEE sample consists of one central electron with $E_T > 22$ GeV selected with the same quality cuts as the WENU channel, and in addition a second electromagnetic cluster. There are 133805 events in the ICE sample, 28107 in the WENU and 3533 in the ZEE.

Starting from the ICE data sample we applied the following cuts:

- $E_T > 20$ GeV
- E/P < 1.5
- $|\eta| < 1.0$
- E(had)/E(elm) < 0.05
- $|\Delta x| < 1.5$ cm
- $|\Delta z| < 3.0$ cm
- $\mathcal{L}_{shr} < 0.2$
- $\chi^2_{strip} < 15.$

- $Z - v < 5$ cm
- $z_{vertex} < 60$ cm.

The electron identification efficiency has been determined from a sample of $Z^{\circ} \rightarrow ee$ events, and was found to be 84 $\pm$ 2 %. In this sample, the accurate selection of one electron and the requirement of the Z° invariant mass are sufficient to assure that the second particle is an electron.

We also applied a cut on the isolation variable, defined as the ratio between the calorimeter transverse energy in the towers within a cone of radius R = $\sqrt{\eta^2 + \phi^2}$ = 0.4 centered on the electron but excluding the electron cluster energy, and the electron transverse energy itself:

- Iso < 0.1.

4.3 Muon identification and selection

Muons are identified in the central region ($|\eta| < 1.0$) by requiring a match between a CTC track extrapolated through the calorimeter and the absorber and a track segment reconstructed in the muon chambers CMU, CMP or CMX, within the error due to multiple scattering which the particle undergoes. The following muon identification variables are used to distinguish muons from punching–through hadrons and from hadron decay in flight:

- an energy deposition in the electromagnetic (E(elm)) and hadronic (E(had)) calorimeters consistent with a minimum–ionizing particle;
- the impact parameter, which is the closest approach of the reconstructed track to the beam line: d_o;
- the distance in the z direction $Z - v$ between the interaction vertex and the reconstructed track : z–vertex match;

- the transverse distance in the $r - \phi$ plane between the extrapolated CTC track and the track segment in the muon chambers: Δ(CMU) and Δ(CMX).

For the muons, we used two subsamples referred to as ICM (*Inclusive Central Muon*) and WZMU ($W \rightarrow \mu\nu$ and $Z \rightarrow \mu\mu$). The ICM sample consists of central muons with at least 18 GeV transverse momentum, which pass very loose minimum ionization and quality cuts. The WZMU sample is a rather inclusive sample of W and Z° candidate events. There are 83051 events in the ICM sample and 22743 events in the WZMU sample.

We applied the following cuts on the ICM sample:

- $P_T > 20$ GeV/c
- $|\eta| < 1.0$
- E(elm) < 2 GeV
- E(had) < 6 GeV
- E(elm) + E(had) > 0.1 GeV
- $d_\circ < 3$ mm
- $Z - v < 5$ cm
- Δ(CMU) < 2 cm
- Δ(CMX) < 5 cm
- $z_{vertex} < 60$ cm.

The overall muon identification efficiency was determined from a sample of $Z^\circ \rightarrow \mu\mu$ and was found to be 90 ± 2 %.

In analogy with the electrons, we also required the muon to be isolated. The isolation variable is defined as the ratio between the energy in a cone of radius R = 0.4 around the muon excluding the muon tower, and the muon P_T. We required:

- Iso < 0.1.

4.4 Lepton–candidate from the isolated tracks

After we selected the sample of events with one high P_T lepton (electron or muon) we look for a second high P_T isolated track. For electron and muon candidates we require $P_T(\text{track}) > 20$ GeV/c, as for the first lepton. The 20 GeV/c cut on both leptons strongly reduces the $b\bar{b}$ and $c\bar{c}$ background (since leptons from light quark pairs have in average smaller P_T).

In order to increase the efficiency for tau leptons, we require $P_T(\text{track}) > 15$ GeV/c for tau candidates (since these tracks are the results of a double decay, the P_T is in average smaller than for electrons and muons; compare figures 3.2 and 3.3). We restrict the study to tracks at $|\eta| < 1.0$.

The track isolation is defined by requiring that the transverse momentum sum of all the tracks contained in a cone of radius R = 0.4 centered on the lepton candidate track is:

$$\sum P_T < 0.1 \times P_T(\text{track}).$$

The cone of radius 0.4 has been chosen in analogy to the usual isolation cuts defined in the calorimeter which are applied to electrons and muons.

The isolation requirement is the same for electrons, muons and taus. By requiring the leptons to be isolated we reduce the background from $b\bar{b}$ and $c\bar{c}$ decays, where usually there are charged hadrons not far from the leptons.

Once the isolated track has been selected, we require the primary lepton and the track to be consistent with a single primary vertex in the beam direction: $\Delta z(\text{lepton–track}) <$ 20 cm. This cut is rather loose, but it enables us to remove events where the two lepton candidates come from two well distinct vertices.

In addition we required the invariant mass of the lepton–track system to be greater than 10 GeV/c^2. Doing this we removed the events that had two reconstructed "mirror"

tracks corresponding to the crossing of one particle only. These errors in the track reconstruction give tracks with the same ϕ and a slighly different η, which have a very small invariant mass. This cut does not cause any efficiency loss for top events.

Looking for an isolated track to identify a lepton is not enough: if for instance the reconstruction code makes a particularly severe mistake in the polar angle measurement, a track which is part of a jet could look isolated. We have found indeed some high P_T tracks which had the same ϕ of a big jet, but were displaced in pseudorapidity. However, in these cases the tracks are pointing to calorimeter cells which do not contain any significant energy deposition. This is not sensible: it would mean that the particle passed through the calorimeter without releasing any energy. Therefore the track can be rejected.

In order to associate the selected track to a lepton category we used the information from the calorimeter. We required always a minimum energy deposition in the calorimeters. Then we classified the track as electron, muon or tau based on the quantity of deposited energy. The definition for the three lepton categories has been chosen so that it is exclusive (e.g. a track can belong to only one of the three categories) and as much as possible complementary (e.g. a lepton excluded from its class because of a particularly unlucky fluctuation can be regained in a different category).

4.4.1 Identification efficiency of a high P_T isolated track

The CDF central tracking chamber has a very high reconstruction efficiency for high P_T tracks. From Montecarlo calculation it has been estimated to be close to 100%. This result was checked using a sample of cosmic rays which cross the detector close to the center, and resulted to be about 99%.

In order to study the efficiency of the isolation requirement one could start studying a sample of Z° events. In this case the efficiency of the isolation cut is very high (97%, compare reference [40]).

In the final analysis the isolation efficiency depends on the physics process under study and cannot be derived with absolute certainty from different processes. We expect this

efficiency to be lower in top events than in Z° events. Indeed in top events there are more jets and charged tracks. The difference can be evaluated by Montecarlo calculations. The error on this estimate will depend on the uncertainty of the theoretical model used by the Montecarlo program for the top fragmentation and decay and on the uncertainty introduced by the detector simulation. The isolation requirement efficiency for high P_T tracks in top events obtained from the Isajet Montecarlo is $\sim$ 85%.

4.4.2 Electrons

The isolated track is classified as an electron candidate if:

- $0.5 <$ E(elm)/P < 2.0
- E(elm)/E(tot) > 0.8

where E(elm) is the energy deposited in the electromagnetic compartment of the tower traversed by the particle, E(tot) is the total energy and P is the track momentum measured in the CTC.

In order to evaluate the inefficiency introduced by the cuts on the deposited energy we used the data sample ZEE, which contains two electromagnetic clusters. We require that one electron passes the standard identification criteria. Then we look for a second isolated track, as previously described. In figure 4.1 we show the invariant mass of the two tracks corrisponding to the "good" lepton and the isolated track. In this plot there are both good Z° and background events. In a second step we require $0.5 <$ E(elm)/P < 2.0. The invariant mass of the events which do not pass this cut is shown in figure 4.2. Comparing figure 4.1 and figure 4.2 we found that the efficiency of the E/P cut is 99 $\pm$ 1%. Concerning the requirement E(elm)/E(tot) > 0.8, it does not introduce any inefficiency because the tracks which do not pass this cut will be studied anyhow, and will be catalogued as taus.

4.4.3 Muons

The isolated track is classified as a muon candidate if the energy deposited in the electromagnetic and hadronic compartments of the tower traversed by the particle is:

- E(elm) < 2 GeV
- E(had) < 5 GeV.

In addition we require a minimum energy deposition in at least one of the two compartments of the tower hit by the particle:

- E(elm) > 0.05 GeV or E(had) > 0.5 GeV.

The last requirement is necessary, as mentioned before, because often tracks which are part of jets are misreconstructed in pseudorapidity, so that they appear to be isolated. These tracks must be rejected.

In order to evaluate the loss of efficiency caused by the minimum ionization requirement for a muon candidate track, we used the WZMU data sample. In addition to the "good" muon we required a second isolated track selected as previously described. In figure 4.3 we show the invariant mass of the two tracks system. Then we require the isolated track to be consistent with a minimum ionizing particle. The two tracks invariant mass for the events which do not have this characteristic is shown in figure 4.4. The peak seen in figure 4.4 suggests that sometimes in $Z^{\circ} \rightarrow \mu\mu$ events there are muons which do not appear as minimum ionizing particles. Some of these events have been studied in details. It resulted that usually they hit the calorimeter close to the module boundaries, where the energy measurement is more dubious. Comparing figure 4.3 and 4.4 we found that the efficiency of the cuts applied to select muon candidate tracks is: 92 ± 2 %.

4.4.4 Taus

We restricted the tau analysis to the so called "one prong" decay channel (i.e. when the tau decays to one charged hadron, a tau neutrino and neutral hadrons). This channel

accounts for 50% of the tau decays. Isolated tracks with $P_T > 15$ GeV/c, which are neither classified electrons nor muons, are called "tau" if:

- $E_\tau/P > 0.5$

where E_τ is the total energy of the tower traversed by the particle summed to the energy of the adjacent towers. The definition used for the tau candidates is very loose. Electrons and muons which did not pass their selection criteria because of an abnormal fluctuation might also enter the tau category.

4.5 Jet reconstruction

A jet corresponds to a group of collimated particles. It is defined by an energy deposition localized in a specific part of the calorimeter. The CDF jet reconstruction algorithm, called JETCLU, looks for regions in the η - ϕ space of fixed radius ($R = \sqrt{\eta^2 + \phi^2}$) with a concentration of deposited energy. We used a reconstruction cone of radius R = 0.4. The jet identification process consists of two steps. First, calorimeter seed towers with $E_T > 1.0$ GeV are listed. The towers inside a circle of radius 0.4 centered around a seed tower and with $E_T > 100$ MeV are summed. Secondly, the cluster centroid is calculated, weighting the towers with their transverse energy and a new cone is formed. The process is repeated until the list of towers in the circle remains unchanged. If two clusters overlap such that one shares more than 75% of its energy with another one, the two clusters are merged. Otherwise they are mantained distinct, and towers in common are assigned to the nearest cluster.

The jet energy as measured by the calorimeter was corrected to take into account the detector effects, in particular the non–linearity in calorimeter response and its anomalous behaviour in the "*cracks*" region, (i.e. the mechanical conjuctions among the calorimeter modules, which do not contain scintillator material). In addition, a correction was applied to take into account two physics effects:

- subtraction of the *underlying event* (which should originate from spectator partons not participating in the hard process $q\bar{q}(gg) \rightarrow t\bar{t}$). It contributes with a spurious term to the energy deposited in the clustering cone.

- addition of the energy from particles produced in the fragmentation of the parton of interest, which falls out of the clustering cone because of fluctuations in the fragmentation process. These particles are lost and their energy is called "*out of cone*" energy.

The correction functions are obtained studying the energy balance in events with two jets (or one jet and one photon), and using Montecarlo programs. The whole of these corrections has the purpose, for every jet detected in the calorimeter, to give in average the best estimate of the energy of the original partons [72]. In the analysis we will always refer to jet energy corrected for the aforesaid effects.

We required at least two jets in the events, satisfying the following conditions:

- E_T(jet1), E_T(jet2) > 15 GeV;

- ΔR(lepton–jet) > 0.5;

- ΔR(track–jet) > 0.5;

- ΔR(jet–jet) > 0.7;

- $|\eta|$(jet1), $|\eta|$(jet2) < 2.0.

The ΔR cut on the distance between pairs of leptons and jets can be interpreted as an isolation requirement. It implies the giving up of the study of leptons inside jets or very close to them. The ΔR cut between two jets is consistent with the choice of a jet reconstruction cone of radius R = 0.4. One wants to avoid that a jet unusually extended on many calorimeter towers is wrongly interpreted as two separated jets by the reconstruction algorithm. The efficiency for these requirements obtained from the Isajet

Montecarlo is $\sim$ 80% for a top mass of 170 GeV/c^2. For a top mass of 140 GeV/c^2 this efficiency is $\sim$ 70%.

4.6 Transverse energy carried by neutrinos

The neutrinos do not interact with any detector component. Therefore they cannot be detected directly. This causes an apparent unbalance of the final state prongs in the event (which is called missing energy because it is determined by a calorimeter energy measurement). A large fraction of the $p\bar{p}$ collision energy escapes undetected at small angles from the beam direction. Therefore longitudinal energy balance in the beam direction cannot be exploited, and the longitudinal component of the neutrino momentum cannot be deduced. However, on the plane transverse to the beam direction the momentum unbalance can be measured through the transverse missing energy vector, which is defined as:

$$\vec{\not\!\!E}_{Tu} = -\sum_i \vec{E}_T^i$$

where $\vec{E}_T^i$ is the vector corresponding to the transverse energy deposited in a single calorimeter tower. The sum is extended to all the calorimeter towers at $|\eta| < 3.6$.

The transverse energy measured by the calorimeter must be corrected for the presence of muons. Muons deposit little energy in the calorimeter and contribute to the apparent event energy unbalance. The muon momentum is measured by the tracking system. For events with muon candidates, the vector sum of the calorimeter transverse energy is corrected by vectorially subtracting the energy deposited in the tower traversed by the muon and then adding the $\vec{P}_T$ of the muon candidate as measured in the CTC.

In events with a large hadron activity it is possible that the jet energy is mismeasured, because of non-linearities in the calorimeter response or because of the larger energy losses in uninstrumented regions. This effect can manifest itself as an apparent energy unbalance in the event. Therefore we evaluated the missing energy after applying the jet corrections. We corrected the clusters with E_T(uncorrected) $>$ 5 GeV, by applying all

standard jet corrections, including "*out of cone*" and "*underlying events*" corrections. We do not correct for unclustered energy.

We choosed this way to correct the $\not\!\!E_T$ because it resulted to be the best one to distinguish W events from non–W events [73]. We can summarize as follows the corrections applied:

$$\vec{\not\!\!E}_{Tc} = \vec{\not\!\!E}_{Tu} - \sum_{cluster>5GeV} (\vec{E}_{Tc} - \vec{E}_{Tu}) - (\sum_{muons} \vec{P}_T - \sum_{muons} \vec{E}_T^{\mu-tower}).$$

In our analysis we finally applied the following cut:

- $\not\!\!E_{Tc} > 25$ GeV.

The efficiency of this cut has been obtained from the Isajet Montecarlo in top decay events with two high P_T leptons in the final state. For a top mass of 170 GeV/c^2 this efficiency is $\sim$ 84%. For a top mass of 140 GeV/c^2 it is $\sim$ 70%.

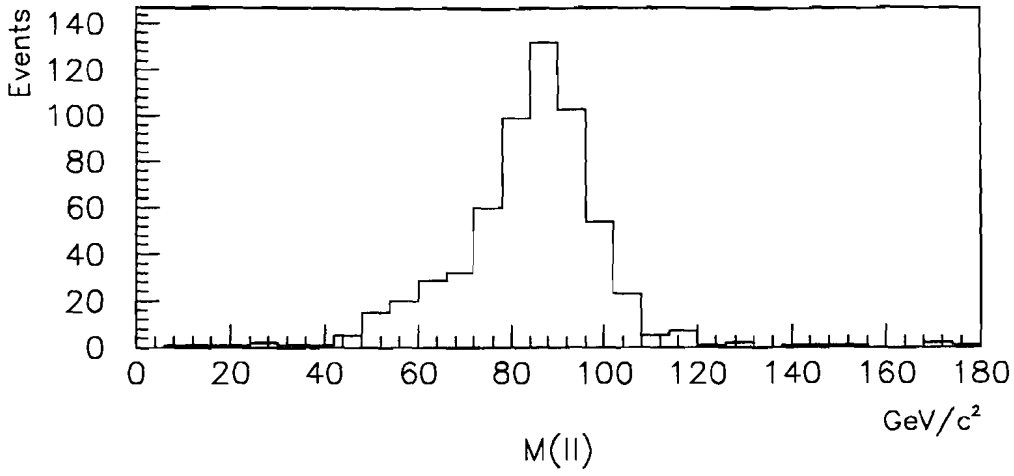

Figure 4.1: Invariant mass of the two electron tracks in Z° → *ee* events.

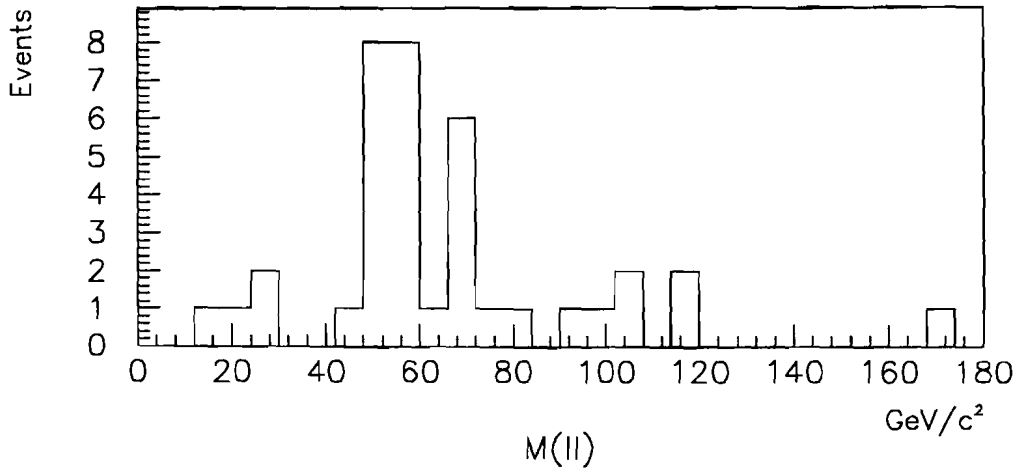

Figure 4.2: Invariant mass of the two tracks in the fraction of Z° →*ee* events which do not pass the E/P cut.

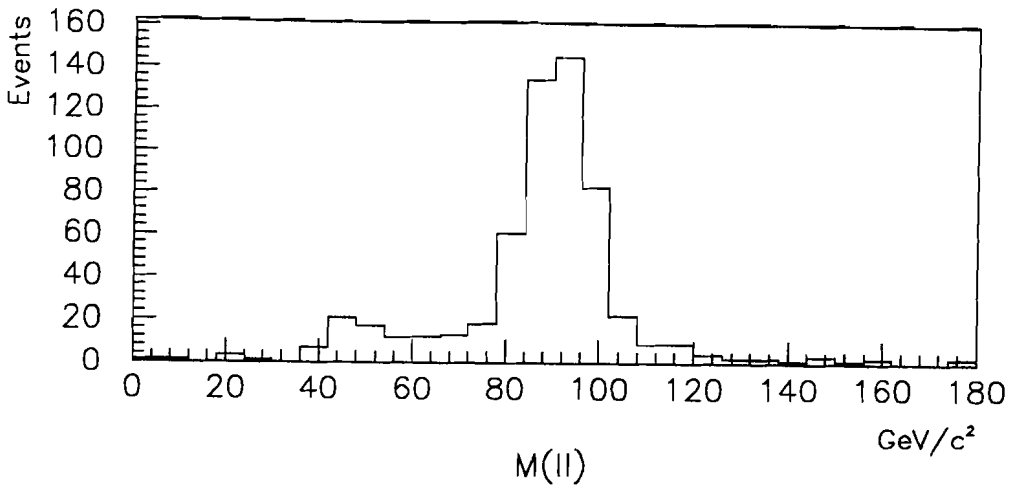

Figure 4.3: Invariant mass of the two muon tracks in $Z^\circ \rightarrow \mu\mu$ events.

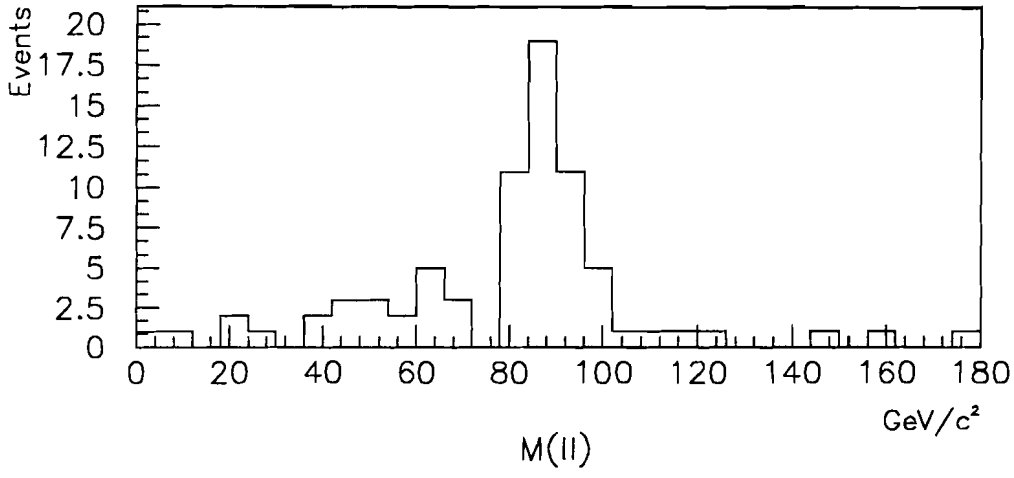

Figure 4.4: Invariant mass of the two tracks in the fraction of $Z^\circ \rightarrow \mu\mu$ events which do not satisfy the minimum ionization requirements.

Chapter 5

Background Study

In this Chapter we describe the study of the contamination from several possible background sources in our selected events sample. We examined both "physical" and "technical" backgrounds.

The physical background consists of correctly reconstructed events which passed the analysis cuts but do not come from top decay. An example of this kind of background is WW production and subsequent leptonic decay. It is difficult to compute this kind of background without the use of some physics simulation program, like the Isajet Montecarlo. This dependence on Montecarlo calculations imposes to use of a highly reliable program, and at the same time to adopt a conservative attitude.

Much progress has been made in this field recently. Programs which contain the correct QCD matrix element to generate several exclusive processes are now available [55]. We think that these developments will be of great help for any future analysis. However, we would like to perform more extensive studies to establish their reliability and systematic errors in the framework of the CDF simulation software. For the time being we are using the Isajet Montecarlo for the purpose of physics simulation, which includes a number of adjusted phenomenological parameters. Since there are indications that Isajet overestimates the physical background to top, in as much as gluon radiation is overestimated in general in hard processes, its use is conservative in the context of this thesis.

The technical background comes from a wrong interpretation of the parameters measured by the experiment, as for events where one of the lepton candidates is in reality a hadron which appears as a high P_T isolated track and shows in the calorimeter muon, electron or tau characteristics.

It is difficult to evaluate the technical background using Montecarlo programs. The isolated tracks constitute the tail of the jet fragmentation function, and the Montecarlo programs in that region may have considerable uncertainties. Moreover, tracks may appear to be isolated because of a wrong operation of the tracking chamber or of the calorimeter. Therefore we used the data to evaluate this kind of background [69]. For similar reasons we used the data also to evaluate the background due to $b\bar{b}$ events.

Expecially for taus, the major background reduction comes from the isolation requirement.

5.1 Probability to observe a calorimeter cluster associated to an isolated track

We will call "fake lepton" probability, the rate with which a QCD jet has multiplicity equal to one, and looks like one single isolated track in the CTC. In some of these cases, the energy deposited in the calorimeter could be consistent with our definition of electron, muon or tau.

In order to calculate this background we used part of a data sample called QCD–JET50 [70]. The trigger with which these data were recorded required one single tower over threshold at Level 1 and a significant transverse electromagnetic and hadronic energy deposition at Level 2 ($E_T > 50$ GeV). We expect most of these events to be QCD jets. There are only few leptons in the sample.

We started our study measuring the probability to find a calorimeter jet associated to an isolated track in the CTC. Then we evaluated the probability that the track be interpreted respectively as an electron, muon or tau. The presence of isolated tracks in

the QCD–JET50 sample can be due to fluctuations in the fragmentation process, or to a spatial misreconstruction of the track. In figure 5.1 we show the jet E_T distribution for jets at $|\eta|< 1.0$ (there are 39900 jets in the plot). Next we look for isolated tracks in this sample of jets, with different thresholds on the P_T of the track: $P_T > 5$ GeV/c, 10 GeV/c and 15 GeV/c. The isolation is defined in the CTC, requiring: $\sum P_T(0.4) < 0.1 \times P_T(\text{track})$. This is the same isolation requirement used to search for lepton + isolated track events, as described in Chapter IV. In figures 5.2, 5.3 and 5.4 we show the E_T distributions of the subsample of jets associated to an isolated track with $P_T(\text{track}) >$ 5, 10 and 15 GeV/c respectively. The ratio between figures 5.2, 5.3, 5.4 and figure 5.1 gives the probability for a jet to contain an isolated track, for a certain P_T(track) cut, as a function of the E_T of the jet. This probability decreases with increasing the P_T cut on the track, as shown in figures 5.5, 5.6 and 5.7 respectively.

With the cut $P_T(\text{track}) > 15$ GeV/c, the probability for a jet to be associated to an isolated track varies between 0.5% and 1%. Presumably there are also some real leptons in the jet sample. Therefore this probability, when interpreted as the hadronic contamination of the lepton sample, represents an upper limit to the true contamination.

The trigger used to collect these events could introduce some bias in the jet characteristics. For instance, since low track multiplicity jets might be more collimated than jets with a high number of tracks, close to the trigger threshold the trigger might have a higher efficiency for the low multiplicity jets. In order to avoid trigger effects, as a check we excluded the leading jet from our study. The probability for a jet to contain an isolated track turned out to be lower. Therefore, including the first leading jet (which caused the trigger) in the probability calculation is conservative.

Other considerations on possible trigger effects can be found in appendix B.

5.1.1 Fake tau probability

In order to evaluate the probability for a jet to be identified as a tau, we looked for isolated tracks with $P_T >$ 15 GeV/c, satisfying the tau candidate definition described in

Chapter IV: $E_\tau/P > 0.5$. E_τ is the sum of the energy deposited in the tower traversed by the track and in the adjacent ones. In figure 5.8 we show the E_T distribution of the jets which pass the tau requirements. The ratio between figure 5.8 and figure 5.1 provides the fake tau probability as a function of jet energy. The probability is about $P(\tau) = 0.6$ % per jet (figure 5.9). The result is consistent with what we found for the fake isolated track probability: the background reduction is due essentially to the isolation requirement. Requiring a τ–like energy deposit in the calorimeter does not change the result by much.

In order to verify the probability function that was obtained, we selected a sample of high P_T μ + 1 jet events. We applied the probability function shown in figure 5.9 to the jet E_T distribution of this new sample to obtain the number of expected "fake taus".

We used the muon sample only, in order to avoid a contamination from $Z^\circ \rightarrow ee$ where one of the electrons is mismeasured and is identified as a tau (this category of events will be the object of a separate study in paragraph 5.3). We required one and only one jet with $E_T > 15$ GeV and $|\eta(jet)| < 1.0$. The E_T(jet) and $\Delta\phi$(muon–jet) distributions are shown respectively in figures 5.10 and 5.11.

We looked among these jets for a high P_T isolated track classified as a tau candidate. We found 12 events. Their E_T and $\Delta\phi$(muon–jet) are shown in figures 5.12 and 5.13 respectively. There is clear evidence for a component of events with the muon and the jet exactly back to back in ϕ. This topology is typical in the Z° decay without jets.

We generated with the Isajet Montecarlo a sample of $Z^\circ \rightarrow \tau\tau$ events to study the ϕ correlation between the tau decay products. We applied exactly the same requirements as in the data. In figures 5.14 and 5.15 the E_T and $\Delta\phi$(muon–jet) distributions are shown, for $Z^\circ \rightarrow \tau\tau$ events where one tau decays to a charged hadron. The $\Delta\phi$ distribution shows an evident peak at 180°.

Some of the events observed in the μ + 1 jet sample might come from $Z^\circ \rightarrow \tau\tau$ events, where one of the two taus decays to muon and the other one decays to a charged hadron. They could also come from a $Z^\circ \rightarrow \mu\mu$, where one of the two muons hits a critical region of the detector (lightguide), faking the deposit of a large energy.

For this reason, in order to verify the expected number of QCD jets wrongly identified as tau in the μ + 1 jet sample, we selected only the events with $\Delta\phi$(muon–jet) < 150°. The E_T distribution of these jets is shown in figure 5.16. We applied the probability function of figure 5.9 to this distribution.

We obtained an expectation of 1.2 ± 0.4 fake taus in the μ + 1 jet sample. For jets which are not back to back in ϕ to the muon the calculation works well, since in this ϕ range we observe 2 events (see figure 5.13) which pass the tau identification criteria.

5.1.2 Fake electron probability

The procedure used to calculate the probability that a hadronic jet appears as an electron is very similar to that previously described for taus. We looked for isolated tracks with P_T > 20 GeV/c. In addition we required: 0.5 < E(elm)/P(track) < 2 and E(elm)/E(tot) > 0.8. In figure 5.17 we show the E_T distribution of the jets which satisfy these requirements. The ratio between figure 5.17 and figure 5.1 gives the fake electron probability as a function of jet E_T (figure 5.18). It is possible that the QCD sample contains a small fraction of real electrons (for instance from W + jets and Z° + jets decays, where the presence of jets caused the trigger). If among the jets shown in figure 5.17 there are also some real electrons, the measured fake probability is an upper limit of the true one. We find that the fake probability increases with jet E_T: this effect is due to the cut on the track P_T. At higher jet E_T it seems to level at about P(e) = 0.1 % per jet.

5.2 Fake muon probability

The fake probability calculation for taus and electrons was based on calorimeter jets. Hadrons which fake minimum ionizing muons have to traverse the calorimeter without a large energy deposit. Isolated fake muons will not appear as jets. We therefore base our background calculation for muons on tracks only. There are two possibilities: extrapolating the number of isolated, minimum ionizing tracks either from the number of observed non–isolated tracks, or from the number of observed isolated tracks wich are not

minimum ionizing. However, the last category of events, in the data sample of "W(e) + jets" (from which the background to our candidate events comes from), is dominated by $Z^\circ \rightarrow ee$ events where one of the electrons is mismeasured and deposits little energy in the calorimeter. This kind of background does not exist in the QCD jet sample. Therefore one cannot do a direct comparison of jets in the QCD and in the W + jets samples. For this reason we based the muon background calculation on the comparison between the number of minimum ionizing tracks which are isolated and the number of tracks which are non–isolated.

For this study we used again the QCD–JET50 data sample. We looked for $P_T > 20$ GeV/c tracks with $\sum P_T > 0.15 \times P_T(\text{track})$ in a cone of R = 0.4. Then we looked for isolated tracks ($\sum P_T < 0.1 \times P_T(\text{track})$) which pass the minimum ionization requirements (E(had) < 5 GeV, E(elm) < 2 GeV and either E(elm) > 0.05 GeV or E(had) > 0.5 GeV). In addition we required the isolated track to be far in ϕ from all jets in the event ($\Delta\phi$(track–jet)> 0.3). As already mentioned, this last requirement is needed because the minimum ionization cuts alone are not sufficient to reject from the JET50 sample tracks belonging to a jet and badly reconstructed in η. It would be possible to identify these events by performing a detailed technical study of the track properties. In order to simplify the analysis we preferred to explicitly require that the track be sufficiently far in ϕ from the jets.

After applying these cuts, we are left with 6 events. They have been studied one by one. Three of these events are likely to be W's (one of them might be a Z°) because they have high P_T muon candidates and large missing transverse energy. The remaining 3 events are our candidates for fake muons. We obtain a ratio of isolated minimum ionizing to non–isolated tracks R = 0.0015 ± 0.0009. We evaluated the mean number of jets per event. Based on this number we corrected the R ratio for the effect of the $\Delta\phi$(track–jet) > 0.3 cut between track and jets. We obtained: R= 0.0016 ± 0.0009. In analogy with the electron and tau background, one would like to give the muon fake rate as a function of P_T(track). We cannot do that because we do not have enough fake muon candidates.

We should mention that the three non–W muon candidates which we found are all close to a jet and very close to the $\Delta\phi$(track–jet) cut. Therefore our estimate of the fake muon background depends strongly on this variable. Changing the isolation requirement the fake muon probability also changes. This point will be discussed more in appendix A.

5.3 Background from Z° decay

Drell–Yan events should be eliminated essentially by imposing a lower limit on the transverse missing energy, because these events do not contain neutrinos. However, because of non–uniformities and non–linearities in the calorimeter response, a jet (or an electron) can occasionally be much underestimated (or overestimated) with respect to the true energy of the initial parton. This could cause an apparent high $\not\!\!E_T$ in the event and let some Drell–Yan + jets event leak into the sample.

In order to estimate the background from Z° events we used the Isajet Montecarlo as well as the CDF Z° $\rightarrow ee, \mu\mu$ data sample. With Isajet we generated Z° events forcing the decay to leptons. We generated Z° $\rightarrow ee$ events corresponding to an integrated luminosity of 198 pb^{-1}, Z° $\rightarrow \mu\mu$ corresponding to 74 pb^{-1} and finally Z° $\rightarrow \tau\tau$ corresponding to 300 pb^{-1}.

Since we do not want to rely on how well Isajet reproduces the associated gluon radiation, we compared Z° $\rightarrow ee$ events produced by Isajet with a data sample of real Z° $\rightarrow ee$ and Z° $\rightarrow \mu\mu$. The Z° $\rightarrow \ell^+\ell^-$ data were selected applying the cuts described in Chapter IV and requiring them to be inside the Z° mass window ($70 < M(\ell^+\ell^-) < 110$ GeV/c^2). In both samples, Montecarlo and data, we required at least two jets in the events with $E_T > 12$ GeV. In figure 5.19 we compare the E_T distribution of the second leading jet for Montecarlo and data. The two distributions have been normalized to the same number of total Z° events in the two samples. Isajet shows a spectrum which is more energetic, although not violently in disagreement with the data. We conclude that the background calculation obtained from Isajet is conservative.

5.4 Background from WW and WZ pairs

We produced with Isajet samples of vector boson pairs WW and WZ, corresponding to an integrated luminosity of 2842 pb^{-1} and 2692 pb^{-1} respectively (σ_{WW} = 9.5 pb [55], σ_{WZ} = 2.6 pb [71]). The theoretical uncertainty in the cross section is about 30%. We used these samples to get the absolute number of expected WW and WZ events faking tops. Because of the uncertainty in the Isajet gluon radiation prediction, a better approach would have been to use a Montecarlo with the correct matrix element for the WW + jets process. A Montecarlo program which generates WW + n jets, with n = 0, 1, 2, and WZ events and contains the full matrix element for each one of these processes has been made available by T.Han. It is based on the calculations done by V. Barger *et al.* [55]. This Montecarlo program is relatively new and it is being tested at present. The preliminary results that we obtained tend to confirm that Isajet produces too much radiation.

5.5 Background from $b\bar{b}$ pairs

The background from $b\bar{b}$ pair production can be estimated considering that our analysis starts from the W + jets data sample. It is well known from several studies made on this sample that the background from non–W events is of the order of 10 % [74].

As discussed above, we calculated the probability to find a jet with a high P_T isolated track starting from a sample of QCD jet events. This QCD sample might contain a fraction of $b\bar{b}$ pairs which is different from the $b\bar{b}$ content of the W + jet sample. If the probability that a b quark results in a high P_T isolated track is different from that for a light quark or gluon, then our "fake" lepton background calculation might be sistematically wrong for the W + jets sample.

First, there is a small fraction (a few percent) of W events which contain a $b\bar{b}$ pair (W + $b\bar{b}$ events). These events are not of great concern for our sample because those b quarks are of low P_T.

Secondly, there is a contamination (of about 5%) in the W + jets sample from events

where the high P_T isolated lepton is not from a (real) W decay, but comes from the decay of a b quark ($b\bar{b}$ events). The second b quark in these events might be of high P_T, and therefore might be more likely to result in a high P_T track, which then might be isolated. However, this b content hardly can influence our background calculation, because it is small. In addition, it is known from various studies that the kinematical structure of b quark jets and different jets are very similar.

In order to derive in a quantitative way the probability that in b enriched events a jet is identified as an isolated lepton we studied a sample of events with non–isolated leptons. We required one high P_T ($P_T > 20$ GeV/c) lepton of good quality (applying the cuts described in paragraph 4.2), which is not isolated: $0.1 < \text{Iso} < 0.5$. While in the W candidate sample of isolated leptons the fraction of b events is of the order of 5%, in the large P_T non–isolated lepton sample typically 50% of the events come from b decays. We required at least one jet with $E_T > 15$ GeV. We then studied whether this b enriched jet sample shows an increased fraction of jets with isolated high P_T tracks, compared with that found in the QCD–dominated sample. In figure 5.20 we show the E_T distribution for the jets at $|\eta| < 1.0$ (these might fake a lepton). Figure 5.21 shows the E_T distribution of the jets identified as taus. In figure 5.22 the probability that a jet appears as a tau is shown, as a function of the jet E_T, in analogy to what was done for the QCD jet sample. A comparison between figure 5.22 and figure 5.9 shows no evidence for an increased probability to observe a jet with an associated isolated track. The same study was done for electron and muon candidates. No increase in the corresponding probabilities was found as well [1].

In conclusion, in a sample which is enriched in b quarks we did not find any evidence for an excess of high P_T isolated tracks. Consequently, the expected number of high P_T isolated tracks in the W + jets sample, based on the method which will be described in chapter VI, is an adequate background estimate which includes the contribution from $b\bar{b}$

[1] A sample of b quarks should show an excess of good electrons and muons. However, our electron and muon requirement is very loose, so the signal–background separation is correspondingly low.

events.

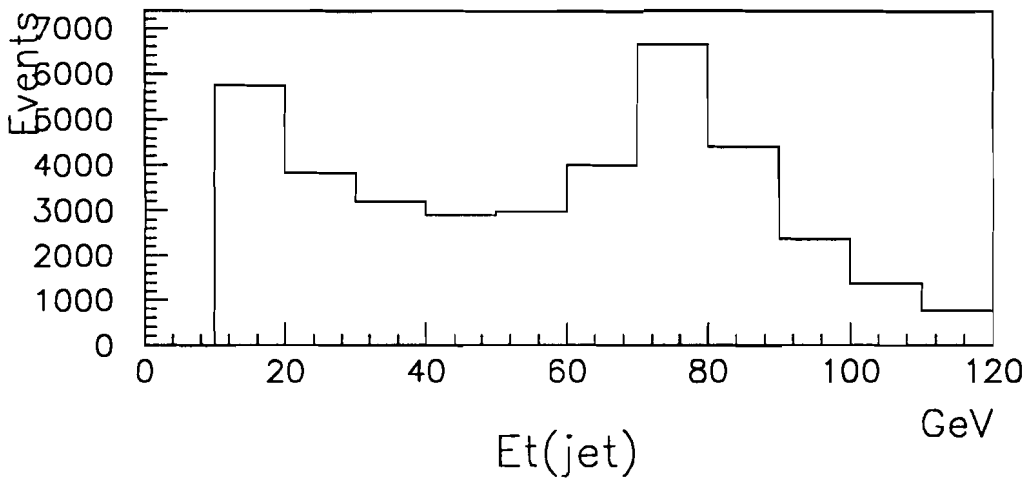

Figure 5.1: E_T distribution of the jets at $|\eta|<1.0$ in the JET50 sample. The shape of the distribution is a reflection of the trigger threshold. This has no impact on the study, since we work out only probabilities per jet to appear as a fake.

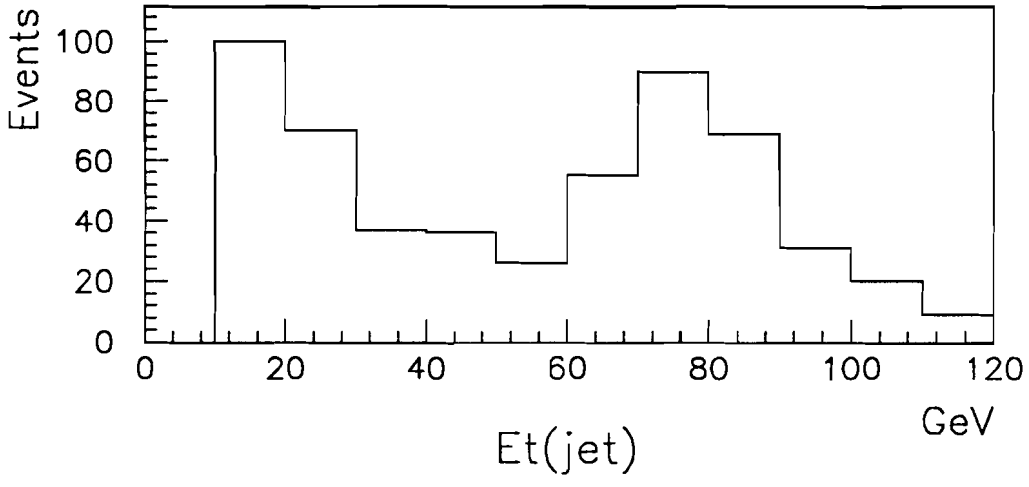

Figure 5.2: E_T distribution of the jets associated to an isolated track in a cone of radius R=0.4 around the track and $P_T>$ 5 GeV/c (JET50 sample).

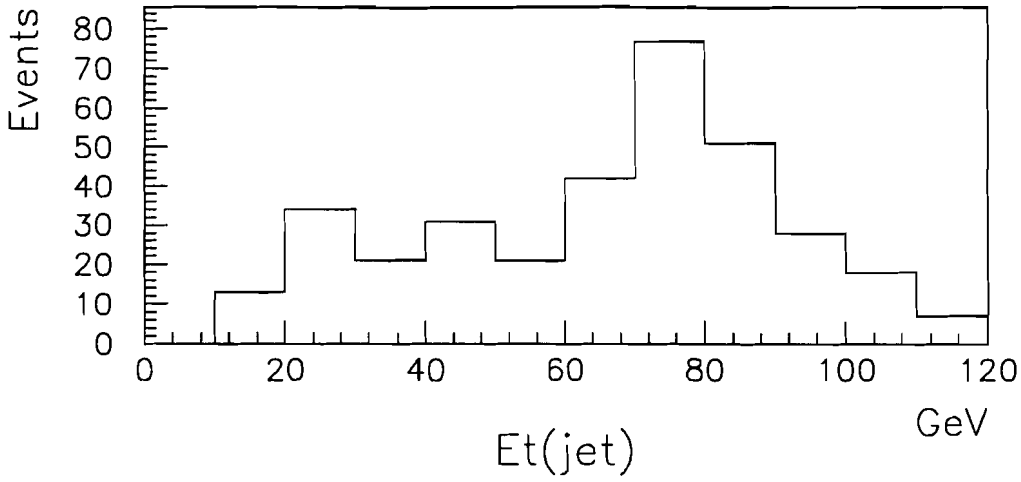

Figure 5.3: E_T distribution of the jets associated to an isolated track with $P_T > 10$ GeV/c (JET50 sample).

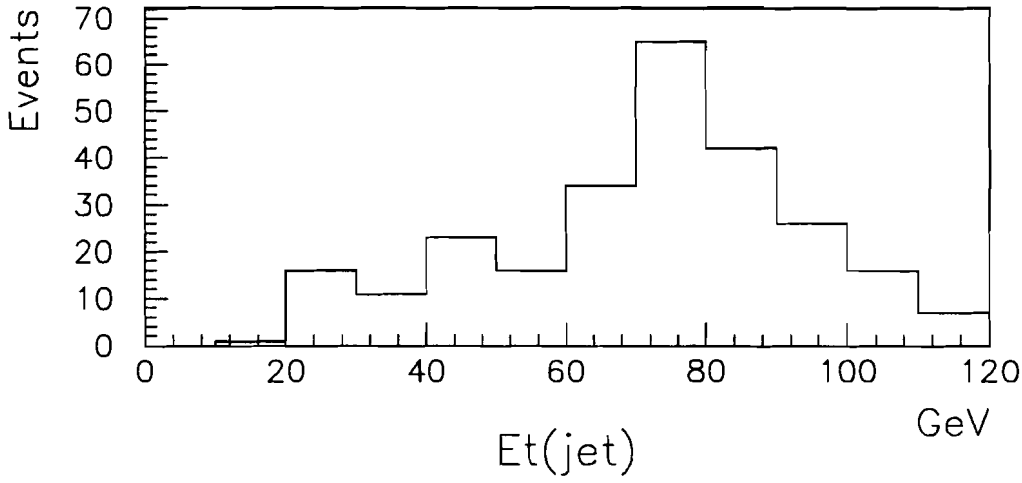

Figure 5.4: E_T distribution of the jets associated to an isolated track with $P_T > 15$ GeV/c (JET50 sample).

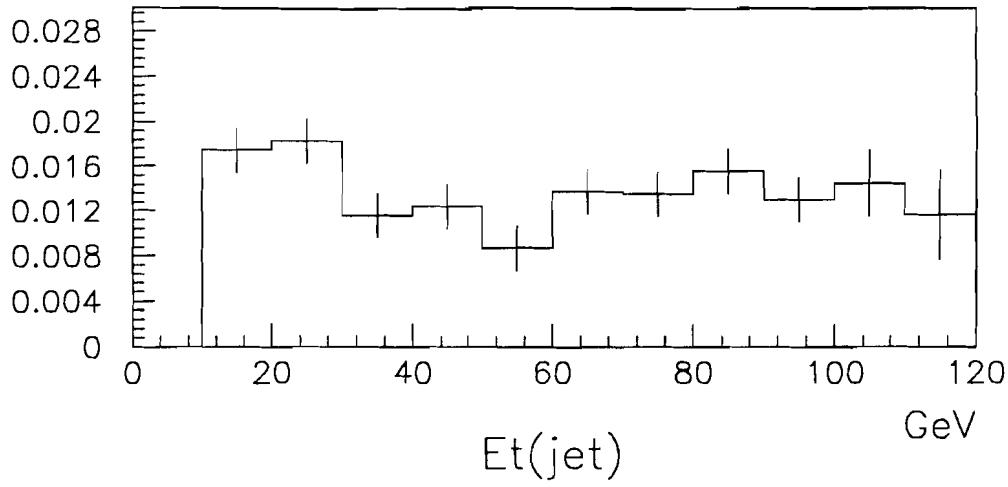

Figure 5.5: Probability for a jet to be associated to an isolated track with $P_T > 5$ GeV/c as a function of the jet E_T (JET50 sample).

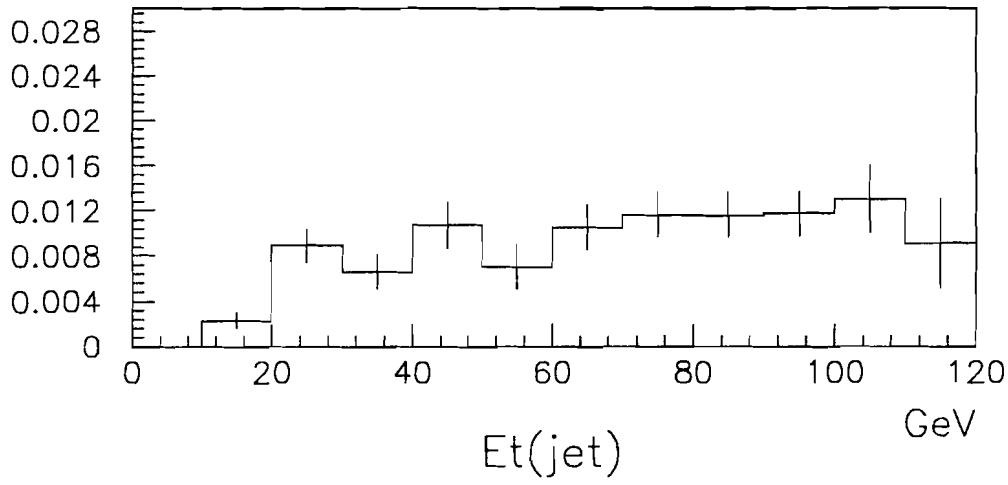

Figure 5.6: Probability for a jet to be associated to an isolated track with $P_T > 10$ GeV/c (JET50 sample).

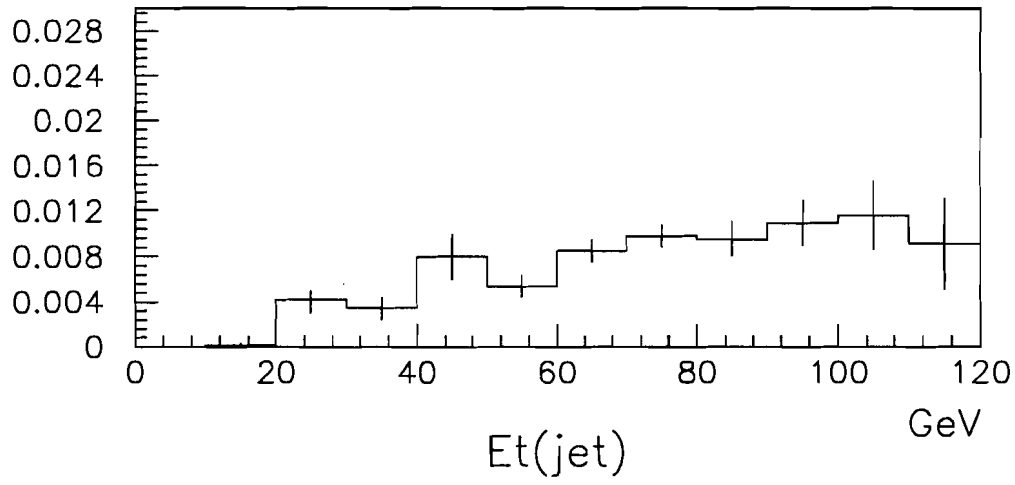

Figure 5.7: Probability for a jet to be associated to an isolated track with $P_T > 15$ GeV/c (JET50 sample).

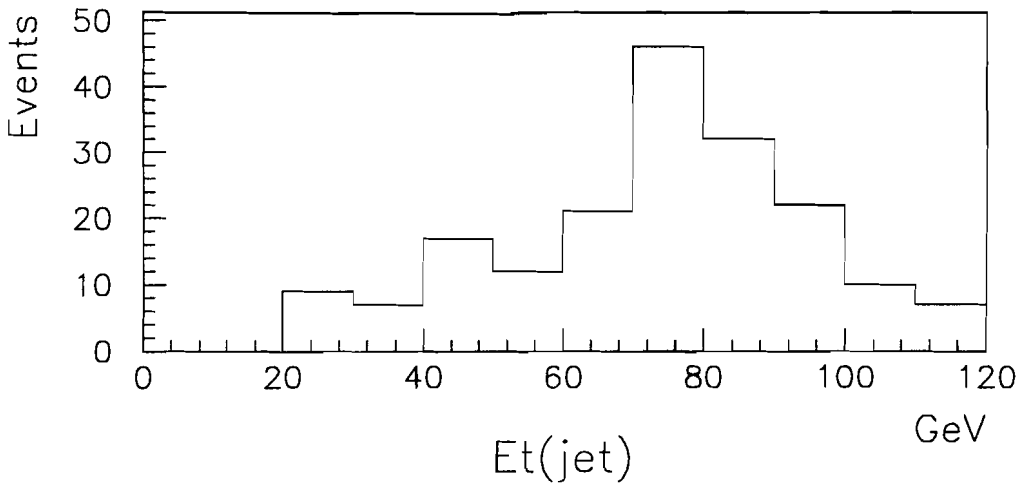

Figure 5.8: E_T distribution of the tau candidate jets (JET50 sample).

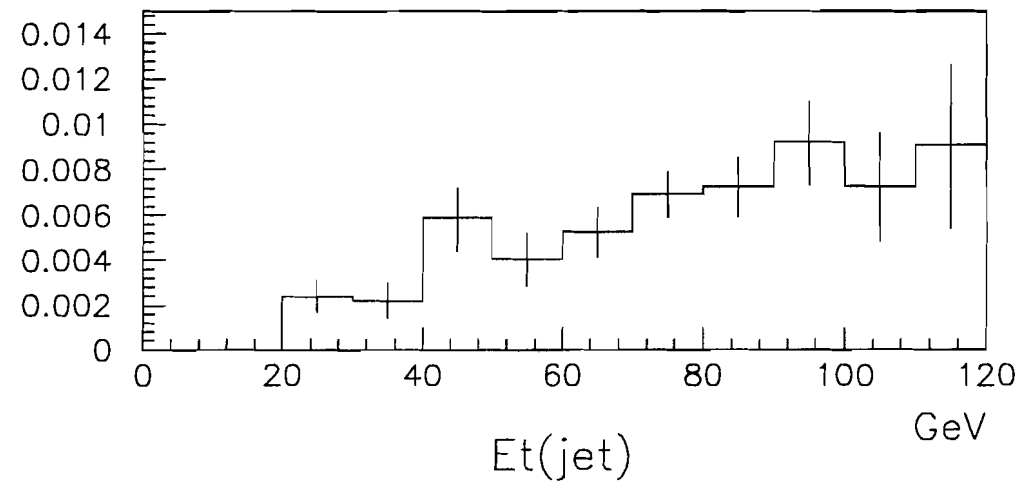

Figure 5.9: Probability for a jet to be identified as a tau (JET50 sample).

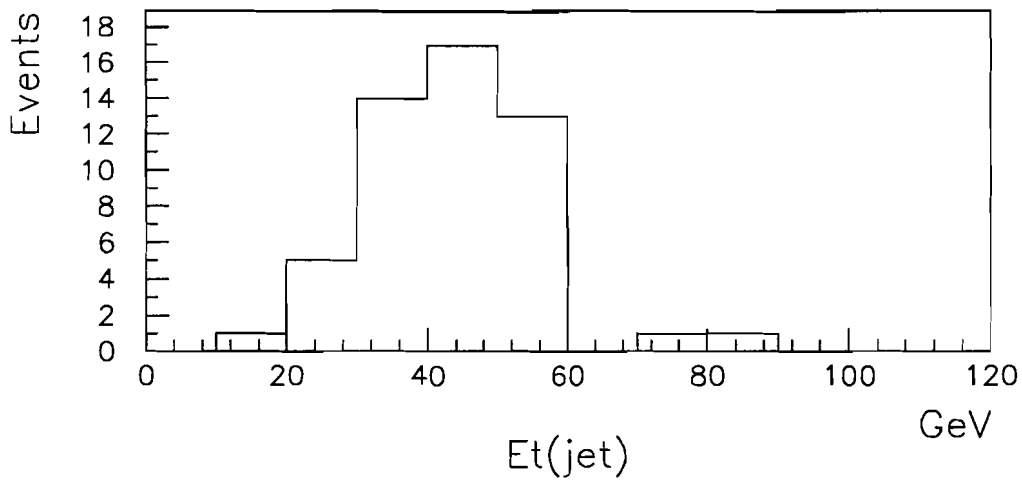

Figure 5.14: E_T distribution of tau candidate jets in $Z^\circ \rightarrow \tau\tau$ events (Isajet Montecarlo).

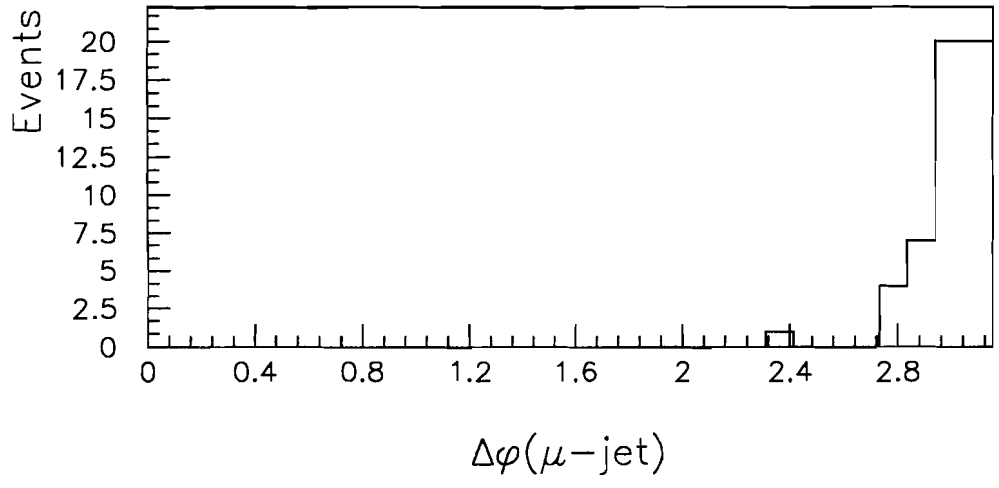

Figure 5.15: $\Delta\phi$(muon–jet) in $Z^\circ \rightarrow \tau\tau$ events (Isajet Montecarlo).

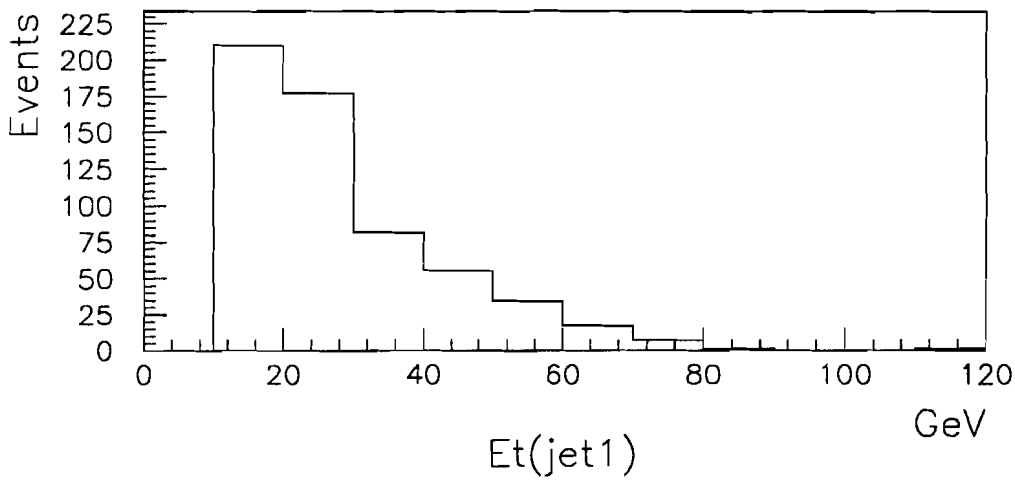

Figure 5.16: E_T distribution of central jets in μ + 1 jet events, with $\Delta\phi$(muon–jet) < 2.6.

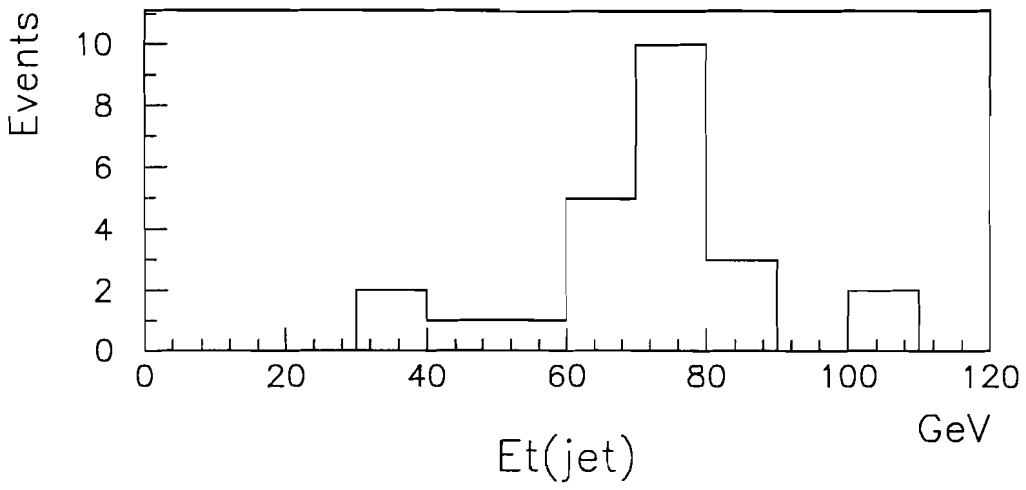

Figure 5.17: E_T distribution of electron candidate jets (JET50 sample).

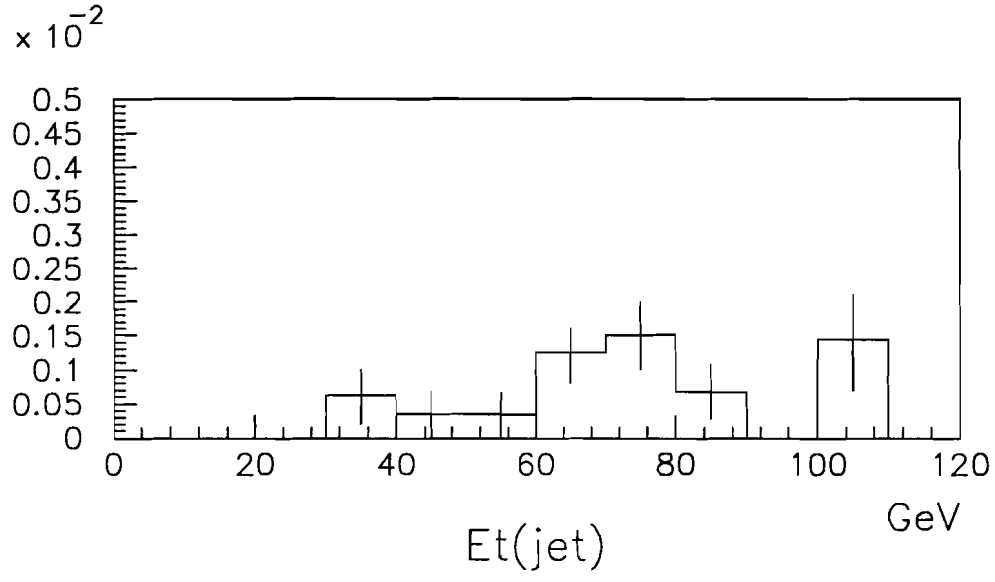

Figure 5.18: Probability that a jet is identified as an electron (JET50 sample).

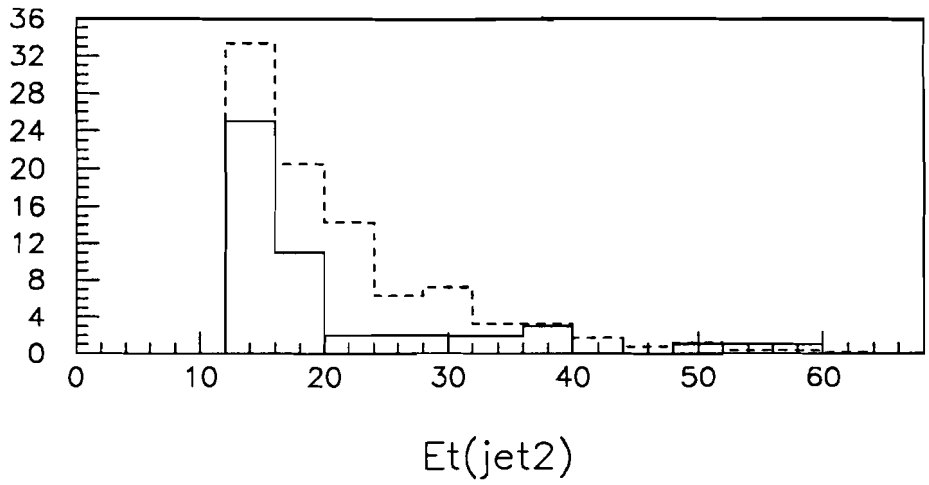

Figure 5.19: E_T distribution of the second leading jet in $Z^\circ + \geq 2$ jet events (electrons and muons, solid line) compared to the $Z^\circ \rightarrow ee$ in the Isajet Montecarlo (dashed line).

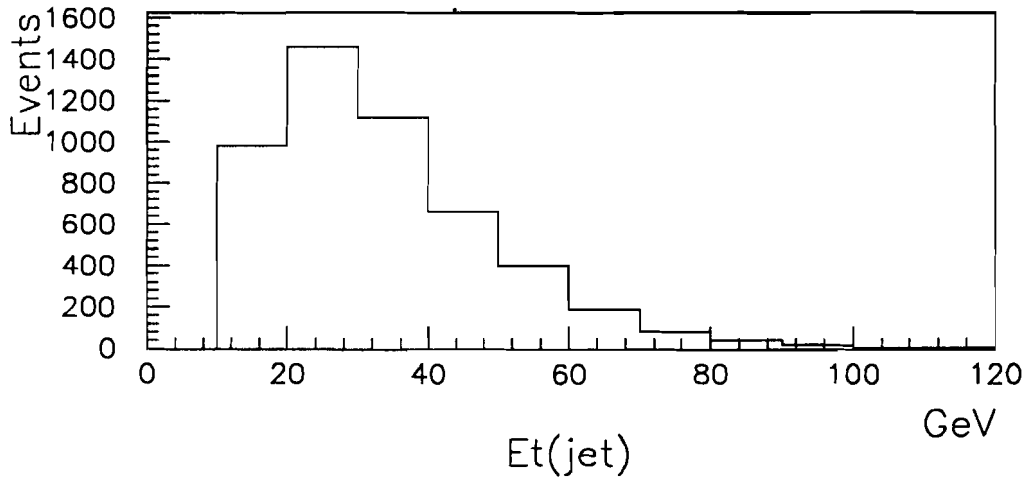

Figure 5.20: E_T distribution of central jets in b enriched events (containing a good quality non-isolated lepton).

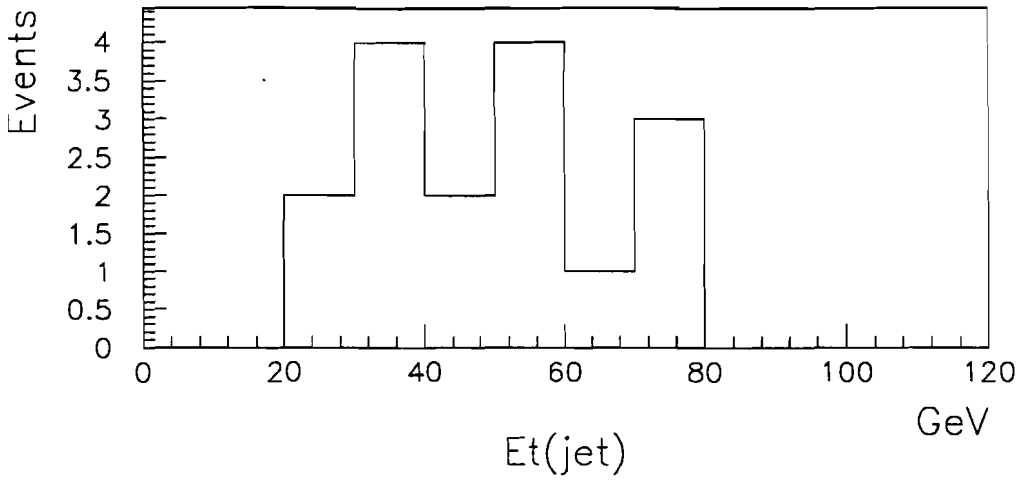

Figure 5.21: E_T distribution of tau candidate jets in b enriched events (containing a good quality non–isolated lepton).

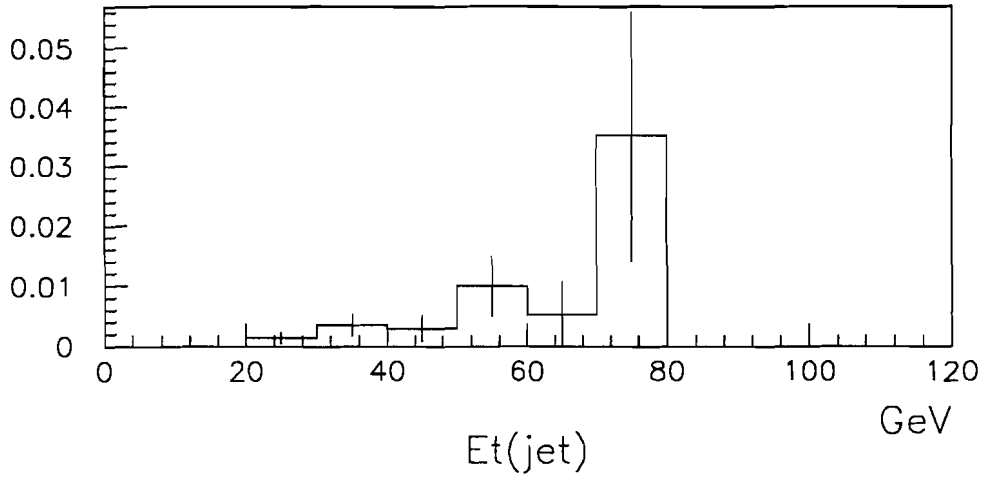

Figure 5.22: Probability for a jet to be identified as a tau, as a function of the jet E_T, in b enriched events.

Chapter 6

Search for top candidates

6.1 The event sample selection cuts

We summarize here all the cuts we used to obtain the final sample of candidate events:

- A lepton (e o μ) with P_T> 20 GeV/c, which passes *standard* identification requirements for high quality leptons, as described in Chapter IV.

- A track at $|\eta| < 1.0$ with P_T> 20 GeV/c for electron and muon candidates and with P_T> 15 GeV/c for tau candidates, isolated in the CTC: $\sum P_T$ (R=0.4) < 0.1 × P_T(track). This track has been then classified as electron, muon or tau based on the calorimeter energy deposit:

  - electron: 0.5 < E(elm)/p < 2.0, E(elm)/E(tot) > 0.8.
  - muon: E(elm) < 2.0 GeV, E(had) < 5.0 GeV,
    either E(elm)>0.05 GeV or E(had) > 0.5 GeV.
  - tau: E_τ/P > 0.5.

- Corrected missing energy: $\not\!\!E_T$ > 25 GeV.

- The first two leading jets in the event must have E_T(corrected) > 15 GeV and $|\eta(jet)| < 2.0$.

6.2 The ee, $\mu\mu$ channels

In the ee and $\mu\mu$ channels we required the invariant mass of the two leptons to be out of the Z° region: $75 < M(\ell^+\ell^-) < 105$ GeV/c^2. After applying this cut there is no candidate event left in the ee channel. In the $\mu\mu$ channel we have instead 1 candidate event. The invariant mass of this event is $M(\mu,\mu) = 136$ GeV/c^2. Its characteristics are summarized in table 6.1.

Run 47311 Event 71056	Charge	P_T(GeV/c)	ϕ (deg)	η
Lepton μ (CMX)	–	52.6	175	-0.76
Track μ (CMP)	+	108.5(71.2)	344	-0.20
$\not\!\!E_T$		95.2 (64.8)	196	
Jet 1		65.5	53	-0.20
Jet 2		20.8	238	1.02
Mass M(ll)		136(126)		

Table 6.1: $\mu\mu$ candidate event characteristics. The jet energy and missing energy have been corrected. The values between parentheses have been obtained using the SVX information to measure the momentum of the track–lepton candidate.

This event has been studied in details. The first muon has been detected by the CMX system. The second muon has been detected by the CMP chambers only, at a larger radial distance. It traversed a detector region where CMU was not instrumented (the central muon chambers CMU are located on the back of the wedges which form the calorimeter, and among the wedges there are some regions which are not instrumented). The reconstruction of both high P_T tracks is made difficult by the fact that there are many tracks in the VTX. The probability that one of these tracks gets misreconstructed is high. The VTX reconstructs several vertices in the event, very close to each other.

The error on the measurement of the track curvature, based on the information of the CTC only, is estimated to be about 13%. However there are indications that the error on the P_T measurement could be much larger. If one takes into account the SVX information to measure the track momentum, a track with $P_T = 108$ GeV/c in the CTC gets a $P_T = 71$ GeV/c. If one uses the information from the primary vertex position

to determine the P_T, there is an additional uncertainty because of the ambiguity in the vertex determination.

The two muons are almost back to back in azimuth. This configuration is typical of several kinds of background. The uncertainty in the muon reconstruction is reflected on the missing energy determination, which varies according to the software version used. The missing energy is parallel to one of the muons (as one could expect). The uncertainty on the momentum measurement is transferred also on the measurement of the two tracks invariant mass. The whole of these informations makes uncertain the quality of this event. We do not consider it as a good top candidate.

As described in Chapter 3.5, we expected in the ee and $\mu\mu$ channels some background due to misreconstructions. These detector effects are very difficult to quantify. Therefore for the top search it is preferable not to rely on such problematic events. At the same time the question appears about how to treat in the future this kind of events. With a larger data sample expected from the next data taking (1994), the number of events with ambiguous characteristics due to reconstruction problems will be larger. It will be necessary (and it will be possible, with more statistics) to improve the analysis in the ee and $\mu\mu$ channels. One might study the angular correlations among muon direction, missing energy vector and jets. It might be necessary to require that at least one jet is identified as a b quark ("*b tag*").

In the study described in this thesis we decided not to use these channels further, since they are certainly interesting but problematic.

6.3 The $e\mu$ channel

After applying the cuts described in paragraph 6.1, there is only one candidate event in the $e\mu$ channel. This event contains a muon which passes the standard identification cuts and an isolated track which is identified as an electron candidate. This event enters our sample thanks to the loose requirements on the electron qualities. The electron would not

pass the standard cut on the energy fraction deposited in the hadronic compartment of the calorimeter (E(had)/E(elm) = 0.06 is observed, while the standard cut is E(had)/E(elm) < 0.05) and the χ^2 cut on the electromagnetic shower profile measured in the *strip chambers* ($\chi^2 = 20$ is observed, while the cut is $\chi^2 < 15$). The event characteristics are reported in table 6.2

Run 45047 Event 104393	Charge	P_T(GeV/c)	ϕ (deg)	η
Lepton μ	-	45.5	116	-0.36
Track e	+	22.6	251	0.42
$\not\!\!E_T$		130.4	313	
Jet 1		71.9	117	-1.2
Jet 2		33.9	117	0.91
Mass M(ll)		65		

Table 6.2: $e\mu$ candidate event characteristics.

This event has kinematical characteristics compatible with top decay: large missing energy, leptons and jets well separated from each other. On the other hand, the muon has the same ϕ as the two jets. Therefore we considered the possibility that the muon could be a misidentified hadron. The muon has been studied in detail. It resulted to be of very good quality. The jets are energetic and central. In figure 6.1 we show the distribution of E_T(jet2) versus E_T(jet1) obtained from Isajet Montecarlo for top events with two leptons in the final state (M_{top} = 170 GeV/c^2). For comparison the energy values of the two jets in the candidate event have been indicated.

6.3.1 The expected background

In Chapter V we described the probability calculation for a QCD jet to fluctuate and be wrongly identified as a lepton, as a function of the jet E_T. The probability for the electrons was $\approx$ 0.1 % per jet.

The background due to tracks wrongly identified as electrons comes predominantly from the W(μ) + $\geq$ 3 jets sample, where one of the jets at $|\eta| < 1.0$ fragments and interacts in the detector in such a way as to be interpreted as an electron. The W(μ) + $\geq$

3 jet events, selected requiring $E_T(\text{jet}) > 15$ GeV and $|\eta|(\text{jet}) < 2.0$, are 47. In figure 6.2 we show the E_T distribution of the jets at $|\eta| < 1.0$ found in these events (84 jets). These jets could potentially mimic electrons. We evaluated the contamination of our sample from the fake lepton background applying the probability function obtained in Chapter V (figure 5.18) to the E_T distribution of central jets in $W(\mu) + \geq 3$ jet events, shown in figure 6.2. We found a prediction of 0.03 ± 0.02 background events with a real muon and a fake electron.

Concerning the background from tracks wrongly identified as muons, we calculated in Chapter V the probability for a track to appear as a muon using a sample of QCD jets. We compared the number of isolated minimum ionizing tracks to the number of non–isolated tracks in that sample. The different method with respect to electrons was necessary because fake isolated muons do not appear as jets.

Nevertheless, the muon background estimate is relatively more complicated. If a jet fragments and interacts in the calorimeter in such a way as to fake an isolated muon, no jet will be observed in the calorimeter. To estimate the frequency of these cases one can base the background estimate on a sample of $W(e) + 3$ jet events, where one can isolate cases of $W(e) + 2$ jets $+ \mu$. However, it is still possible that a large jet "splits" into a fake muon and a smaller residual jet. For these cases one would use the W + 2 jet sample for the background estimate. We did a conservative overestimate of the background by using the $W(e)$ + "at least" 2 jet events. In these events we looked for non–isolated tracks and found 60 tracks. Combining this number with the ratio found in Chapter V ($R = 0.0016 \pm 0.0009$) we obtain the number of expected electron + fake muon track events: 0.10 ± 0.05. This result is reported in table 6.3, with the result obtained when requiring the jets to be at $|\eta| < 2.0$: 0.06 ± 0.03.

The background from $b\bar{b}$ pair production has been estimated in Chapter V using a sample of non–isolated leptons (enriched in b quarks). We found that b enriched jets do not have an appreciably larger probability to correspond to an isolated track, compared to QCD jets. The contribution from this kind of background is included in the fake lepton

$e + \mu$ channel	Lepton+Track+$\not\!\!E_T$	+ 2 jets	+ $\|\eta$(j1,j2)$\|$ <2.0
$e + \mu$ track		0.10 ± 0.05	0.06 ± 0.03
$\mu + e$ track		0.04 ± 0.01	0.03 ± 0.02
WW	1.1 ± 0.2	0.14 ± 0.04	0.11 ± 0.03
WZ	0.14 ± 0.03	0.04 ± 0.02	0.02 ± 0.01
Z→ $\tau\tau$		0.05 ± 0.04	0.03 ± 0.03
Total:			0.25 ± 0.06

Table 6.3: Expected events from the various sources of background in the $e\mu$ channel, under different cuts.

background calculation which has been obtained from the QCD jet sample.

The WW, WZ and Z $\rightarrow \tau\tau$ backgrounds were computed using the absolute prediction from the Isajet Montecarlo. All the contributions have been reported in table 6.3. The total background was obtained by adding linearly the different contributions. The error on the total background was obtained by adding in quadrature the errors on the single background sources. The main background contribution in the $e\mu$ channel comes from the WW pair production process.

Overestimating some of the background contributions is acceptable in the adopted strategy of identifying a signal rather than inferring a lower limit on the top mass. Indeed, it puts us in a conservative position. The significance of observing 1 event over an expected background of 0.25 ± 0.06 will be discussed later (paragraph 6.6).

In figure 6.3 we show on a logarithmic scale the second leading jet E_T distribution which is expected from background. The various contributions from each background source have been normalized to the number of expected events and added. The contribution from fake electrons has been obtained using the jet distribution shown in figure 6.2. For each jet we determined the probability as a function of jet E_T that the jet be identified as an isolated electron candidate. We used this probability to weight the event. The integral of distribution 6.3 corresponds to the total expected background. We also show in the plot the position of the observed candidate event.

6.3.2 Top into $e\mu$ events predicted from Montecarlo

The number of $t\bar{t}$ events expected in the $e\mu$ channel was computed by applying the analysis cuts on various $t\bar{t}$ samples corresponding to different top masses, produced by the Isajet Montecarlo. The results are reported in table 6.4. The errors are statistical only. A further uncertainty of about 30% is due to the top production cross section. The cross section values have been obtained from reference [32]. The Montecarlo predicts O(1) events.

M(top)(GeV/c^2) :	140	150	160	170	180
σ(pb) : $e+\mu$ channel	16.9	11.7	8.16	5.83	4.21
Lepton+Track+$\not\!\!E_T$	2.1 $\pm$ 0.3	1.2 $\pm$ 0.2	0.9 $\pm$ 0.1	0.8 $\pm$ 0.1	0.59 $\pm$ 0.07
Et(jet2)>15 GeV	1.6 $\pm$ 0.2	1.1 $\pm$ 0.2	0.8 $\pm$ 0.1	0.66 $\pm$ 0.09	0.52 $\pm$ 0.07
$\|\eta\|$(jets)<2.0	1.55 $\pm$ 0.20	1.0 $\pm$ 0.2	0.75 $\pm$ 0.10	0.66 $\pm$ 0.09	0.50 $\pm$ 0.07

Table 6.4: Events expected from Montecarlo (Isajet) in the $e\mu$ channel for various cuts and top masses. Errors are statistical only.

6.4 The $e\tau$, $\mu\tau$ channels

After applying the cuts summarized in paragraph 6.1, we obtained 6 candidate events, 4 in the $e\tau$ channel and 2 in the $\mu\tau$ channel. The characteristics of these events are reported in tables 6.5 and 6.6. In these channels we expect the background from hadrons wrongly identified as taus to be larger than in the electron and muon cases. Also the Z° $\rightarrow \tau\tau$ background might be larger than in the $e\mu$ channel. The reasons can be traced to both the branching ratio of taus to a charged hadron (50%), which is larger than the branching ratio to electron or muon (18% in each channel), and to the track P_T cut which is lower than for electron and muon candidates ($P_T(\tau) > 15$ GeV/c). Finally, we expect a background contribution from the Z° $\rightarrow ee$ channel also, where one of the electrons is mismeasured and is interpreted as a tau.

1) Run 42727 Event 81408	Charge	P_T(GeV/c)	ϕ (deg)	η
Lepton e	−	47.4	109	-0.44
Track τ	+	34.4	187	0.23
$\not\!\!E_T$		31.3	273	
Jet 1		73.9	8	-0.02
Jet 2		29.6	235	-1.15
M(ll)		53.7		
2) Run 42899 Event 110482	Charge	P_T(GeV/c)	ϕ (deg)	η
Lepton e	+	70.7	148	0.10
Track τ	+	20.4	304	-0.26
$\not\!\!E_T$		25.7	197	
Jet 1		88.8	263	-0.20
Jet 2		79.4	46	-0.92
M(ll)		73.5		
3) Run 45880 Event 31838	Charge	P_T(GeV/c)	ϕ (deg)	η
Lepton e	−	27.6	255	0.16
Track τ	+	32.3	355	-0.18
$\not\!\!E_T$		80.1	137	
Jet 1		60.8	245	1.09
Jet 2		31.0	66	0.376
M(ll)		45.6		
4) Run 46935 Event 384578	Charge	P_T(GeV/c)	ϕ (deg)	η
Lepton e	−	51.3	179	-0.53
Track τ		+ 15.8	338	-0.21
$\not\!\!E_T$		33.5	100	
Jet 1		51.8	304	0.66
Jet 2		25.7	120	-0.91
M(ll)		63.2		

Table 6.5: Parameters of the 4 $e\tau$ candidate events.

1) Run 40732 Event 24012	Charge	P_T(GeV/c)	ϕ (deg)	η
Lepton μ	+	24.3	115	0.52
Track τ	-	16.0	295	-0.81
$\not\!\!E_T$		33.3	121	
Jet 1		23.3	353	0.14
Jet 2		22.9	213	-1.18
M(ll)		49.5		
2) Run 43139 Event 284949	Charge	P_T(GeV/c)	ϕ (deg)	η
Leptone μ	+	22.6	7	0.93
Track τ	-	37.4	30	0.41
$\not\!\!E_T$		42.9	230	
Jet 1		34.2	154	0.35
Jet 2		21.6	225	-1.08
M(ll)		19.5		

Table 6.6: Parameters of the 2 $\mu\tau$ candidate events.

Observations based on the "*CDF Display*"

The CDF tracking system is located inside a magnetic field. This gives the possibility to measure the lepton and track charge sign. We notice that in the second event reported in table 6.5 the tau candidate track has the same sign as the electron. This is not possible, if the event is due to a standard top decay and if the detected leptons come from the decay of the two W's.

The probability to have two high P_T isolated leptons with the same sign from top decay is $\sim$ 4% and does not depend on the top mass. The electromagnetic shower parameters and the E/p ratio for this event are excellent. The tau candidate track is of good quality. The energy deposited in the tower traversed by the track is about 10 GeV (4 in the electromagnetic compartment and 6 in the hadronic compartment). There is a large energy deposits in the adjacent towers. Including these towers in the tau definition this track has been identified as a tau candidate. One of the remaining jets is rather close to the tau candidate jet (ΔR = 0.57). This suggests that it could come from b decay.

Concerning the third event in the list, observing a lateral view of the event in the

$z - \phi$ plane, we notice that the tau candidate track hits the electromagnetic calorimeter very close to a crack.

6.4.1 The expected background

In Chapter V we computed the probability that a QCD jet be identified as a tau lepton, in analogy to what we did for the electrons. We evaluated this probability as a function of the jet E_T and we found a value of $\approx 0.6\%$ per jet.

The background due to isolated tracks wrongly classified as taus is due primarily to W + $\geq$ 3 jet events, where one of the jets at $|\eta| < 1.0$ fluctuates and is identified as a tau, with a probability which depends on its transverse energy. The W + $\geq$ 3 jet events (in both $W \rightarrow e\nu$ and $W \rightarrow \mu\nu$ channels) were selected requiring at least 3 jets with $E_T >$ 15 GeV at $|\eta| < 2.0$. They are 128. In figure 6.4 we show the E_T distribution of the jets at $|\eta| < 1.0$ (239 jets), which can give origin to a fake tau.

We obtain the absolute value for the expected background in our sample applying the probability function found in Chapter V (figure 5.9) to the jet E_T distribution in W + $\geq$ 3 jet events shown in figure 6.4. The prediction for events with a good electron (or muon) and a track wrongly identified as tau is 0.8 ± 0.3 events.

The background from WW and WZ pair production and the background from Z^0 decaying to $\tau\tau$ or ee (where one of the electrons is mismeasured and identified as a tau) were estimated using the Isajet Montecarlo, as described in Chapter V. In contrast to the $e\mu$ channel, in the $e\tau$ and $\mu\tau$ channels the background from WW pair production represents the smallest contribution.

The backgrounds from the various sources have been summarized in table 6.7.

In figure 6.5 we show the E_T distribution of the second leading jet, expected from background. The contribution from fake taus has been evaluated in analogy to what was done for the distribution in figure 6.3. The various background contributions have been added after normalizing to the absolute number of expected events. Therefore the integral of the distribution corresponds to the absolute value of the expected background for the

Channel $e/\mu + \tau$	Lepton+Track+2 jets	+ $\|\eta(j1,j2)\|$ <2.0
Fake leptons	1.0 ± 0.4	0.8 ± 0.3
WW and WZ	0.14 ± 0.04	0.12 ± 0.03
$Z^\circ \to \tau\tau$	0.7 ± 0.2	0.6 ± 0.2
$Z^\circ \to ee$	0.6 ± 0.2	0.5±0.2
Total:		2.0 ± 0.4

Table 6.7: Events due to the several sources of background in the $e\tau$ and $\mu\tau$ channels, under different cuts. The errors are statistical only.

M(top)/GeV/c^2 :	140	150	160	170	180
σ/pb : Channel $e/\mu + \tau$	16.9	11.7	8.16	5.83	4.21
Lepton+Track+$\not\!\!E_T$	1.0 ± 0.2	0.75 ± 0.1	0.65 ± 0.10	0.42 ± 0.07	0.32 ± 0.05
Et(jet2)>15 GeV	0.8 ± 0.2	0.7 ± 0.1	0.50 ± 0.09	0.40 ± 0.07	0.27 ± 0.06
$\|\eta\|$(jets)<2.0	0.8 ± 0.2	0.6 ± 0.1	0.45 ± 0.09	0.35 ± 0.07	0.25 ± 0.06

Table 6.8: Number of events predicted by the Isajet Montecarlo in the $e\tau$ and $\mu\tau$ channels, for different top masses and various cuts. The errors are statistical only.

$e\tau$ and $\mu\tau$ channels, which is 2.0 ± 0.4 events. The black circles with the statistical errors show the six observed events.

6.4.2 Top into $e\tau$, $\mu\tau$ events predicted from Montecarlo

In order to extract the number of top events expected in the $e\tau$ and $\mu\tau$ channels, we used the data samples generated by Isajet, for different values of the top mass. We applied all the analysis cuts to the Montecarlo samples, and used the cross section values from reference [32]. The results are reported in table 6.8.

6.5 Search for beauty jets in the candidate events

Wa can have more information on the nature of the candidate events by looking for some evidence of the presence of b quarks. CDF developed two methods to identify b in jets (they are called b "*tagging*" methods).

One method consists in looking for relatively low P_T electrons or muons inside the

jets. These low P_T leptons are supposed to come from b quarks through the decay $b \rightarrow l$ ($l = e$ or μ) and $b \rightarrow c \rightarrow l$. The minimum P_T threshold for these leptons is 2 GeV/c. The efficiency of this tagging method is about 16% and is slowly varying in the top mass region of interest ($140 \div 180$ GeV/c^2). The background due to a wrong track identification has been estimated to be of the order of 1% per track. We will refer to this method as the SL ("*Soft Lepton*") [75], [76].

Another method which CDF can use is the search for secondary vertices in the plane transverse to the beam, exploiting the information from the silicon vertex detector (SVX). Because of the relatively long lifetime of the B mesons, tracks corresponding to particles from B decay originate in general at a measurable distance from the primary interaction vertex. The SVX measures four points along the track at a few centimeters from the beam, with a resolution of the order of 15 μm. Therefore the displacement (which is of the order of a hundred μm) can be measured and secondary decay vertices can be found. The efficiency of this kind of *tagging* in top events is about 22% and does not depend on the top mass in the region of interest. The background due to fake secondary vertices is of the order of 2% per jet contained in the SVX. However it depends on the jet E_T, multiplicity and position in the detector. This mean value was obtained studying a sample of QCD jets which may contain a small component of real b quarks. Therefore it is inclusive of signals due to errors and to "non–relevant" b's. CDF developed three different SVX tagging algorithms [75]. We will refer to them as JSVX (*Jetvtx*) [77], JP (*Jet Probability*) [78] and Dϕ [79].

We looked for some evidence of b quarks in the selected events. In table 6.9 we report the results obtained using the three different SVX algorithms and the *Soft Lepton* method. In the table we reported also the position of the primary vertex along the z axis (we remind that only events at $|z| < 25$ cm are inside the vertex detector acceptance).

Concerning the $e\mu$ candidate, the JSVX algorithm reconstructs a secondary vertex in the leading jet, the D–ϕ algorithm in the second leading jet, and the JP algorithm in both

N run – N event	Channel	z (cm)	JSVX	JP	Dϕ	SL
45047 – 104393	$e + \mu$	7.5	$\star$	$\star\star$	$\star$	
40732 – 24012	$\mu + \tau$	12.2				
43139 – 284848	$\mu + \tau$	34.5				
42727 – 81408	$e + \tau$	-6.3				
42899 – 110482	$e + \tau$	8.3	$\star$	$\star$	$\star$	
45880 – 31838	$e + \tau$	-17.0				$\star$
46935 – 384578	$e + \tau$	6.0				

Table 6.9: b quark content of the candidate events selected in the dilepton channel.

jets. The study done with the vertex detector also showed that the electron candidate track has a relatively large impact parameter (about 300 μm) and appears to be clearly displaced from the primary vertex.

Concerning the $e\tau$ and $\mu\tau$ channels, a secondary vertex has been identified in one event only. It is the event where electron and tau candidates are like–sign. The two high P_T tracks corresponding to the e and τ are both displaced with respect to the primary vertex (they have an impact parameter of the order of 100 μm). Although the dilepton charge signs are not typical of the $t\bar{t}$ process, its kinematical properties (energetic jets and b–tag) are hardly interpreted in terms of background.

Finally, one of the $e\tau$ candidate events contains a *SL tag*, which is a 2.5 GeV electron inside a jet.

6.6 Interpretation of the result

We observe a slight excess of events in the $e\mu$, $e\tau$ and $\mu\tau$ channels, with respect to the expected background. In the $e\mu$ channel we observe 1 event, with an expected background of 0.25 ± 0.06 events. In the $e\tau$ and $\mu\tau$ channels we observe 6 events, with a total expected background of 2.0 ± 0.4 events.

Separately in the $e\mu$ channel and in the $e\tau$–$\mu\tau$ channels we calculated the probability that the estimated background has fluctuated up to the number of observed candidate events or greater. This calculation is done using Poisson statistics where the mean is

Expected (m ± Δm):	1±0.2	2±0.4	3±0.6
P(N), N=6 (%)	0.08	2.1	9.5
P(5) (%)	0.5	6.0	19.4
P(4) (%)	2.1	15.0	35.3
P(3) (%)	8.4	32.4	56.5

Table 6.10: Probability to observe $\geq$ N events from the background when m ± Δm are expected.

given a Gaussian smearing in order to account for the error on the expected background events.

In the $e\mu$ channel, the probability to observe 1 or more background events when we expect 0.25 ± 0.06 is 22%. In the $e\tau$ and $\mu\tau$ channels, the probability to observe 6 or more background events when we expect 2.0 ± 0.4 is 2%.

As was discussed and justified in Chapter V, the background calculation for fake muons is conservative. In addition, the Isajet Montecarlo may overestimate the expected background because it appears to predict more jet activity than experimentally observed, (as was shown by comparing the jet E_T distribution in Z° generated by Isajet and real data in paragraph 5.3). Therefore we think that the background contributions obtained from Isajet are also conservative. We want to analyze better how the significance of the observed excess depends on the background calculation, and how many signal events are likely to be in the sample. For this reason we calculated the probability to observe a certain number of events (from the background) varying the expected background value. The results are shown in table 6.10.

Since we made conservative background estimates, the observation of an excess of events over the background in two different channels is more significant than what it would have been in one channel only. On the other hand, a possible signal which points out the presence of some top quarks must be discussed with a conservative attitude. Therefore we would like to use more information before coming to any conclusion.

The $e\mu$ candidate event shows evidence of a secondary vertex from b decay in two jets. Also one of the $e\tau$ candidate events contains a secondary vertex.

In figure 6.6 we show the distribution of the E_T of the second leading jet versus the transverse missing energy for the candidate events. The two events which contain secondary vertices have been indicated. In figure 6.7 the same distribution is shown for the processes which contribute most of the background. Figure 6.7 c) has been obtained using a sample of W + $\geq$ 3 jet events. For each jet we determined the probability as a function of jet E_T that the jet be identified as an isolated lepton candidate. We used this probability to weight the event (this is the same procedure used to obtain the fake lepton background in figures 6.3 and 6.5).

The largest contribution to the background in the $e\mu$ channel comes from WW pair production. The Isajet Montecarlo predicts only 2.$\pm$2.% of the WW events to have a missing energy greater or equal to that of the observed $e\mu$ event (compare figure 6.7 b)).

The main contribution to the background in the $e\tau$ and $\mu\tau$ channels comes from Z° decays and fake leptons. We observe in figures 6.7 a) and c) that the distribution in $\not\!\!E_T$ versus E_T of the second jet for these processes contains only few events in the kinematical region where the candidate events with a secondary vertex are found (figure 6.6).

The two events with secondary vertices are compatible with the top hypothesis. However some of their characteristics are not typical of top events. More statistics available will be crucial for detailed studies of the candidate events properties and check that they behave in average as expected.

Concerning the observation of secondary vertices in the SVX, the probability that a secondary vertex is reconstructed inside a jet has been estimated as a function of the jet E_T, its track multiplicity and its position in the detector, as already mentioned. Assuming a probability of 2% per generic jet per algorithm is rather conservative. We have 7 events, with a total of 14 jets. In 2 of these 7 events secondary vertices have been reconstructed. We find an expectation of 0.3 background events with a reconstructed fake vertex in the sample of candidate events, while we observe 2. The probability to observe 2 or more cases when we expect 0.3 is 4.%. This value is conservative, because we did not take into account the fact that in one of the two events there are two secondary vertices. A

background event with these characteristics is very rare.

The expected number of *b tags* was calculated on the base of the observed events, which are found to be more than expected from background. The probability to observe an excess of events is independent of the probability to observe two *b tags*.

Finally, one of the $e\tau$ candidate events contains a *SL tag* in a jet. This is also not very likely in such a small sample of events, if their jets were "generic" jets.

Taking into account the above considerations, we conclude that the global picture is in favour of the interpretation that a few top quark events are present in the sample.

6.7 Comparison with the result in the single lepton channel

Looking for a confirmation of the above indication, we compared it with the result of the analysis done in the channel with one charged lepton, one neutrino and hadronic jets in the final state [66].

The direct comparison of the two analyses was made easier by the fact that many of the applied selection cuts are the same. In the single lepton channel an additional cut on the $|cos\theta^*|$ of the jets has been applied ($|cos\theta^*| < 0.7$). This cut reduces by 50% the top signal but allows to reduce by a factor of 3.5 the background from W produced in association with QCD jets. We calculated from Montecarlo the relative efficiency of the analysis in the dilepton channel with respect to the single lepton channel. This efficiency is $29 \pm 4\%$.

The single lepton channel analysis selected a data sample of 15 events, with an excess of about 10 events over expectation from QCD background.

The 10 events observed in the single lepton channel are consistent with 2–3 events to be observed in the dilepton channel.

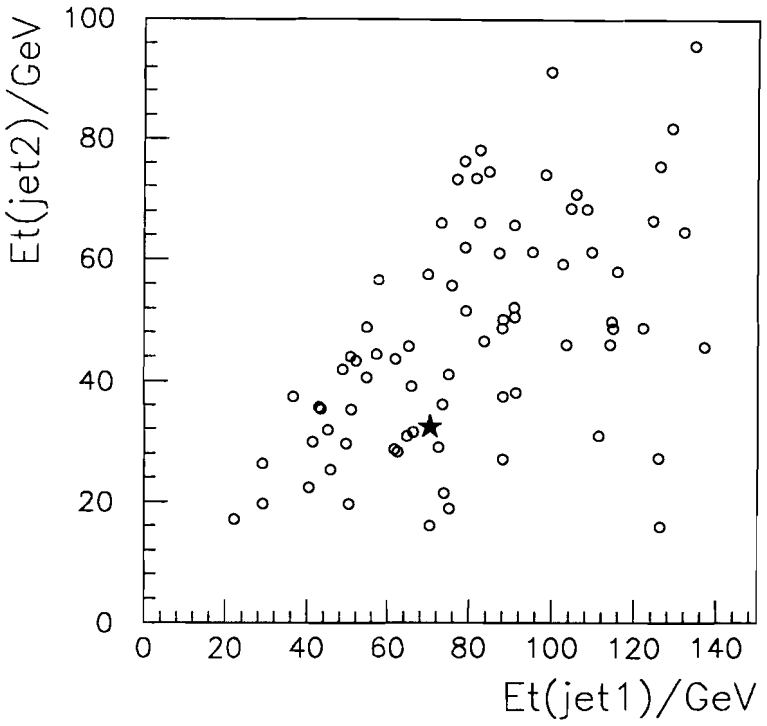

Figure 6.1: E_T distribution of the two leading jets in top events with two charged leptons in the final state (Montecarlo Isajet, M_{top} = 170 GeV/c^2). The star indicates the representative point of the $e\mu$ candidate.

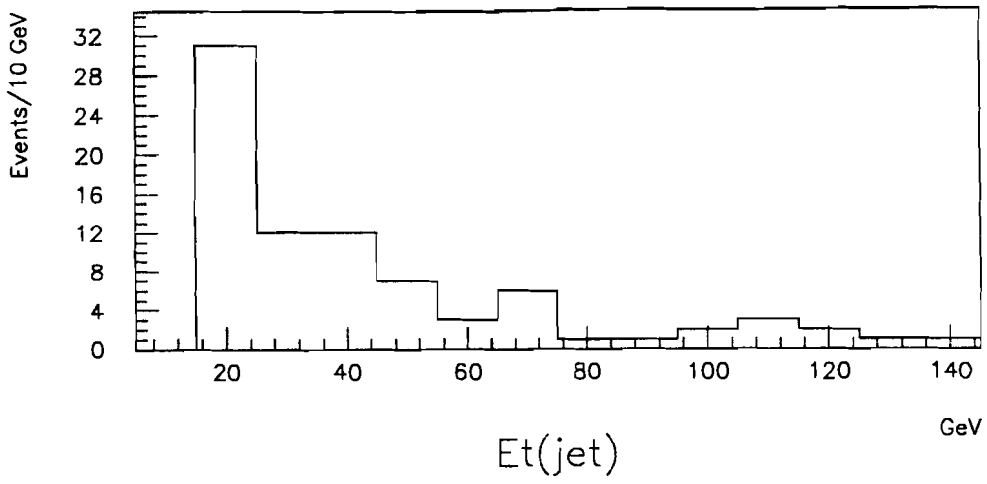

Figure 6.2: E_T distribution of the jets at $|\eta|< 1.0$ in W(μ) + 3 jet events.

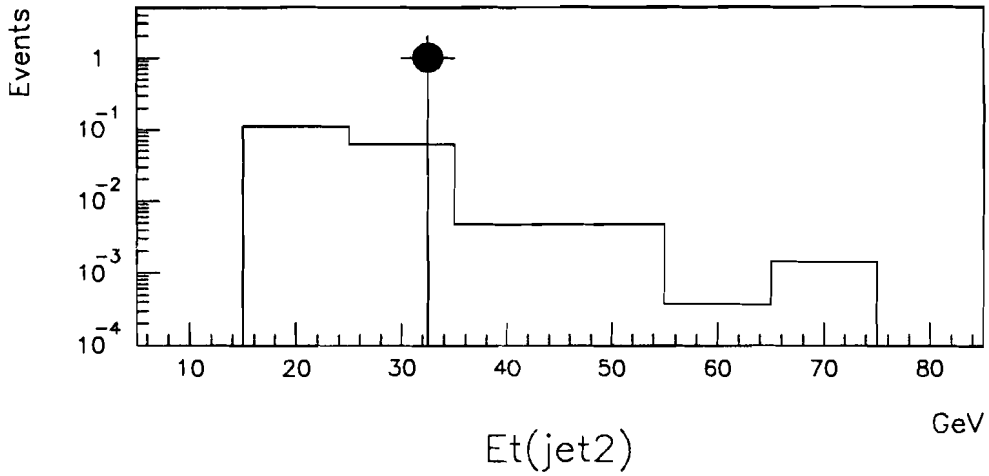

Figure 6.3: E_T of the second leading jet in the $e\mu$ candidate event, compared to the E_T distribution of the overall background (solid line).

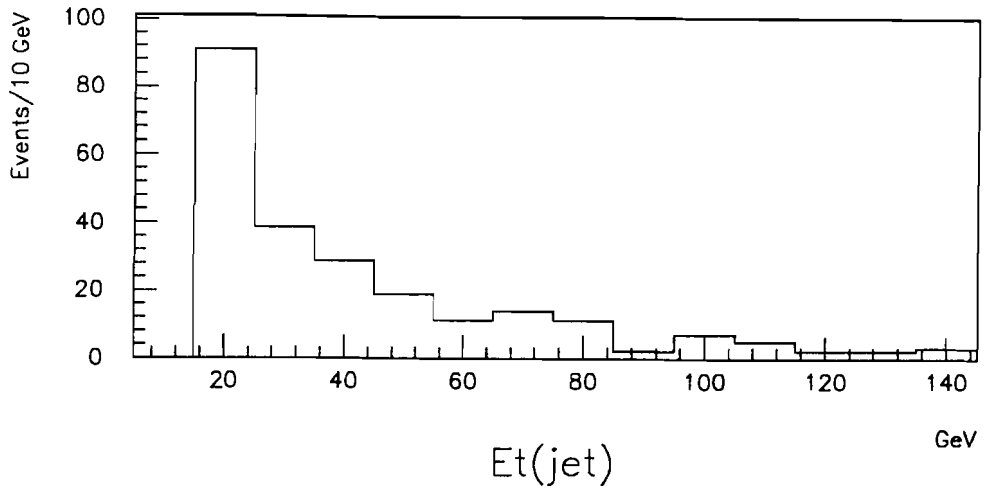

Figure 6.4: E_T distribution of the jets at $|\eta| < 1.0$ in W + 3 jet events.

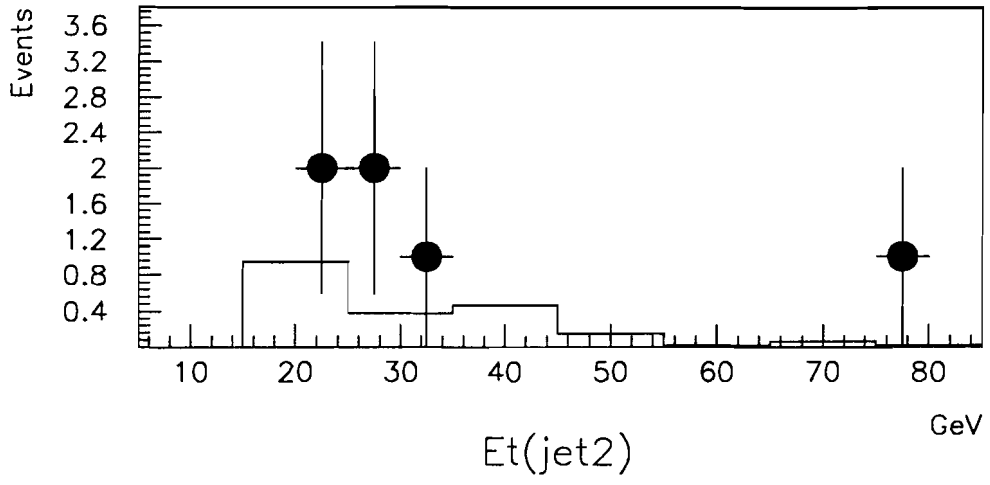

Figure 6.5: E_T distribution of the second leading jet in $e\tau$ and $\mu\tau$ candidate events, compared to the E_T distribution of the overall background (solid line).

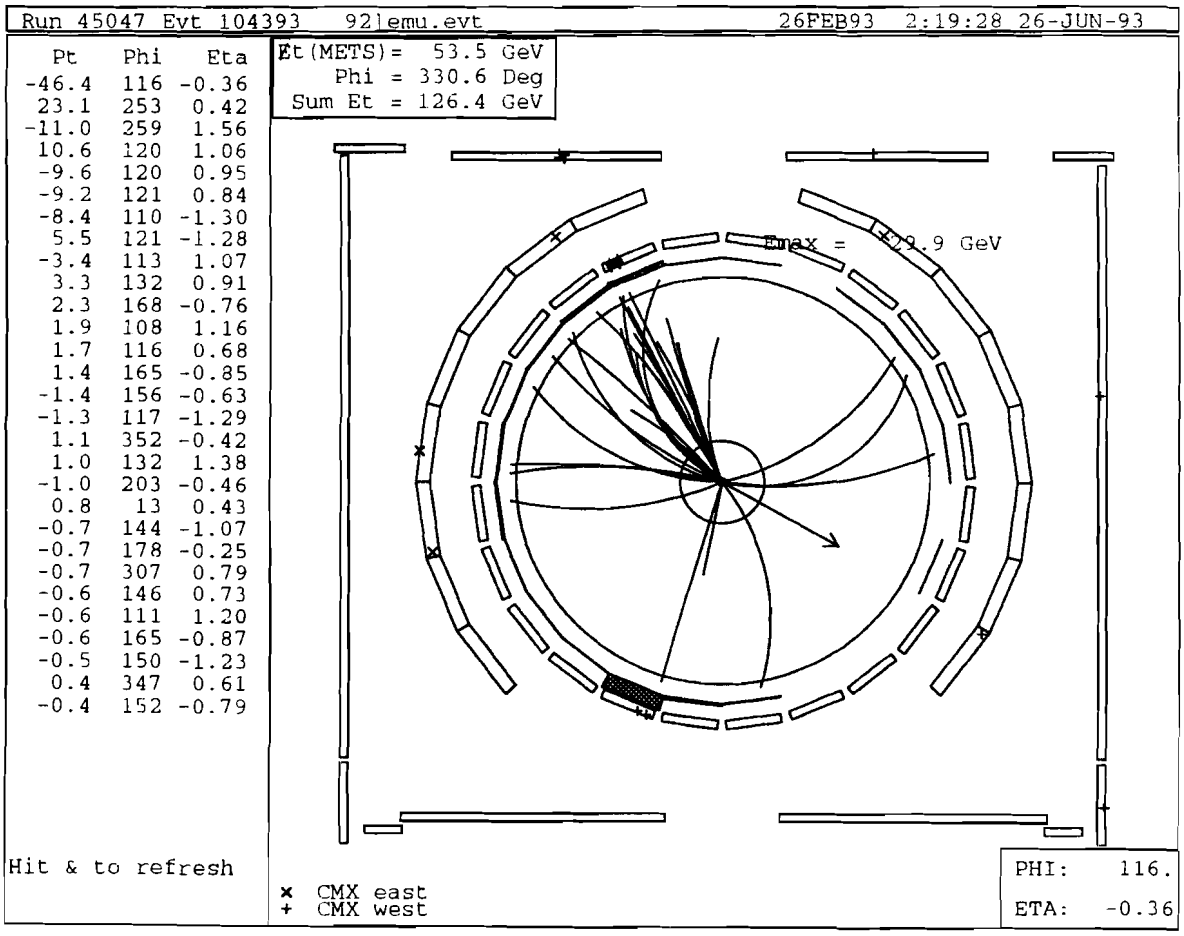

Figure 6.8: "*CDF Display*" of the CTC and the muon detectors for the $e\mu$ candidate event.

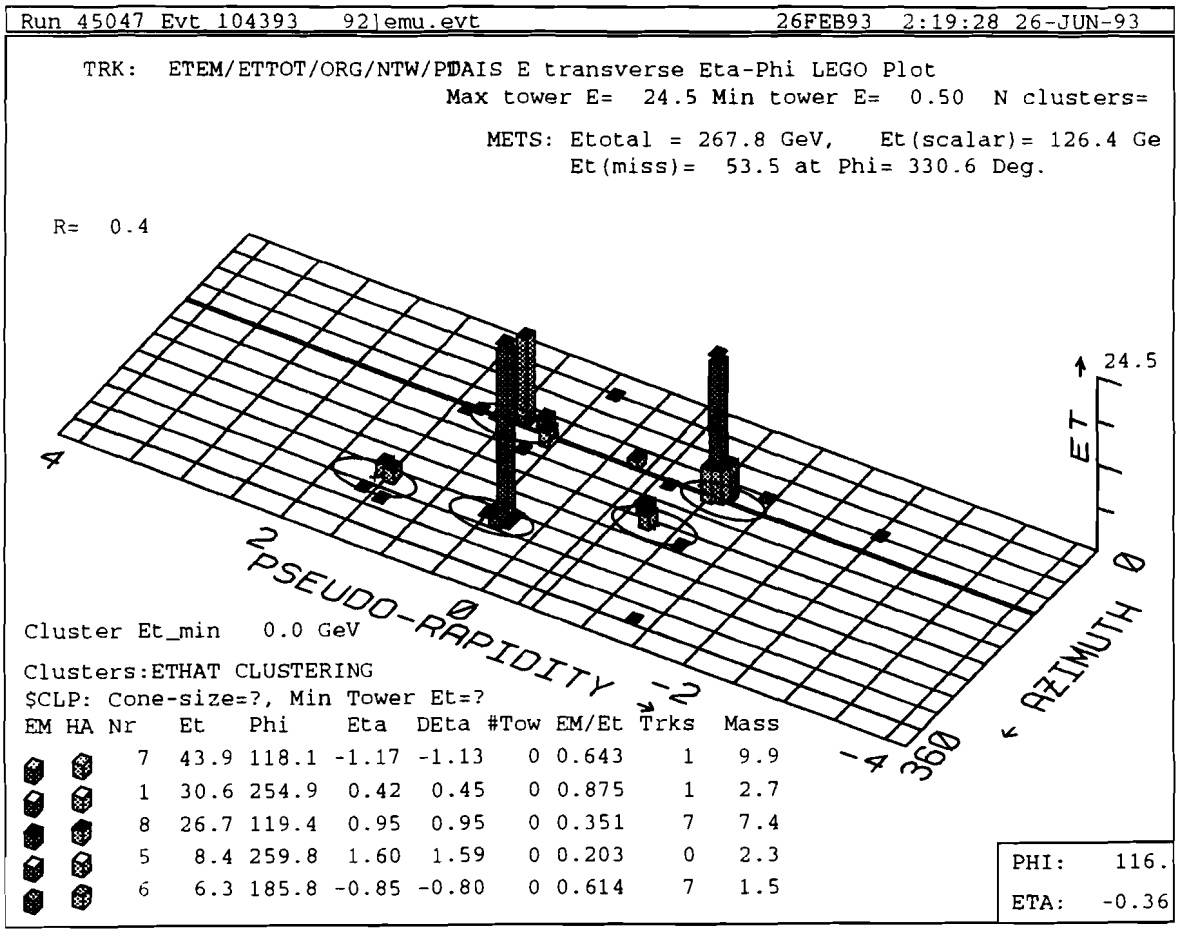

Figure 6.9: "*CDF Display*" of the *Lego* plot for the $e\mu$ candidate event.

Conclusions

In this thesis we described a top quark search in the channel where both tops decay semileptonically ($e\mu$, $e\tau$, $\mu\tau$ channels). The analysis has been extended for the first time to the $e\tau$ and $\mu\tau$ channels.

We observed 1 event in the $e\mu$ channel, over an expectation of 0.25 ± 0.06 events from background, and 6 events in the $e\tau$ and $\mu\tau$ channels over an expectation of 2.0 ± 0.4 events from background.

Considering only the number of observed events, there is already some evidence of a signal. This indication is strengthened when considering that some fraction of the expected background has been evaluated using a Montecarlo (Isajet) which appears to overestimate the gluon radiation.

We looked for evidence of b quarks in the selected sample. The $e\mu$ candidate event contains two secondary vertices detected by the SVX. One of the $e\tau$ candidates contains a secondary vertex, another one contains a *soft lepton* tag.

These three "b-tagged" events have kinematical characteristics – large transverse missing energy and/or large jet transverse energy – compatible with being from top decay. However, one of them has equal-sign leptons, which is not likely – albeit possible – for a $t\bar{t}$ decay.

The probability that the observed excess of events, as well as the excess of secondary vertices, are due to a background fluctuation is small.

In conclusion, the sample of events with two isolated high P_T leptons which we selected is unlikely to be explained in terms of the known background. In the context of the Minimal Standard Model, the natural explanation which is left for the excess of events is

that some of them are due to $t\bar{t}$ pair decays.

Given the few events observed in the 1992–1993 run with 21.4 pb^{-1} integrated luminosity, the expected data for the 1994 run of about 75 pb^{-1} should just be enough to clarify the situation and reach a conclusive statement.

Appendix A

Discussion of the $e\mu$ events selected by a different line of analysis

A group of CDF collegues made an independent analysis, also searching for the top quark in the channel with two high P_T leptons in the final state. Their analysis addressed the $e\mu$, $\mu\mu$ and ee channels. The results of that analysis have been presented in public several times and submitted for publication. We will refer to it as the "official analysis" [34], [75].

They observe 2 candidate events in the $e\mu$ channel with an expectation of $0.56^{+0.25}_{-0.13}$ events from the various backgrounds. There are no candidate events in the $\mu\mu$ and ee channels.

There is no overlap between our $e\mu$ event and the two $e\mu$ events in the official sample. We asked ourselves::

1) if we can improve our analysis applying some of the cuts of the official analysis;

2) how the official top candidate events behave with respect to our sample of events, and if we could accept one of or both the official events by modifying in a simple way the cuts of our analysis.

The characteristics of these two events are summarized in the following table.

The main differences between the two analyses are:

1) The official analysis applies a cut on the minimum distance $\Delta\phi$ between $\not\!\!E_T$ and

Run 41540 Event 127085	Charge	P_T(GeV/c)	ϕ (deg)	η
Electron	−	22.6	32	0.84
Track μ	+	46.5	14	0.17
$\not\!\!E_T$		139.5	180	
Jet 1		139.6	352	0.11
Jet 2		61.5	215	-0.54
Jet 3		27.0	113	-2.94
Run 47122 Event 38382	Charge	P_T(GeV/c)	ϕ (deg)	η
Electron	+	49.4	25	0.93
Muon	−	33.9	4	-0.74
$\not\!\!E_T$		67.5	143	
Jet 1		89	218	0.64
Jet 2		20.3	344	-3.31
Jet 3		18.0	344	1.38

Table A.1: Characteristics of the two $e\mu$ candidate events of the official analysis.

leptons and between $\not\!\!E_T$ and jets, requiring $\Delta\phi > 20°$, for the events with $\not\!\!E_T < 50$ GeV.

This cut does not reject any event in the official analysis. It is used to decrease the expected background. If we apply this cut to our sample, we do not loose any of the three events which show some b decay evidence. On the other hand, the background expectation would decrease, so that the statistical significance of the result would increase.

2) the lepton isolation.

The official analysis defines an isolation cone of radius R = 0.25 for the leptons, and requires at least one of the two leptons to be isolated. We have a similar but more restrictive request, with a cone of R = 0.4. The event 41540–127085 is in that sample and not in ours for this reason. In the fake muon background calculation described in Chapter V we saw that the background increases when we do not require the track to be far from the jets. In order to better understand this behaviour, we used the isolation cut of the official analysis and we looked for muon candidates in the QCD jet sample. In figure A.1 we show the minimum ΔR (muon–jet). We see a component of muon-track candidates

close to jets. Clearly more background is accepted by a cut at $\Delta R = 0.25$ than at $\Delta R = 0.4$. These muons could come from b quark decays and be good muons. However, in our analysis we look for muons from W decays.

Applying our background calculation as described in Chapter VI, we find that the expectation from tracks wrongly identified as muons in W(e) + $\geq$ 2 jet events, when we define the isolation in a cone of radius R = 0.25 instead of R = 0.4, becomes about 0.6 events instead of 0.06. The efficiency for top events increases by only 10%. The event 41540–127085 has ΔR(muon–jet) = 0.38 and $\sum P_T$ (R=0.4) $\sim$ 40 GeV/c.

In the event 47122–38382 both leptons are of good quality and pass our isolation requirement. The event is not in our sample because we required the two leading jets to be at $|\eta| < 2.0$. We notice that there is a third central jet. If we compare the energy of the jets in this event with the distribution in figure 6.1 of the E_T of the second leading jet versus the E_T of the first jet, we see that an 18 GeV jet would be in the tail of the distribution, for a top of mass $M_{top} = 170$ GeV/c^2.

The event 45047–104393, $e\mu$ candidate in our analysis, is not in the sample selected by the official analysis. The electron candidate does not pass some of the electron identification requirements (see paragraph 6.3). However, this event is part of the sample selected by the official analysis in the single lepton channel, which requires one good quality lepton and at least 3 jets. In the analysis which looks for secondary vertices from b decays, the electron candidate is classified as a jet: the event appears as a W(μ) + 3 jets. The analysis which uses the *Soft Lepton* tag method to identify b's counts the electron candidate both as a *soft lepton* and as a jet. Therefore it classifies the event as a W(μ) + soft electron + 3 jets.

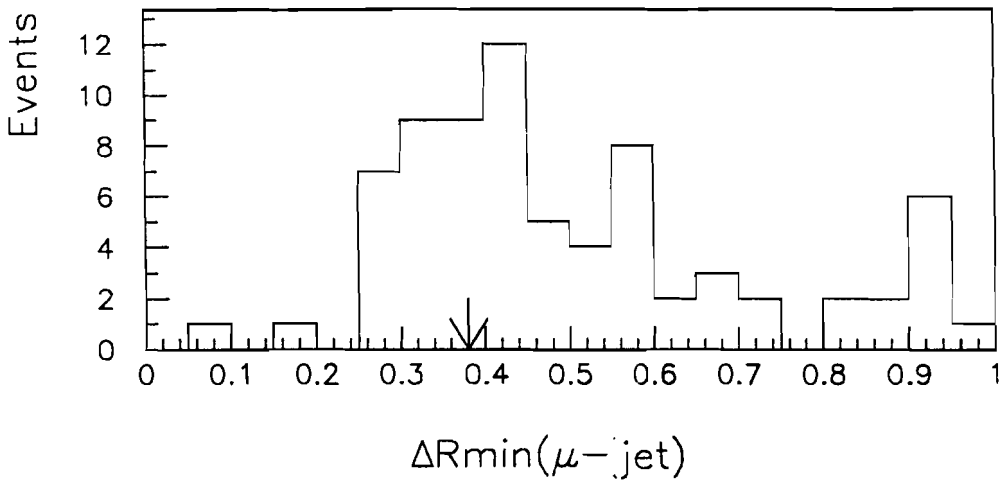

Figure A.1: Minimum distance between muon candidate tracks and jets in the QCD jet sample. The arrow indicates the position of event 41540–127085.

Appendix B

Test of the τ identification algorithm

As an example of the application of the tau identification algorithm described in this thesis, we briefly show a search for $Z^\circ \rightarrow \tau\tau$ events done by Michele Gallinaro and Hans Grassmann [80]. The process $Z^\circ \rightarrow \tau\tau$ has never been observed before in CDF. In their study they looked for events where one of the τ's decays to electron or muon and the other one decays to a charged hadron. They require the presence of a good quality, high P_T lepton (e or μ) and then look for tracks with $P_T > 5$ GeV/c, isolated in a cone of radius R = 0.7 around the track [1], and associated to a jet. The P_T track cut has been lowered with respect to the cut applied in this thesis, to increase the efficiency in the process under study. The lepton must be opposite in azimuth to the tau candidate jet. No other jet is allowed in the event, in addition to the tau jet.

The background study has been made in a very similar way to what was described in Chapter V. Several samples of jets have been used: QCD–JET50, QCD–JET20 and jets contained in events with a high P_T non–isolated muon. In these three samples it is assumed that the tau content is small. In figure B.1 we show the probability for a jet to contain an isolated track, as obtained from the three different samples, and for two different isolation cones (R=0.4 and R=0.7). The background suppression power is lower, with respect to the distribution shown in figure 5.9, because of the lower cut on the P_T

[1] In our analysis a cone of radius R = 0.4 was used instead of 0.7 to define the track isolation. One expects the τ–decay track to be less isolated in top events because there is more hadronic activity than in Z° events.

of the track. Otherwise, the results of Chapter V are confirmed.

For energy values close to the trigger threshold, we observe a higher probability for the JET20 sample. This is in agreement with our observation that in the JET50 sample the leading jet (which caused the trigger) has a higher probability to contain an isolated track. Therefore, in the analysis described in this thesis, using the JET50 sample to calculate the background is reasonable: there might be effects due to the trigger in the sample, but we expect them to appear at high values of the jet energy, in a region where there are only few events in the data sample used for top search.

In figure B.2 we show the E_T distribution of the tau candidate jets, for the two different cones used to define the isolation of both lepton and track. The shaded area corresponds to the background expected from hadrons which contain an isolated track and are wrongly identified as taus. In figure B.3 we show the same distributions as in figure B.2, but after requiring that lepton candidate and isolated track have opposite charge. One observes more events than predicted from QCD background. The excess is more pronounced if we apply tighter cuts.

In figure B.4 we compare the E_T distribution of the tau candidate jets of figure B.2 d) with the expectation obtained from a sample of $Z^\circ \rightarrow \tau\tau$ generated by the Isajet Montecarlo (dashed line). The absolute normalization of the histogram has been obtained comparing $Z^\circ \rightarrow ee$ events generated by Isajet and data. There are 14 events. 8 of these are $\mu + \tau$–track candidates. The remaining 6 are $e + \tau$–track candidates.

From this preliminary study we conclude that one observes a $Z^\circ \rightarrow \tau\tau$ signal, well described by the Isajet Montecarlo. This observation, which is based on the tau identification strategy described in this thesis, confirms the results of our analysis.

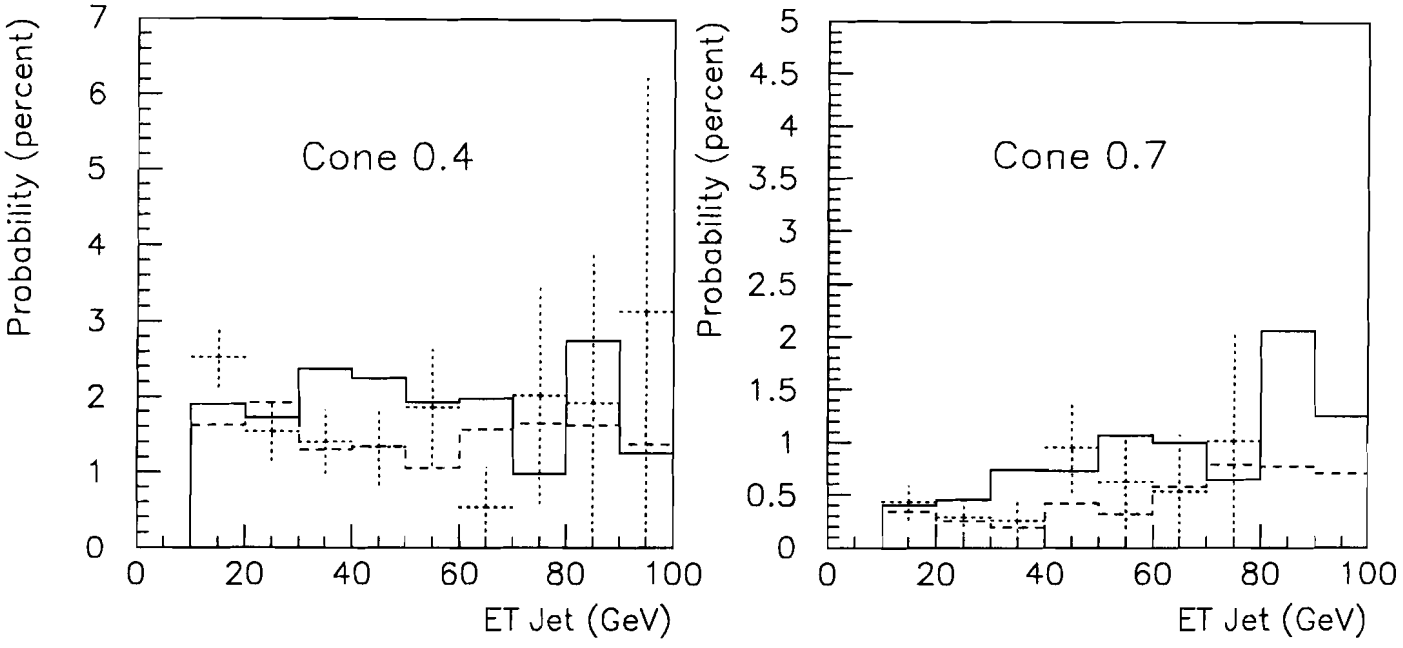

Figure B.1: Probability for a jet to contain an isolated track in the samples JET20 (solid line), JET50 (dashed line) and in the sample of non isolated muons (points with error bars). a) Isolation cone of radius R = 0.4. b) Cone of radius R = 0.7.

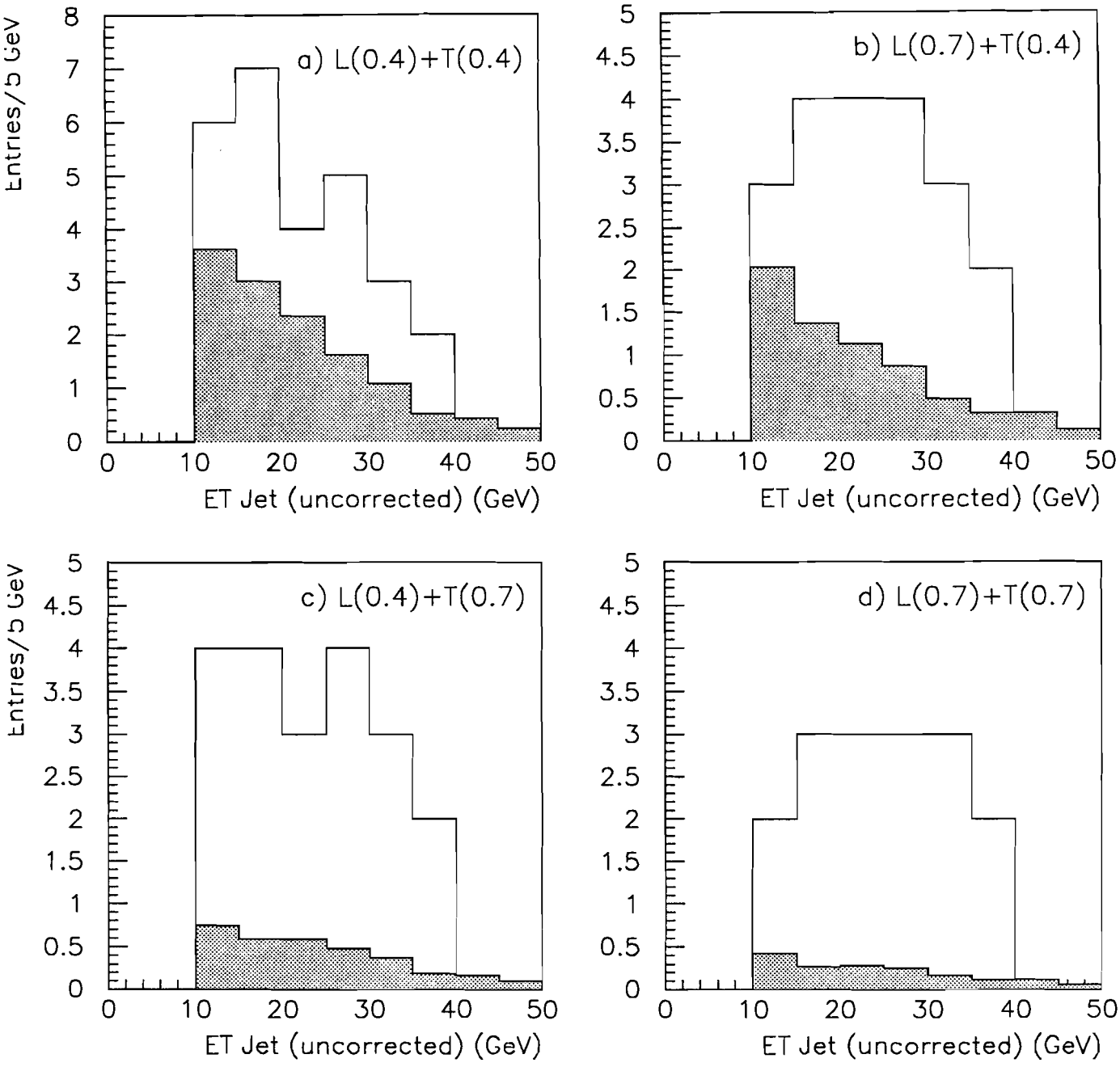

Figure B.2: E_T distribution of the tau candidate jets in e/μ + isolated track events. Data and background expectations are shown for two isolation cone: R = 0.4 and R = 0.7. The lepton isolation is defined in the calorimeter, while the track isolation is defined in the CTC.

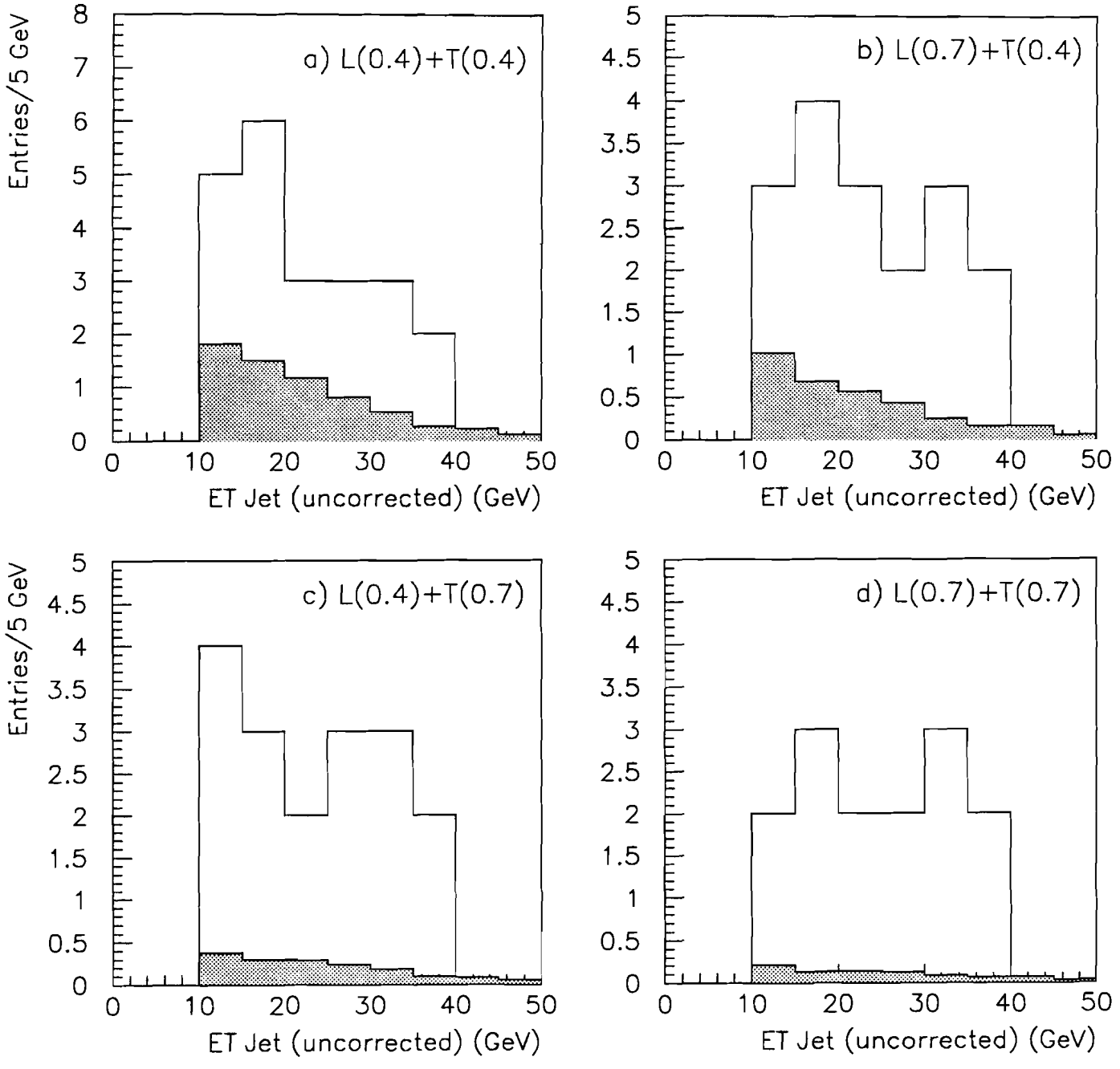

Figure B.3: E_T distribution of tau candidate jets in e/μ + isolated track events. The lepton and the track are required to be unlike sign.

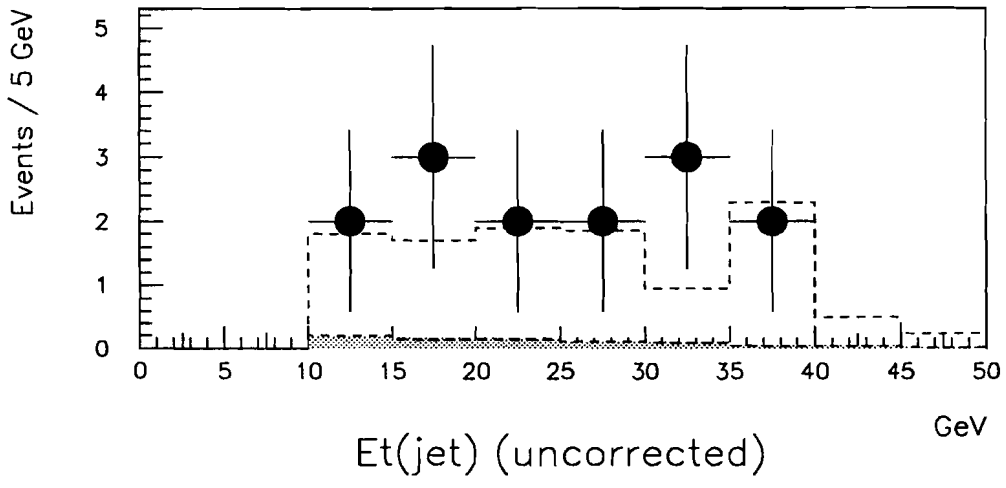

Figure B.4: E_T distribution of tau candidate jets in $Z^0 \rightarrow \tau\tau$ events, compared to the absolute prediction obtained from the Isajet Montecarlo. The isolation for both lepton and track is defined in a cone of radius R = 0.7.

References

[1] N.C. Yang and R.L.Mills,*Phys. Rev.***96** (1954) 191;
M. Gell-Mann, *Suppl. Nuovo Cimento*, **9** (1972) 733;
H. Fritzsch, M. Gell-Mann and H. Leutwyler, *Phys. Lett. B* **47** (1973) 365;
D.J. Gross and F. Wilczek, *Phys. Rev. Lett* **30** (1973) 1343 ; *Phys. Rev.* **D 8** (1973) 3633.

[2] S.L. Glashow, *Nucl. Phys.* **22** (1961) 579;
S. Weinberg, *Phys. Rev. Lett.* **19** (1967) 1264;
A. Salam, *"Elementary Particle Theory: Relativistic Groups and Analyticity"*, Proc. 8th Nobel Symposium Aspenasgarden, Stockholm, (1968) 367.

[3] G. Arnison *et al.*, UA1 Collaboration, *Phys. Lett. B* **122** (1983) 103;
M. Banner *et al.*, UA2 Collaboration, *Phys. Lett. B* **122** (1983) 476;
G. Arnison *et al.*, UA1 Collaboration *Phys. Lett. B* **126** (1983) 398;
P. Bagnaia *et al.*, UA2 Collaboration *Phys. Lett. B* **129** (1983) 130.

[4] W. Hollik, in *Proceedings of the XVI International Symposium on Lepton-Photon Interactions* August 1993; o CERN/PPE/93-157.

[5] Particle Data Group *Phys. Rev.* **D 45** (1992).

[6] P.W. Higgs, *Phys. Lett.* **12** (1964) 132; *Phys. Rev.* **145** (1966) 1156.

[7] R. Hollebeek in: "*Proceedings of the Twentieth SLAC Summer Institute on Particle Physics*", July 1992.

[8] G.L. Kane and M.E. Peskin, *Nucl. Phys.* **B 195** (1989) 29.

[9] A. Bean *et al.*, *Phys. Rev.* **D 35** (1987) 3533.

[10] W. Bartel *et al.*, *Phys. Lett.* **146 B** (1984) 437.

[11] G. Kane, Winskonsin Top Symposium (1992).

[12] S.L. Glashow, J. Iliopoulos and L. Maiani, *Phys. Rev.* **D 2** (1970) 1285.

[13] M.K. Gaillarde, B.W. Lee, *Phys. Rev.* **D 10** (1974) 897.

[14] H. Albrecht *et al.*, *Phys. Lett.* **B 192** (1987) 245.

[15] M. Artuso *et al.*, *Rev. Lett.* **62** (1989) 2233.

[16] H. Schroder, in *B Decays*, S. Stone World Scientific, Singapore, 1992.

[17] F. Abe *et al.*, CDF Collaboration *Phys. Rev. Lett.* **67** (1991) 3351.

[18] F. Sefkow, in *Proceedings of the XXVIII Rencontre de Moriond*, Les Arcs, France, March 1993. CERN–PPE/93–105.

[19] C. Kim, J. Rosner and C. Yuan, *Phys. Rev.* **D 42** (1990) 96.

[20] W. Marciano and A. Sirlin, *Phys. Rev.* **D 29** (1984) 945;
D. Bardin *et al.*, *Z. Phys.* **C 32**, (1986) 121;
U. Amaldi *et al.*, *Phys. Rev.* **D 36**, (1987) 1385;
P. Langacker, *Phys. Rev. Lett.* **63**, (1989) 1920.

[21] F. Abe *et al.*, CDF Collaboration, *Phys. Rev.* **D 44** (1991) 29.

[22] F. Abe *et al.*, CDF Collaboration, *Phys. Rev.* **D 43** (1991) 2070; *Phys. Rev. Lett.* **65** (1990) 2243.

[23] A.A. Akhundov, D.Y. Bardin and T. Riemann, *Nucl. Phys.* **B 276** (1986) 1;
W. Beenakker and W. Hollik, *Z. Phys.* C **40** (1988) 141;
J. Bernabeu, A. Pich and A. Santamaria, *Phys. Lett.* **B 200** (1988) 569.

[24] F. Abe *et al.*, CDF Collaboration, *Phys. Rev. Lett.* **67** (1991) 1502.

[25] G.L. Lin, J. Liu and Y.P. Yao, *Mod. Phys. Lett.* **A 6** (1991) 1333.

[26] J. Alitti *et al.*, UA2 Collaboration, *Phys. Lett* **B 276** (1992) 354.

[27] H. Abramowicz *et al.*, CDHS Collaboration, *Phys. Rev. Lett.* **57** (1986) 298;
A. Blondel *et al.*, CDHS Collaboration, *Z. Phys.* C **45**, (1990) 361.

[28] J.V. Allaby *et al.*, CHARM Collaboration, *Phys. Lett.* B **177** (1986) 446; *Z. Phys.* C **36**, (1987) 611 .

[29] M. Shaevitz for the CCFR Collaboration, M. Shaevitz, in *Proceedings of the Rencontres de Physique de la Vallée D'Aoste* La Thuile, Italy 1993.

[30] W.J. Stirling, in *Proceedings of the 1990 CERN School of Physics*, CERN 92–06.

[31] P. Nason, S. Dawson and R.K. Ellis, *Nucl. Phys.* **B 303** (1988) 724;
G. Altarelli, M. Diemoz, G. Martinelli and P. Nason, *Nucl. Phys.* **B 308** (1988) 724.

[32] E. Laenen, J. Smith and W.L. Van Neerven, *Nucl. Phys.* **B 369** (1992) 543;
E. Laenen, J. Smith and W.L. Van Neerven, Fermilab-PUB-93/270-T (1993).

[33] B. Denby, in *Proceedings of the 9th Topical Workshop on Proton–Antiproton Collider Physics* Tsukuba, Japan, October 1993.

[34] T. Chikamatsu, in *Proceedings of the 9th Topical Workshop on Proton-Antiproton Colllider Physics* Tsukuba, Japan, October 1993;
CDF Collaboration, FERMILAB–Conf–93/212-E.

[35] T. Kamae in *Proceedings of the XXIV International Conference on High Energy Physics* Munich, 1988 (Springer–Verlag, 1898).

[36] F. Dydak, in *Proceedings of the 25th International Conference on High Energy Physics*, Singapore, 1990 (World Scientific, Singapore, 1991).

[37] G. Arnison *et al.*, UA1 Collaboration, *Z. Phys.* **C 48** (1990) 1.

[38] T. Akesson *et al.*, UA2 Collaboration, *Z. Phys.* **C 46** (1990) 179.

[39] F. Abe *et al.*, CDF Collaboration, *Phys. Rev.* **D 45** (1991) 2070.

[40] F. Abe *et al.*, CDF Collaboration, *Phys. Rev. Lett.* **68** (1992) 447; Phys. Rev. **D 45** (1992) 3921.

[41] F. Abe *et al.*, *Nucl. Instr. Meth.* A **271** (1988) 387.

[42] D. Amidei *et al.*, *Nucl. Instr. Meth.* A **289** (1990) 388.

[43] CDF internal note n. 1172 (*Proposal for an Upgraded CDF Detector*).

[44] F. Bedeschi *et al.*, *Nucl. Instr. Meth.* A **268** (1988) 75.

[45] S. Bhadra *et al.*, *Nucl. Instr. Meth.* A **268** (1988) 268.

[46] CDF internal note n. 1248.

[47] L. Balka *et al.*, *Nucl. Instr. Meth.* A **267** (1988)272.

[48] S. Bertolucci *et al.*, *Nucl. Instr. Meth.* A **267** (1988) 301.

[49] G. Ascoli *et al.*, *Nucl. Instr. Meth.* A **268** (1988) 33.

[50] CDF internal notes n. 1500 and 1964

[51] CDF internal note n. 1614.

[52] D. Amidei *et al.*, *Nucl. Instr. Meth.* A **269** (1988) 51.

[53] G. Ascoli *et al.*, *Nucl. Instr. Meth.* A **269** (1988) 63.

[54] G. Foster *et al.*, *Nucl. Instr. Meth.* A **269** (1988) 93.

[55] V. Barger *et al.*, *Phys. Rev.* **D 41** (1990) 2782;
J. Ohnemus, Phys. Rev. **D 44** (1991) 1403.

[56] H. Baer *et al.*, *Phys. Rev.* **D 37** (1988) 3152.

[57] F. Paige and S.D. Protopopescu, BNL Report n. BNL 38034 (1986).

[58] E.Eichten, I. Hinchcliffe, K.Lane and C. Quigg, *Rev. of Modern Physics*, 56 (1984) 579.

[59] V. Barger and R. Phillips, Collider Physics, Addison–Wesley (1987).

[60] S. Leone, "*Ricerca del quark top nel canale a due leptoni in CDF*", presented at the LXXVII SIF Conference, L'Aquila, Italy (1991); "*Ricerca del quark top nel decadimento in τ in CDF*", presented at the LXXVIII SIF conferece, Pavia, Italy (1992).

[61] F. Abe *et al.*, CDF Collaboration, *Phys. Rev. Lett.* **68** (1992) 3398.

[62] F. Abe *et al.*, CDF Collaboration, *Phys. Rev.* **D 43** (1991) 2070.

[63] M. Cobal, H. Grassmann and S. Leone, SSCL–Preprint-480 June 1993, and Il Nuovo Cimento, **107 A** (1994) 75.

[64] H. Grassmann, "*Status Report from CDF*", Fermilab-Conf-92/105.

[65] S. Leone in *Proceedings of the XV International Conference on Neutrino Physics and Astrophysics*, Granada, Spain , June 1992.

[66] M. Cobal, University of Pisa Ph.D. Thesis, December 1993.

[67] R.H. Dalitz and G.R. Goldstein, *Phys. Rev.* **D 45** (1992) 1531.

[68] M.Cobal, H.Grassman and S.Leone, to be published on Il Nuovo Cimento; CDF internal note n. 1913.

[69] M.Cobal, H.Grassman and S.Leone, CDF internal note n. 2136.

[70] M.Cobal, H.Grassman and S.Leone, CDF internal notes n. 2140 and 2246.

[71] J. Ohnemus, *Phys. Rev.* **D 43** (1991) 3626.

[72] F. Abe *et al.*, CDF Collaboration, *Phys. Rev.* **D 47** (1993) 4857.

[73] M.Cobal, H.Grassman and S.Leone, CDF internal notes n. 2323 and 2135.

[74] F. Abe *et al.*, CDF Collaboration, *Phys. Rev. Lett.* **70** (1993) 4042.

[75] F. Abe *et al.*, CDF Collaboration, submitted to Phys. Rev. **D**, April 22, 1994.

[76] C. Campagnari, P. Sphicas, A. Yagil and B. Farhat, CDF internal notes n. 1961 and 2098.

[77] R. Hughes *et al.*, CDF internal note n. 2068.

[78] D. Amidei *et al.*, CDF internal note n. 2091.

[79] S. Dell'Agnello, University of Pisa Ph. D. Thesis, December 1993.

[80] M. Gallinaro and H. Grassman, CDF internal note n. 2490.

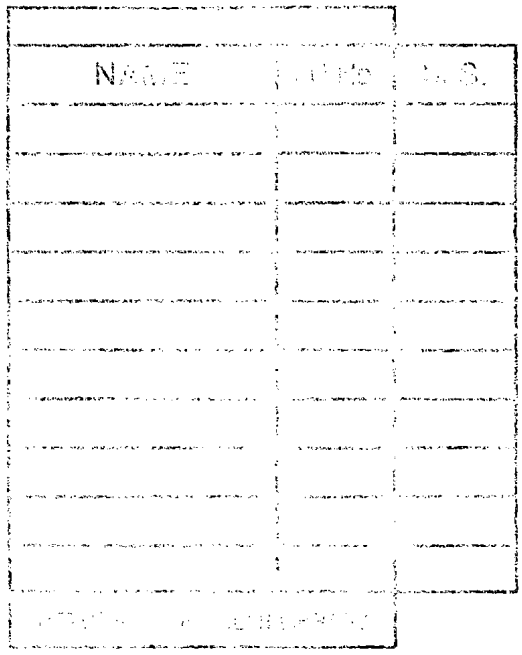
NAME